

AD-A073 520

AIR FORCE ROCKET PROPULSION LAB EDWARDS AFB CA
ASSESSMENT OF IN SITU DIAGNOSTICS FOR APPLICATION TO ROCKET PRO--ETC(U)
JUN 79 W K MCGREGOR
AFRPL-TR-78-62

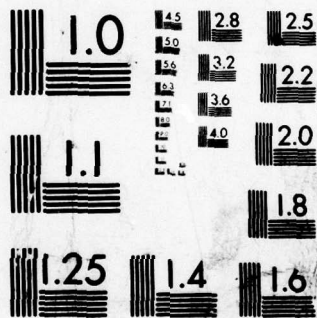
F/G 21/2

UNCLASSIFIED

NL

1 of 2
AD
A073520





MICROCOPY RESOLUTION TEST CHART
NATIONAL BUREAU OF STANDARDS-1963-A

LEVEL II

B.S. 2

AFRPL-TR-78-62

AD A 073 520

ASSESSMENT OF IN SITU DIAGNOSTICS FOR APPLICATION
TO ROCKET PROPULSION PROBLEMS

AUTHOR: W. K. MCGREGOR

JUNE 1979

DDC
RECEIVED
SEP 10 1979
C



*Approved for public release;
distribution unlimited*

DDC FILE COPY

AIR FORCE ROCKET PROPULSION LABORTORY
DIRECTOR OF SCIENCE AND TECHNOLOGY
AIR FORCE SYSTEMS COMMAND
EDWARDS AFB, CALIFORNIA 93523

79 09 5 024

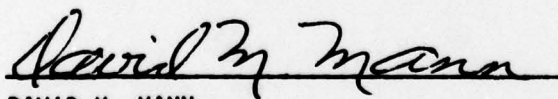
NOTICES

"When U.S. Government drawings, specifications, or other data are used for any purpose other than a definitely related government procurement operation, the Government thereby incurs no responsibility nor any obligation whatsoever, and the fact that the Government may have formulated, furnished, or in any way supplied the said drawings, specifications or other data, is not to be regarded by implication or otherwise, as in any manner licensing the holder or any other person or corporation, or conveying any rights or permission to manufacture, use, or sell any patented invention that may in any way be related thereto."

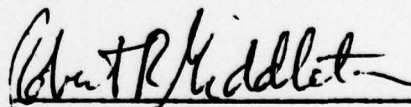
FOREWORD

This work was performed in-house at the AFRPL under project number 2308M2UC, Combustion/Plume Diagnostics--Advanced Techniques. The author was on a temporary appointment to the AFRPL while on leave of absence from SVERDRUP/ARO, Inc., contract operator of the AFSC's Arnold Engineering Development Center. The author wishes to express his appreciation to the AFRPL for the opportunity to conduct the study reported herein and to acknowledge the many constructive discussions with his colleague, Dr. David M. Mann, which contributed materially to this report.

This report has been reviewed by the Information Office/XOJ and is releasable to the National Technical Information Service (NTIS). At NTIS it will be available to the general public, including foreign nations. This technical report has been reviewed and is approved for publication; it is unclassified and suitable for general public release.



DAVID M. MANN
Chief, Plume Technology Section



ROBERT MIDDLETON, Capt., USAF
Chief, Combustion and Plumes Branch

FOR THE COMMANDER



JOHN I. WASHBURN, Lt. Col., USAF
Chief, Propulsion Analysis Division

UNCLASSIFIED

SECURITY CLASSIFICATION OF THIS PAGE (When Data Entered)

| REPORT DOCUMENTATION PAGE | | READ INSTRUCTIONS BEFORE COMPLETING FORM |
|---|-----------------------|--|
| 1. REPORT NUMBER AFRPL-TR-78-62 | 2. GOVT ACCESSION NO. | 3. RECIPIENT'S CATALOG NUMBER 9 |
| 4. TITLE (and Subtitle) Assessment of In Situ Diagnostics for Application to Rocket Propulsion Problems | | 5. TYPE OF REPORT & PERIOD COVERED Final Report Feb 77 to Mar 78 |
| 7. AUTHOR(s) W. K. McGregor | | 6. PERFORMING ORG. REPORT NUMBER |
| 9. PERFORMING ORGANIZATION NAME AND ADDRESS Air Force Rocket Propulsion Laboratory/PACP Edwards Air Force Base Ca 93523 | | 8. CONTRACT OR GRANT NUMBER(s) |
| 11. CONTROLLING OFFICE NAME AND ADDRESS Air Force Rocket Propulsion Laboratory/PACP Edwards Air Force Base Ca 93523 | | 10. PROGRAM ELEMENT, PROJECT, TASK AREA & WORK UNIT NUMBERS 2308M2UC 17 M2 |
| 14. MONITORING AGENCY NAME & ADDRESS (if different from Controlling Office) 12 [53p.] | | 12. REPORT DATE June 1979 |
| | | 13. NUMBER OF PAGES |
| | | 15. SECURITY CLASS. (of this report) Unclassified |
| | | 15a. DECLASSIFICATION/DOWNGRADING SCHEDULE |
| 16. DISTRIBUTION STATEMENT (of this Report) Approved for public release, distribution unlimited. | | |
| 17. DISTRIBUTION STATEMENT (of the abstract entered in Block 20, if different from Report) | | |
| 18. SUPPLEMENTARY NOTES | | |
| 19. KEY WORDS (Continue on reverse side if necessary and identify by block number) diagnostics remote temperature/composition measurement combustion rocket propulsion particle size particle velocity | | |
| 20. ABSTRACT (Continue on reverse side if necessary and identify by block number) A compelling need for knowledge of the properties (temperature, density, velocity, composition, etc.) of the flows produced by propulsion systems has recently surfaced in many areas. Of specific interest to the Air Force Rocket Propulsion Laboratory (AFRPL) is knowledge of properties within combustion chambers, particularly for solid fueled motors employing metalized propellants, and properties affecting exhaust plume observables (e.g., smoke, infrared radiation signatures, ultra-violet radiation signatures, radar cross sections, etc.). Methods of making measurements within | | |

DD FORM 1473 1 JAN 73 EDITION OF 1 NOV 65 IS OBSOLETE

UNCLASSIFIED
SECURITY CLASSIFICATION OF THIS PAGE (When Data Entered)

307 720 mt

20. combustion flows must avoid influencing the very phenomena to be measured and, generally, must be made from without (nonintrusive) because of the harsh environment. This report is aimed at defining the needs for "combustion diagnostics" associated with rocket propulsion, assessing the status and utility of the applicable techniques, and establishing a basis for the research and development required to provide techniques to meet the defined needs. The conclusions reached during the study are listed as follows: (1) For the case of purely gaseous flows from modern liquid propellant rockets, the currently existing spectroscopic techniques of measurement were found to be adequate, in principle, to meet rocket propulsion system needs. Refinements in the form of instrumentation improvement, data treatment, and sensitivity and uncertainty analysis will be required. (2) For the case of the combined gas/particle flows from solid propellant combustion, current techniques for measurement of particle properties were found to be inadequate and techniques for measurement of gas properties in the presence of particles were found to be largely untried. (3) X-ray spectroscopy appears promising for measurement of particle composition and mass properties. Further feasibility analysis on all X-ray methods to define instrumentation requirements and data analysis is required, to be followed by proof of principle experiments. (4) Further work is needed on the spectral characteristics of particulates. (5) A systematic modeling and experimental program is required to investigate spectroscopic techniques for gas property measurement in the presence of particles.

| | |
|---------------------------|----------------------|
| Accession For | |
| NTIS | GRA&I |
| DDC TAB | |
| Unannounced Justification | |
| By _____ | |
| Distribution/ | |
| Availability Codes | |
| Dist | Avail and/or special |
| A | |

TABLE OF CONTENTS

| <u>PARAGRAPH</u> | <u>TITLE</u> | <u>PAGE</u> |
|------------------|---|-------------|
| 1. | Introduction | 6 |
| 2. | Measurement Needs for Rocket Propulsion Flows. | 10 |
| 2.1 | General Properties of Combustion Gases | 10 |
| 2.2 | General Needs for Measurements in Combustion Gases | 15 |
| 2.2.1 | Performance of Liquid Propellant Rockets | 15 |
| 2.2.2 | Performance of Solid Propellant Rockets. | 17 |
| 2.2.3 | Rocket Plume Signatures. | 19 |
| 2.2.4 | Fundamental Mechanism Studies. | 23 |
| 2.3 | Summary of Diagnostic Needs. | 25 |
| 3. | Assessment | 30 |
| 3.1 | Techniques for Gas Phase Only. | 30 |
| 3.1.1 | Discussion of Techniques | 30 |
| 3.1.2 | Assessment of Gas Phase Only Diagnostics | 36 |
| 3.2 | Techniques for Gas/Particle Flows. | 37 |
| 3.2.1 | Assessment of Gas/Particle Flow Diagnostics. | 37 |
| 3.2.2 | Assessment of Optical Techniques for Particle Diagnostics. . . | 40 |
| 3.2.3 | Assessment of Gas Phase Diagnostics in Gas/Particle Flows. . . | 44 |
| 4. | Advanced Techniques. | 46 |
| 4.1 | Particle Composition and Mass, X-Ray Methods | 46 |
| 4.1.1 | Absorption - Average Atomic Density. | 48 |
| 4.1.2 | Time Averaged Fluorescence - Space Averaged Atomic Density . . | 49 |
| 4.1.3 | Particle Fluorescence - Number of Atoms in Particle, Velocity, Size | 50 |
| 4.2 | Particle Temperature - Radiation/Absorption Properties | 52 |
| 4.3 | Particle State - Liquid or Solid | 53 |
| 4.4 | Gas Properties - Spectroscopic Methods | 55 |
| 5. | Conclusions. | 58 |
| | References | 61 |
| | Appendix A. Equilibrium Properties of Combustion Products for Several Typical Rocket Propellant Combinations | 66 |

TABLE OF CONTENTS (Continued)

| <u>PARAGRAPH</u> | <u>TITLE</u> | <u>PAGE</u> |
|------------------|--|-------------|
| | Appendix B. Brief Description of Existing Diagnostic Techniques Applicable to Rocket Combustion and Plume Measurements. | 73 |
| | Appendix B-1. IR Band Model Emission/Absorption | 74 |
| | Appendix B-2. UV Resonance Absorption | 88 |
| | Appendix B-3. Rayleigh Scattering | 97 |
| | Appendix B-4. Raman Scattering. | 101 |
| | Appendix B-5. High Resolution Emission and/or Absorption. | 106 |
| | Appendix B-6. E-Beam Fluorescence | 112 |
| | Appendix B-7. Resonance Fluorescence. | 115 |
| | Appendix B-8. Holography. | 119 |
| | Appendix B-9. Laser Doppler Velocimetry (LDV) | 126 |
| | Appendix B-10. Diffusion Correlated Spectroscopy (DCS). | 135 |
| | Appendix B-11. Mie Scattering Inversion | 142 |

LIST OF ILLUSTRATIONS

| <u>FIGURE</u> | <u>TITLE</u> | <u>PAGE</u> |
|---------------|--|-------------|
| 1a. | Illustration of Liquid Rocket Combustion Flow - Low Altitude | 12 |
| 1b. | Illustration of Liquid Rocket Combustion Flow - High Altitude | 13 |
| 2. | Illustration of Air Launched Solid Propellant Rocket Combustion Flow. | 14 |
| 3. | Illustration of Plume Observables. | 21 |
| 4. | Illustration of X-Ray Spectroscopic Technique. | 47 |
| 5. | Scattering Event Chronology for a Particle Passing Through an X-Ray Beam. | 51 |
| 6. | Spectral Radiance of Particles | 54 |
| B-1 1. | Illustration of Radiative Transfer Through Nonhomogeneous Radiating and Absorbing Path Made up of Isothermal, Isobaric Zones | 75 |
| B-1 2. | Schematic of Orientation of Symmetric Zones for Emission/Absorption Technique | 79 |
| B-1 3. | Computational Flow Chart for AEDC IR Emission/Absorption Inversion Method | 81 |
| B-1 4a. | Raw and Smoothed Data from Transtage Engine Exit Plane - Radiance | 84 |
| B-1 4b. | Raw and Smoothed Data from Transtage Engine Exit Plane - Transmittance. | 85 |
| B-1 5a. | Inverted Data from IR Emission/Absorption Technique Applied to Transtage Engine Exit Plane Radiance and Transmittance - Temperature. | 86 |
| B-1 5b. | Inverted Data from IR Emission/Absorption Technique Applied to Transtage Engine Exit Plane Radiance and Transmittance - CO ₂ Partial Pressure | 87 |
| B-2 1. | Illustration of UV Resonance Absorption. | 89 |
| B-2 2. | Computational Flow Chart for AEDC UV Resonance Absorption Inversion Method | 90 |
| B-2 3. | NO Number Density Profiles in Exhaust of Turbojet Engine Combustor at Two Axial Locations as Measured by Sampling Probes and UV Resonance Absorption Techniques. | 93 |

LIST OF ILLUSTRATIONS (Continued)

| <u>FIGURE</u> | <u>TITLE</u> | <u>PAGE</u> |
|---------------|---|-------------|
| B-2 4. | Measured Transmittance at Peak of 0,0 -band (2262Å) Through Exhaust of Turbojet Engine Combustor at Two Axial Locations. | 94 |
| B-3 1. | Configuration for Laser Rayleigh Scattering Measurements . | 97 |
| B-4 1. | Illustration of Laser Raman Scattering System. | 101 |
| B-4 2. | Temperature and Number Density as a Function of Engine Time for a 500lbf N ₂ O ₄ /MMH Rocket Engine | 105 |
| B-6 1. | Configuration for E-Beam Fluorescence Measurements | 113 |
| B-7 1. | Configuration for Laser Induced Fluorescence Measurements. | 116 |
| B-7 2. | State Diagram Illustrating Fluorescence. | 116 |
| B-8 1. | Optical Arrangement for Application of Holography to High Pressure Solid Propellant Combustion Studies (1 of 2). . . | 122 |
| B-8 2. | Example Particle Size Distribution Data from Combustion Bomb Using Solid Propellant Sample at 500 psia, Obtained with Holography of Figure B-8 1. | 125 |
| B-9 1. | Simplest LDV Configuration | 127 |
| B-9 2. | Reference Beam LDV Configuration | 127 |
| B-9 3. | Dual Scatter LDV Configuration | 129 |
| B-9 4. | AC Signal from Dual Scatter LDV. | 129 |
| B-9 5. | Signal from Dual Scatter LDV | 130 |
| B-9 6. | Visibility Function for Dual Scatter LDV | 130 |
| B-9 7. | Velocity Histograms of the Axial Velocity at Nozzle Exit of the Exhaust of an F101-GE-100 Turbofan Engine Obtained by Laser Doppler Velocimetry. | 134 |
| B-10 1. | Orientation for DCS. | 136 |
| B-10 2. | Homodyne Spectrum from Particle Scattering | 136 |
| B-10 3. | Apparatus for Laser Doppler Line Shape Measurement | 140 |
| B-10 4. | Laser Scattered Power Spectrum from C ₂ H ₂ -O ₂ Flame. | 141 |
| B-11 1. | Angular Scattering Orientation | 143 |

LIST OF TABLES

| <u>TABLE</u> | <u>TITLE</u> | <u>PAGE</u> |
|--------------|--|-------------|
| 1a. | Summary of Measurement Needs for Rocket Propulsion Application - Liquid Propellants. | 26 |
| 1b. | Summary of Measurement Needs for Rocket Propulsion Application - Solid Propellants (1 of 2). | 27 |
| 2. | Diagnostic Techniques Available for Gas Phase Measurements | 32 |
| 3. | Cost Analysis for Gas Phase Combustion Diagnostic Techniques | 38 |
| 4. | Optical Diagnostic Techniques for Particle Measurements. . | 39 |
| A-1 | O ₂ /H ₂ | 67 |
| A-2 | LO ₂ /RP-1 | 67 |
| A-3 | N ₂ O ₄ /MMH | 68 |
| A-4 | ClF ₃ /B ₅ H ₉ | 69 |
| A-5 | ClF ₃ /AZ-50 | 70 |
| A-6 | Minimum Smoke Solid. | 71 |
| A-7 | Aluminized (18 percent) Solid. | 72 |

1. INTRODUCTION.

A compelling need for knowledge of the properties (temperature, density, velocity, composition, etc.) of the flows produced by propulsion systems has recently surfaced in many areas. The need has arisen because of the increased effort to obtain higher energy conversion efficiencies from combustion processes, to define visibility and other observable properties of propulsion system exhausts, and to make quantitative assessments of environmental effects caused by exhaust effluents. One area of concern is with rocket propulsion systems. Of specific interest to the Air Force Rocket Propulsion Laboratory (AFRPL) is knowledge of properties within combustion chambers (particularly for solid fueled motors employing metallized propellants) and properties affecting exhaust plume observables (e.g., smoke, infrared radiation signatures, ultraviolet radiation signatures, radar cross sections). Methods of making measurements within combustion flows must avoid influencing the very phenomena to be measured and, generally, must be made from without (nonintrusive) because of the harsh environment. The field of measurement associated with high temperature gas and gas-particle flows is generally referred to as "diagnostics." This report is aimed at defining the needs for "combustion diagnostics" associated with rocket propulsion, assessing the status and utility of the applicable techniques, and establishing a basis for the research and development required to provide techniques to meet the defined needs.

A few definitive statements need to be made to isolate the class of measurement problems to be addressed in this document. Measurements may be categorized in the following ways:

- (1) Ruler - The dimension of the variable to be measured and the observable are the same, usually with a one-to-one correspondence (e.g., ruler, volume vessel, protractor).

- (2) Gauge, meter - The dimension of the variable to be measured is transformed to a mechanical indicator or dial for observation (e.g., pressure gauge, manometer, mercury thermometer, speedometer, voltmeter).
- (3) Transducer - The desired measurement variable induces an electrical signal through the transducer device which is directly relatable to the measurement variable through calibration (e.g., thermocouple, strain gage, photomultiplier, turbine flow meter).
- (4) Diagnostic - The desired measurement variable is relatable to a direct measurement observable through an ab initio model of the physics (e.g., velocity from Doppler frequency shift, temperature from quantum state population distribution, particle size from scattered radiation, molecular density from Raman scattered radiation).

The measurements in categories (1), (2), and (3) are straightforward, although development of sensors, electrical signal conditioning, and computer data handling software often presents formidable problems. The area of work associated with such problems is classed as "instrumentation" development. Category (4), "diagnostics," requires phenomenological knowledge of the fundamental laws and atomic/molecular properties, and thus often requires a considerable amount of scientific research. This document is primarily concerned with the assessment of the diagnostics areas and the required fundamental research required to place the various techniques on sound footing. Instrumentation development (category (3)) will be discussed only when the lack of adequate devices presents a barrier to the development of the diagnostic technique.

Combustion flows, rocket exhausts in particular, present a very hostile environment to probes immersed in the flow. In addition, the presence of the probe often disturbs the flow field and the chemistry so that a representative measurement cannot be made on the gases sampled. Consequently, immersion sampling probes or other sensing objects into the flow are considered undesirable, and nonintrusive, in situ techniques must be employed. Such techniques encompass emission, absorption, and various scattering mechanisms of electromagnetic radiation.

AFRPL interests in measurements are restricted to the temperature and pressure ranges encountered in rocket combustion chambers, nozzles, and exhaust plumes. In the latter case, a wide range of temperature and pressure ranges are of interest, depending upon the altitude regime and the portion of the plume flow field to be considered. The species of concern are the combustion products of typical liquid and solid propellant rockets. This document is devoted to assessing the techniques which have application to rocket propulsion rather than to combustion diagnostics as a whole. Others, such as the following, have addressed the assessment of techniques of combustion diagnostics for other applications:

| <u>Reference</u> | <u>Year</u> | <u>Authors</u> | <u>Application</u> |
|------------------|-------------|---|--|
| 1 | 1976 | R. Goulard, A.M. Mellor and R.W. Bilger | Air Breathing Propulsion Engines |
| 2 | 1976 | R. Goulard | General Combustion Flows |
| 3 | 1977 | S.A. Self and C.H. Kruger | MHD Combustion |
| 4 | 1977 | A.C. Ekberth, P.A. Bonczyk and J.F. Verdick | Turbine Engine Com- bustion and Flows |
| 5 | 1977 | H.W. Coleman, D.R. Hardesty, et. al. | Coal Fired Gas Turbines |

In addition to the various reviews, a number of workshops on combustion diagnostics have taken place in the past few years, at least two of which were devoted to rocket combustion diagnostics.⁶⁻⁷ A valuable contribution to the literature on combustion diagnostics was recently made by the publication of a collection of papers given in 1976 at the American Institute of Aeronautics and Astronautics (AIAA) Aerospace Sciences Meeting (Washington, D.C., January 1976).⁸ The papers describe a wide variety of techniques that have been applied to gas phase and particle diagnostics in combustion flows. Although the material presented in References 1 through 8 covers generally the measurement problem areas applicable to rocket propulsion, none of them adequately brings into focus the pragmatic problems associated with "real world" measurements in rocket combustion flows.

The approach to be taken in this document is somewhat different than that of other reviews and assessments. Techniques which are well established will be considered in the main body of the report only from the standpoint of applicability and adequacy for rocket-oriented problems, and preferred references will be given to cite needed data to support the conclusions drawn. The basic principles of the established techniques will be outlined briefly in the appendices. The plan of the report is to first establish the needed measurement variables, their range, and the required accuracy, based upon the end objective of the measurement (performance, plume signature, etc.). The available techniques will then be listed, status of development and ranges of application will be discussed, and areas of further development will be identified where applicable. Of particular importance is the identification of voids in current capability and introduction of possible new approaches. The feasibility of the proposed approaches will then be studied in a preliminary sense and a research and development procedure suggested.

2. MEASUREMENT NEEDS FOR ROCKET PROPULSION FLOWS.

2.1 General Properties of Combustion Gases.

The combustion process in rockets may produce species in gas, liquid, and solid phases. The specific products produced and their phase depends upon the location within the engine flow (combustion chamber, nozzle, or plume) and the propellants being used. It is not possible to express many generalizations without specifying the system of interest. For the purposes of this study, the classes of propellants divide naturally into those producing only gaseous combustion products and those producing an appreciable concentration of liquid or solid material. Cryogenic propellants utilizing liquid oxygen with liquid hydrogen or hydrazine; storable propellants utilizing oxidizers such as nitrous tetroxide; fuels such as mono-methyl-hydrazine or unsymmetrical-dimethyl-hydrazine; or any of several other such fuels produce combustion products which are almost exclusively gaseous. Liquid oxygen with kerosene-type fuels produce solid carbon soot in addition to the gaseous products, but little attention is given to hydrocarbon fuels in advanced propulsion systems. Solid propellant systems may be either highly metallized, producing large effluxes of liquid and/or solid particulate matter, or, in the case of the smokeless type propellants under current development, may contain only a small concentration of particulate matter. Advanced propellants using holo-genic oxidizers and boron-containing fuels produce gaseous and liquid/solid products, as yet not well defined, and little attention will be given to this class of propellants in this study.

Appendix A contains tables of properties and species concentrations for several propellant combinations based upon one-dimensional equilibrium calculations. The levels of species concentrations and temperatures listed there serve as references for this study. The major species produced in the combustion processes are:

| <u>Propellants</u> | <u>Major Gaseous Species</u> | <u>Major Solid Species</u> |
|--------------------|------------------------------|----------------------------|
| O_2/H_2 | H_2O, H_2 | |
| O_2/C_xH_y | H_2O, CO_2, CO | C_n |
| $N_aO_b/N_xC_yH_z$ | N_2, H_2O, CO_2, H_2, CO | |
| Solids | N_2, H_2O, HCl, CO, H_2 | Al_2O_3 |

The gaseous species listed generally make up about 99 percent of the total gas, with the remainder composed of poorly known concentrations of minor stable species, such as unburned fuel fragments, oxides of nitrogen, alkali metals (Na or K), and free radicals (O, OH, CH, etc.). Thus, gas phase diagnostics is directed toward one or more of the major molecules, unless a specific need exists to determine concentration of one of the minor species.

Solid materials produced consist of either carbon soot (C_n) for the O_2/C_xH_y liquid propellant and some advanced propellants, such as ClF_3/MMH , or metal oxides (mostly Al_2O_3) for the solid propellants. Thus diagnostics of particulates in rocket combustion should be concerned mostly with carbon soot or Al_2O_3 particles. Solid propellant rockets which do not use metals imbedded within the propellant grains do not produce an appreciable number of particulates in the combustion process, but condensation in the far field of the low altitude plume often occurs. The condensate (secondary smoke) is thought to be composed of H_2O/HCl droplets centered on small nucleation sites with the possibility that HCl plays a role in the condensation process.⁹ Such condensates are also subject to diagnostics.

In Figure 1, a schematic of a combustion flow for a liquid propellant rocket is shown for a low altitude afterburning plume (Figure 1a) and a vacuum plume (Figure 1b). In Figure 2, a similar schematic is given for a solid propellant rocket flow at low altitude (air-launched). A temperature and pressure history along the flow paths from the combustion chamber to the far field plume is given in each case. These schematics will be used as maps to indicate the applicability of different diagnostic methods. Those methods which have been used are shown at the appropriate location in the flow schematic. Figures 1 and 2

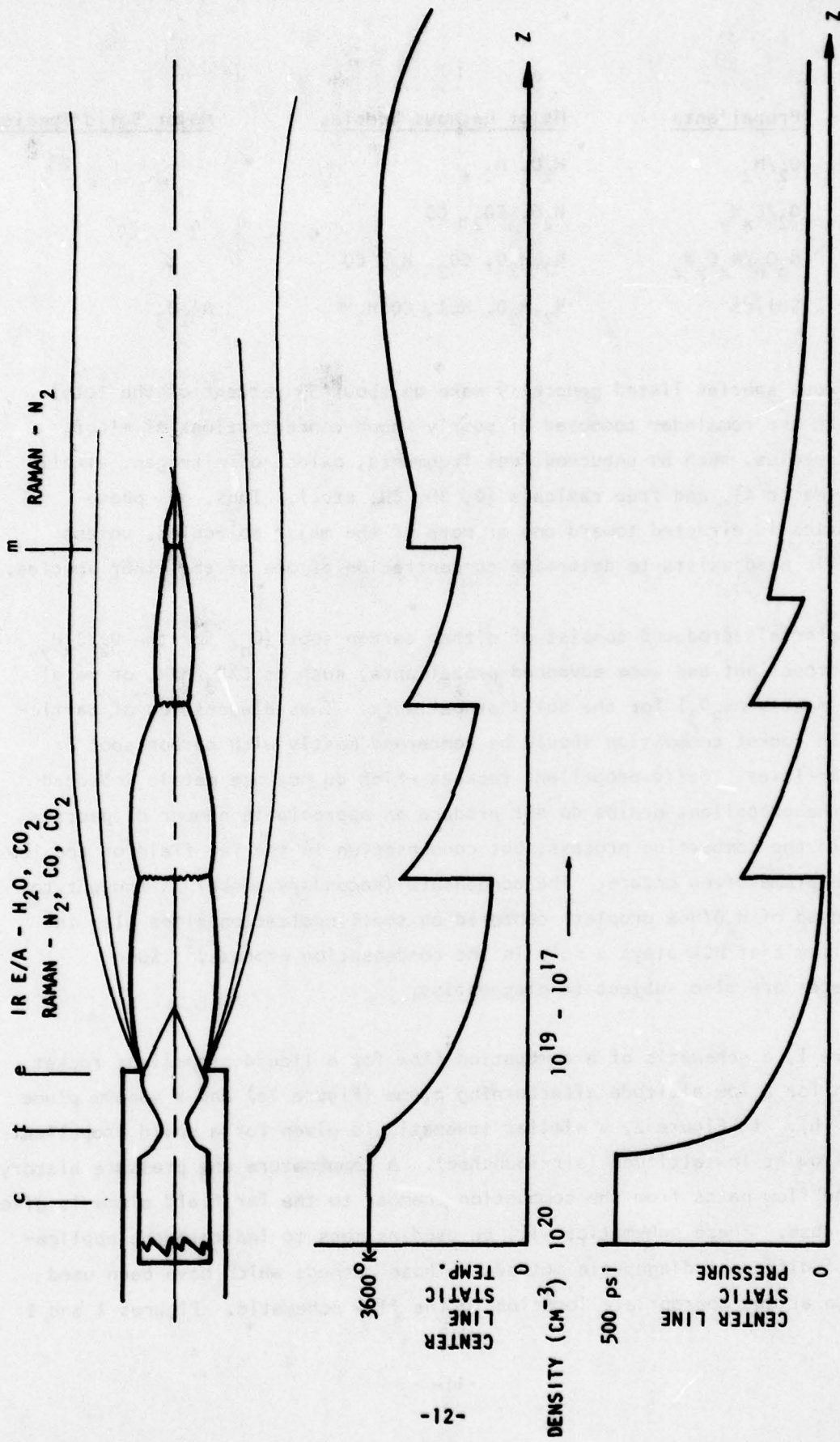


Figure 1a. Illustration of Liquid Rocket Combustion Flow - Low Altitude

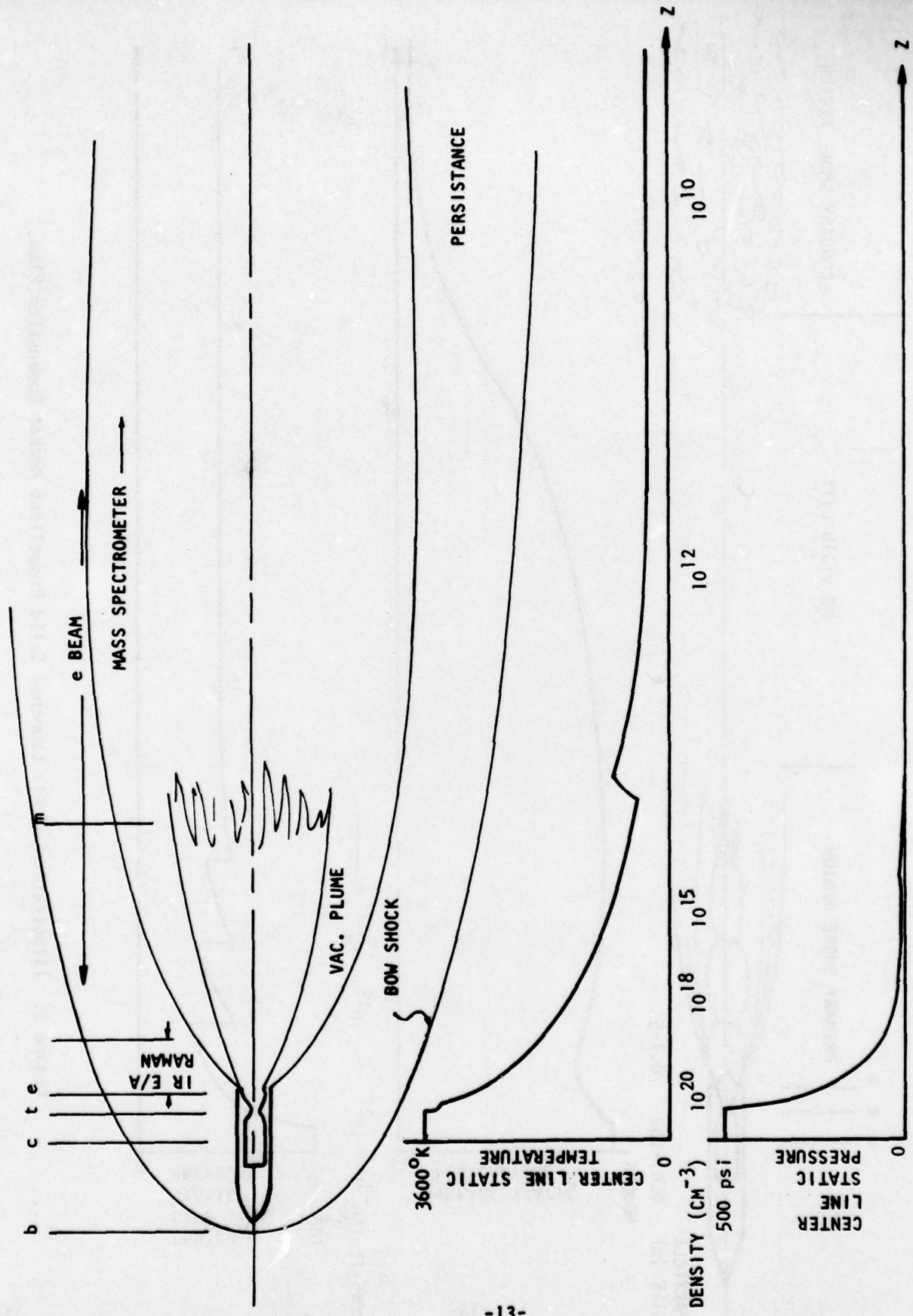


Figure 1b. Illustration of Liquid Rocket Combustion Flow - High Altitude.

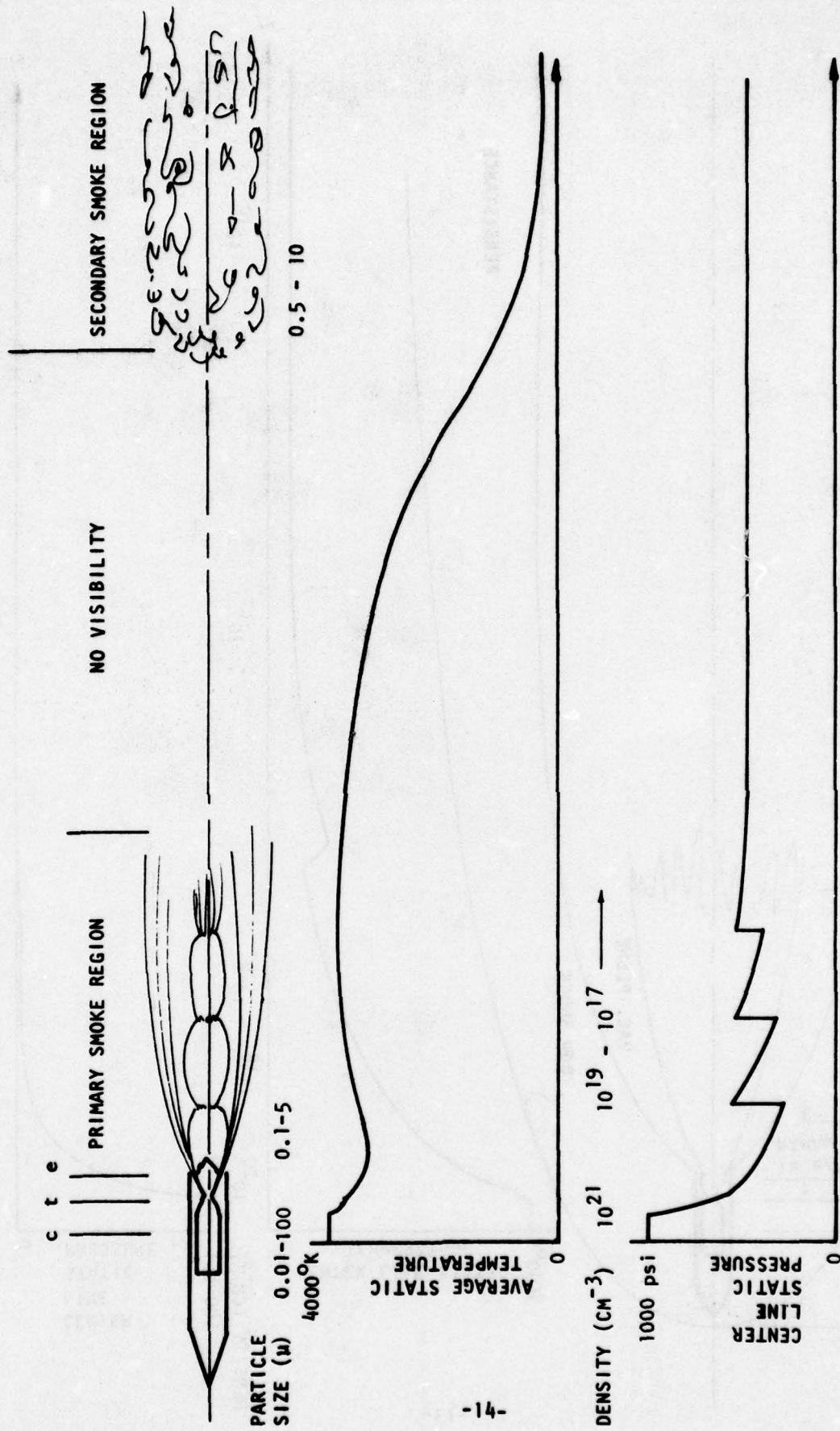


Figure 2. Illustration of Air Launched Solid Propellant Rocket Combustion Flow.

will be discussed in more detail in the next section. The intent at this point is to define the ranges of variables to be dealt with as indicated on the figures.

2.2 General Needs for Measurements in Combustion Gases.

2.2.1 Performance of Liquid Propellant Rockets.

In the development of rocket propulsion systems to meet the requirements of users like the Space and Missile Systems Organization and Aeronautical Systems Division, the major requirement is performance, usually measured in terms of "specific impulse" (I_{sp}), which is defined as

$$I_{sp} = \frac{\text{Thrust (F)}}{\text{Weight flow of propellants } (\dot{W})} \text{ sec} \quad (1)$$

The thrust and weight flow of propellants in a liquid propellant rocket are directly measurable so that I_{sp} is instantaneously determined throughout a firing. The energy release by the chemical reaction of fuel and oxidizer is known from chemical heat of formation data so that the ideal I_{sp} can be predicted. A measure of the performance is then available through comparison of the measured to the ideal I_{sp} . In the actual case, the chemical reactions rarely go to completion, and this, coupled with real gas dynamic behavior, prevents the achievement of perfect performance. The measurement of F and \dot{W} in a gross sense does not indicate the reason for a less than ideal performance; thus, because these have been traditionally the only measurements made, development of rocket engines has evolved as an empirical cut-and-try procedure.

With the advent of the modern, high-speed digital computer and improved understanding of turbulent, chemically reacting flow and droplet burning phenomena, attempts have recently been made at putting the development of liquid propellant rockets on a sound scientific basis through analytical modeling (Reference 10, for example). However, such complex models involve

many assumptions, and gross measurements of F and \dot{W} are seldom sufficient to determine just where a model is deficient. For example, thrust F is determined by

$$F = \frac{1}{g} \iint \rho_e V_e^2 dA_e + \int_0^L (P_w - P_o) \cos \theta 2\pi r_w dz \quad (2)$$

where g is the acceleration of gravity;

ρ_e is the gas density at some position x_e, y_e in the plume of the nozzle exit;

V_e is the gas velocity at some position x_e, y_e in the plane of the nozzle exit;

dA_e is a differential area at a position x_e, y_e in the plane of the nozzle exit;

P_w is the static pressure at the wall at an axial position z from the nozzle throat;

P_o is the static pressure of the ambient surroundings;

θ is the angle which the nozzle makes with the z axis of the nozzle;

r_w is the radius of the nozzle at the axial position z ;

L is the axial length of the nozzle from the throat to the exit plane.

The gas density and velocity at any point in the exit plane are determined by the oxidizer-to-fuel ratio (O/F) at that point and the degree to which combustion has gone to completion, as well as the gas dynamic conditions

imposed by the nozzle expansion. Thus, an accurate computer program for predicting the I_{sp} must start at the propellant injector face and follow the mixing and combustion through the combustion chamber to the nozzle exit. Then it must compute the integrals of Equation (2) point by point. A measurement to test the adequacy of the program must include the local exit plane density and velocity or sufficient other variables to separately calculate them so that point by point comparison between model prediction and measurements can be made. A sufficient set of variables to compute Equation (1) are the temperature, T_e , the O/F, the total pressure profiles, and a mapping of $P_w(z)$. The pressures are directly measurable, but T_e and O/F are not; this is the beginning of the diagnostics problem. Measurement of the temperature and the major species concentrations (H_2O , CO_2 , CO , and perhaps N_2 or H_2) is sufficient to determine a local value of the O/F. If certain assumptions are made about the chemistry, then measurement of the local density of only one or two of these species may be sufficient.

2.2.2 Performance of Solid Propellant Rockets.

In the testing of solid propellant rockets, the weight flow rate of propellants, \dot{W} , is not directly measurable but depends upon the propellant surface burning rate. Since the burning rate is also not measurable, the I_{sp} is usually determined by

$$I_{sp} = \frac{I_t}{W} = \frac{1}{W} \int_0^{t_0} F dt \quad (3)$$

where I_t is the total impulse;

W is the total weight of propellant;

t_0 is the total burn time.

A model to compute the thrust F for solid propellant rockets follows Equation (2) except that now both gas and solid phases must be taken into account in computing P_e , V_e , and P_w . Consequently, the temperature of both phases must be computed, and the composition of both gas and solids must be determined. The interaction of gas and particle flow is a major part of the analytical modeling for solid propellant rocket motors, and a critical variable is the status of the particles in the flow (size, spatial distribution, temperature, and constituency of the particles). By constituency is meant the chemical composition, the porosity, the geometrical shape, and the phase (liquid, solid, crystalline, etc.) of the particles. The only information currently available on particle properties is that obtained through analysis of samples obtained during or after a motor firing. Such particle analyses have shown that carbon soot with a mean particle diameter well below $1 \mu\text{m}$ is formed in the combustion of hydrocarbon fuels (see, for example, Reference 11).

For solid propellant motors to which aluminum has been added, the particles collected are Al_2O_3 , with a wide range of size distributions, the size depending to a large extent on how the samples were obtained.¹² In some cases, the Al_2O_3 particles are porous, or even hollow, with evidence that they were in a liquid state within the nozzle.

The temperature history of the particles depends upon their history in the flow and on their radiative properties. The temperature of the particles may not be the same as the gas temperature because of the gas/particle heat and mass and state changes.

The measurements required to fully evaluate analytical models for the performance of solid propellant rockets are summarized as follows:

| | |
|------------|------------------------------------|
| Gas Phase: | Local gas temperature |
| | Local composition of major species |
| | Velocity |

Condensed Phase: Geometrical size distribution

Composition

Mass distribution

Velocity distribution

State (liquid or solid)

Temperature

Hardly any of these variables is directly measurable by probes because of disturbances induced at the probe entrance. Consequently, in situ diagnostic methods are required. The diagnostic problem for the solid propellant rocket is clearly much more formidable than for the liquid propellant rocket.

2.2.3 Rocket Plume Signatures.

The AFRPL is also responsible for providing information to users on the electromagnetic observables and interferences produced by rocket exhaust plume products. The observables of interest may lie in any wavelength range from vacuum ultraviolet to radio frequency. The applications include surveillance of enemy missile launches, missile warning receivers for aircraft, radar cross sections, transmission or communications signals through plumes, contamination of spacecraft surfaces by plume materials, and various countermeasures to disguise or hide missile launches and maneuvers. The extent of the flight regimes and scenarios is much too broad to rely on flight test or ground test programs to supply complete information over all flight regimes. Therefore, reliance is made on analytical gas dynamic, chemistry, and electromagnetic radiation models to provide the overall predictive capability. Two measurement problems arise: (a) The models require input data (initial conditions), and (b) they must be validated through appropriate testing to insure that the most important physical processes have been modeled.

In order to illustrate the measurements required, consider Figure 3 in which a plume is shown which is emitting radiation and may also scatter radiation from other sources to an observer (detector). Depending upon the orientation of the detector with respect to the plume, the wavelength range, and the orientation of the external radiation source, Figure 3 represents a wide range of scenarios. A generalized expression for the radiation received at the detector may be written as follows:

$$I_{\Delta\lambda}^D = \int_{\Delta\lambda} \int_{\Delta\Omega} \int_{\Delta Z} \sum_i E(T, P_i, \lambda) \frac{\partial}{\partial Z} \tau(T, P_i, \lambda) dz d\Omega d\lambda + \int_{\Delta\lambda} \int_{\Delta\Omega} \int_{\Delta Z} \int_{\Delta\theta} I_o(\theta, \lambda) \sum_i S_i(\theta, P_i, \lambda) \frac{\partial \tau(T, P_i, \lambda)}{\partial Z} dz d\Omega d\lambda d\theta \quad (4)$$

where I_{λ}^D is the detected radiation within some specified wavelength range $\Delta\lambda = \lambda_1 - \lambda_2$;

$E(T, P_i, \lambda)$ is the emission coefficient of the radiation at some position with respect to the detector produced by species i at temperature T and partial pressure P_i at a wavelength λ ;

$\tau(T, P_i, \lambda)$ is transmittance of the radiation at a wavelength λ along the path \vec{z} to the detector;

$I_o(\theta, \lambda)$ is the irradiance from an external source falling on the plume at an angle θ with respect to \vec{z} (such as the sun or a radar beam) which may be scattered into the detector field of view or be attenuated by the plume;

$S_i(\theta, P_i, \lambda)$ is the scattering function of the plume at the angle θ by species (particles) i at the wavelength λ .

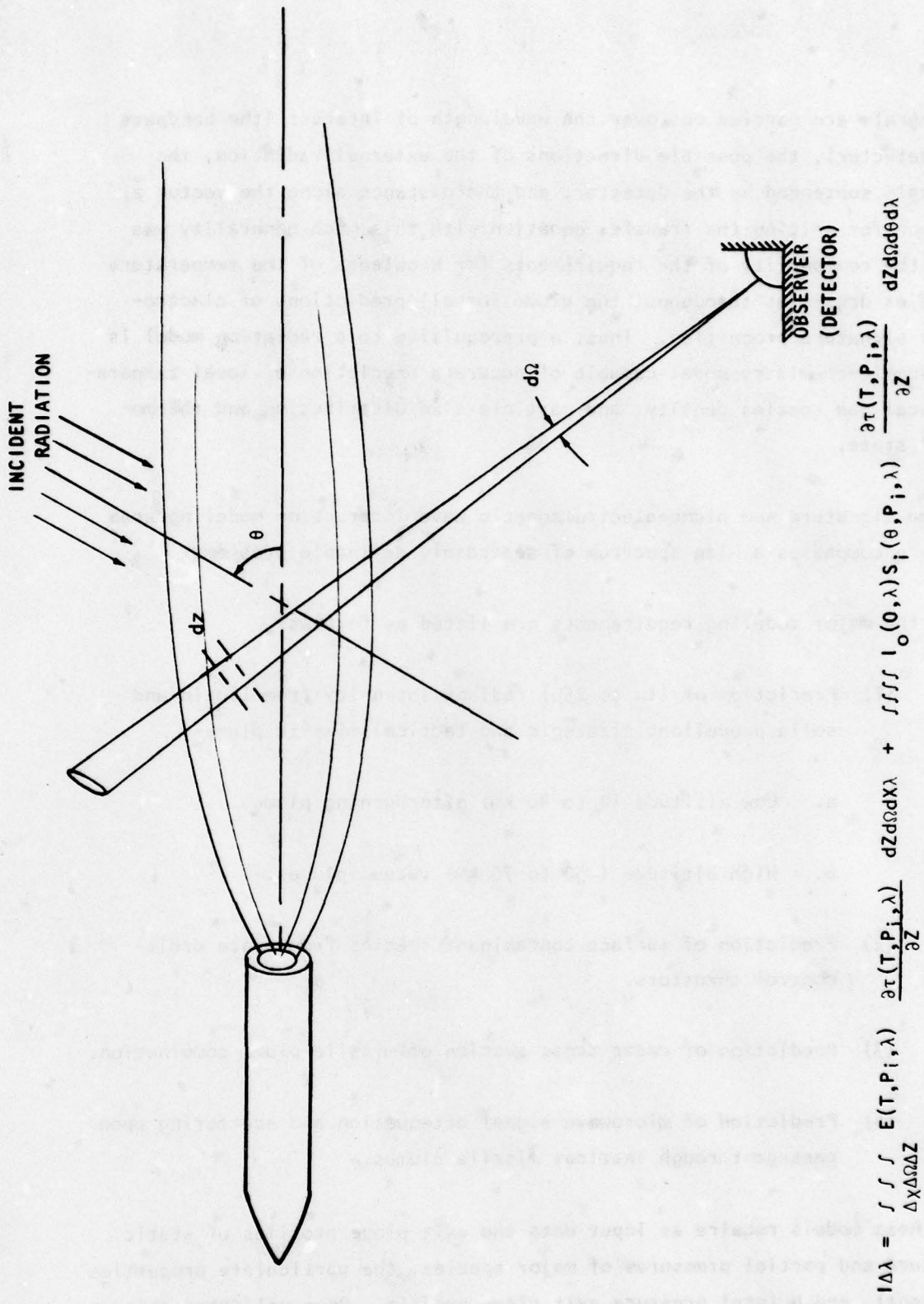


Figure 3. Illustration of Plume Observables.

The integrals are carried out over the wavelength of interest (the bandpass of the detector), the possible directions of the external radiation, the solid angle subtended by the detector, and the distance along the vector \vec{z} . The reason for writing the transfer equation with this much generality was to show the commonality of the requirements for knowledge of the temperature and species densities throughout the plume for all predictions of electromagnetic signature properties. Thus, a prerequisite to a radiation model is a gas dynamic-chemistry model capable of accurate prediction of local temperature, local gas species density, and particle size distribution and thermophysical state.

The plume signature and plume-electromagnetic wave interaction modeling area actually encompasses a wide spectrum of separately definable problems.

Some of the major modeling requirements are listed as follows:

- (1) Prediction of (1μ to 25μ) radiant intensity from liquid and solid propellant strategic and tactical missile plumes.
 - a. Low altitude (0 to 40 km) afterburning plumes.
 - b. High altitude (~50 to 70 km) vacuum plumes.
- (2) Prediction of surface contaminant species from space orbit-control thrusters.
- (3) Prediction of radar cross section of missile-plume combination.
- (4) Prediction of microwave signal attenuation and scattering upon passage through tactical missile plumes.

All of these models require as input data the exit plane profiles of static temperature and partial pressures of major species, the particulate properties (if present), and a total pressure exit plane profile. Once validated through

experiments employing proper diagnostic measurements, the performance models discussed in 2.2.1 and 2.2.2 can provide the exit plane inputs to the plume models. Evaluation of the plume signature prediction models can be accomplished in an "at large" sense by measurement of the predicted variable in either flight test or captive simulation tests. However, field tests are seldom satisfactory, and the deficient elements of the model cannot be detected. Therefore, controlled simulation testing is necessary in which measurements of critical variables (temperature, major species concentration, electron density, etc.) at selected positions in the plume are made.

Other plume-produced phenomena of interest include the following:

- (5) The interaction of plume species with atmospheric species to produce radiation in the far field of high altitude plumes.
- (6) The condensation of particulates in the far field of smokeless propellant tactical missile plumes to form condensation trails.

These phenomena require a different kind of diagnostics than the near field plume phenomena. The high altitude interaction problem requires measurements of minor or trace species concentrations at low density. The low altitude condensation problem requires particle property diagnostics of the condensates. Neither of these phenomena can be studied adequately by flight testing or by rocket firings in captive facilities, but require simulation of the phenomena in some indirect way, making good diagnostics that much more important.

2.2.4 Fundamental Mechanism Studies.

Many fundamental studies are required in the development of new concepts in rocket propulsion and in understanding of plume phenomena. The laboratory experiments conducted during these studies also require diagnostics. Some fundamental studies which currently can be identified are listed below, along with the measurement desired:

(1) Solid propellant combustion.

Objective: To determine burning rate and surface reaction phenomena for a variety of propellants.

Apparatus: Combustion bomb.

Measurement: Geometrical history of reacting surfaces and escaping particles (with definition of gaseous species properties if possible).

(2) Metal combustion phenomena.

Objective: To determine the mechanism of metal oxide formation, nucleation, and particle growth.

Apparatus: Low density reaction furnace.

Measurement: Gaseous specie identification, concentration, and temperature and particle growth history and constituency.

(3) UV radiative mechanisms.

Objective: To identify chemiluminescent excitation mechanisms for UV plume radiators (such as CO, NO, OH, CN, CH, and continuum mechanisms) and determine rate constants.

Apparatus: Gas reactor configuration, shock tubes, etc.

Measurement: Species concentrations and temperature of reaction participants, and UV radiation.

(4) Particle radiative properties.

Objective: To determine spectral emissivity and scattering cross sections of particles as encountered in combustion gases.

Apparatus: Two-phase, heated flow facility.

Measurements: Radiation and scattering function and temperature.

(5) Spectral properties of gas species.

Objective: To determine the radiative constants (molecular properties or band model properties) for molecules of interest in plumes.

Apparatus: Burners and heated flow facilities.

Measurements: Temperature, species density, and spectral radiation.

These are but a few of the many fundamental programs being conducted by the AFRPL which require diagnostic type measurements for proper treatment of the experiments.

2.3 Summary of Diagnostic Needs.

The measurement needs discussed in 2.2.1, 2.2.2, and 2.2.3 are summarized in Tables 1a and 1b for liquid propellant and solid propellant rockets, respectively. The variable to be measured, the region in the plume where the measurement is desired, the applications involved, the ranges of the variables of interest, and the accuracy required to accomplish the objective

TABLE 1a. SUMMARY OF MEASUREMENT NEEDS FOR ROCKET PROPULSION APPLICATION - LIQUID PROPELLANTS.

| <u>VARIABLE</u> | <u>REGION</u> | <u>APPLICATION</u> | <u>RANGE</u> | <u>REQUIRED ACCURACY</u> |
|--|-------------------------------|--|---|--------------------------|
| Local gas temperature | Exit plane | -Performance code evaluation | 1000°-2500°K | ± 5% |
| | Near field low altitude plume | -Plume model inputs -Plume gas dynamic model evaluation | 300°-2000°K | ± 5% |
| Local major species density H ₂ , CO ₂ , CO, N ₂ , H ₂ | Exit Plane | -Performance code evaluation | 10 ¹⁶ -10 ¹⁹ cm ⁻³ | ± 5% |
| | Near field low altitude plume | -Plume model inputs -Plume gas dynamic model evaluation | 10 ¹⁵ -10 ¹⁹ cm ⁻³ | ± 10% |
| Local minor species H _x C _y | Far field high altitude | -Inputs to far field codes | 10 ¹³ -10 ¹⁶ cm ⁻³ | 10% |

TABLE 1b. SUMMARY OF MEASUREMENT NEEDS FOR ROCKET PROPULSION APPLICATION - SOLID PROPELLANTS (1 of 2).

| <u>VARIABLE</u> | <u>REGION</u> | <u>APPLICATION</u> | <u>RANGE</u> | <u>REQUIRED ACCURACY</u> |
|---|-------------------------------|-------------------------------------|------------------------------------|--------------------------|
| Local gas temperature | Nozzle exit | -Performance code evaluation | 1500°-2500°K | ± 5% |
| | | -Input to plume gas dynamic code | | |
| | Near field low altitude plume | -Plume gas dynamics code evaluation | 500°-2000°K | ± 5% |
| | Far field low altitude plume | -Plume visibility code input data | 200°-500°K | ± 10% |
| <hr/> | | | | |
| Average particle temperature | Nozzle exit | -Performance code evaluation | 1500°-2500°K | ± 10% |
| | | -Input to rad. code | | |
| | Near field low altitude plume | -Plume rad. code evaluation | 500°-2000°K | ± 10% |
| | Far field low altitude plume | -Visibility code input data | 200°-350°K | ± 10% |
| <hr/> | | | | |
| Major gas species density (H ₂ O, CO ₂ , CO, HCl) | Nozzle exit | -Performance code evaluation | 10 ¹⁸ -10 ²⁰ | ± 10% |
| | | -Input to plume gas dynamic model | | |

TABLE 1b. SUMMARY OF MEASUREMENT NEEDS FOR ROCKET PROPULSION APPLICATION - SOLID PROPELLANTS (2 of 2).

| <u>VARIABLE</u> | <u>REGION</u> | <u>APPLICATION</u> | <u>RANGE</u> | <u>REQUIRED ACCURACY</u> |
|---|-------------------------------|--|---------------------------------|--------------------------|
| | Near field low altitude plume | -Plume gas dynamic code evaluation | $10^{17}-10^{19}$ | + 10% |
| | Far field low altitude plume | -Plume visibility code inputs | $10^{18}-10^{19}$ | + 10% |
| | Far field high altitude plume | -Contamination code evaluation | $10^{13}-10^{15}$ | + 10% |
| <hr/> | | | | |
| Particle size and weight distribution, and number density | Nozzle exit | -Performance code evaluation | $.01\mu-10\mu$ dia, | + 20% |
| | Low altitude far field | -Input to red code and gas dynamic model | 10^5-10^{10} cm ⁻³ | + 20% |
| | High altitude far field | -Visibility code evaluation | 10^5-10^{10} cm ⁻³ | + 20% |
| | | -Contamination code evaluation | 10^5-10^{10} cm ⁻³ | + 20% |

of the application are given in the tables. The information contained in Tables Ia and Ib will be used to assess the capability of existing diagnostic techniques and to locate inadequacies so that new work can be planned.

3. ASSESSMENT.

3.1 Techniques for Gas Phase Only.

3.1.1 Discussion of Techniques.

The emission or absorption of radiation from atoms or molecules in the gas phase has the property that the absolute value is related directly to the number density of the specie, and the spectral distribution is a function of the temperature through some formulation of the quantum state equilibrium distribution. Several procedures have been used to obtain a "measure" of the absolute distribution function of a specie in a gas flow, including

Passive emitted radiation

Absorbed radiation from a source

Fluorescent radiation induced by a source

Fluorescent radiation induced by electron beams

Scattering from an intense radiation beam (laser) at frequency ν_0

Rayleigh - nonshifted, ν_0

Raman - shifted, $\nu_0 \pm \nu_R$, ν_R = Raman shift

Nonlinear Raman

From these phenomena have come many specialized techniques for gas analysis and measurement of properties of ionized gases (plasmas), flames, and combustion gas flows from turbojet and rocket propulsion systems. The only techniques to be discussed here are those which have been applied to combustion flows and those for which there appears to be no barriers to use in combustion

flows since they have been used successfully in similar flows. The techniques are listed in Table 2 along with the measurements possible with them and the ranges of application. The physical principle, instrument layout, ranges of applicability, and, where possible, the estimated typical uncertainty of each of the techniques listed in Table 2 are discussed in Appendix B.

The measurement of velocity in gas flows by an in situ technique depends upon use of the Doppler frequency shift of an emission spectral line or on the Doppler shift of scattered radiation from a laser beam. In practical combustion flows, the Doppler shifts of emission lines are seldom large enough relative to the line width due to random motion and collisional broadening to be measurable. The technique that has proved most successful for velocity measurement has been the Laser Doppler Velocimeter (LDV) technique in which the frequency shift of the scattering signal from particles imbedded in the gas flow is measured. (This technique is discussed at length in the survey References 1 through 5 and by several papers in Reference 8). The discussion of this technique for rocket propulsion applications properly belongs in the next section on gas/particle flows. Quite obviously, the chief question with regard to measurement of gas flow velocities has to do with whether particles are moving at the same velocity as the gas flow. Generally, particles having diameters less than about $0.5 \mu\text{m}$ will follow the gas flows of rockets at pressures greater than about 1 atm. The question, however, is a much more complex one which requires careful analysis for each application (see References 34 and 35, for example).

The principal application of diagnostic methods to liquid rocket combustion flows has been the measurement of nozzle exit plane temperature and species concentration profiles in simulated vacuum or flight environments. Thus, the discussion to follow will center mostly on these applications.

TABLE 2. DIAGNOSTIC TECHNIQUES AVAILABLE FOR GAS PHASE MEASUREMENTS.

| <u>TECHNIQUE</u> | <u>SPECIES</u> | <u>TEMP RANGE</u> (°K) | <u>DENSITY RANGE</u> (cm^{-3}) | <u>STATUS</u> | <u>REFERENCE</u> |
|----------------------------|---|---------------------------|--|------------------|------------------|
| IR Emission/ Absorption | H_2O , CO , CO_2 | 800°-3000° | 10^{17} - 10^{20} | Operational | 13-17 |
| Resonance Absorption | OH, NO, C_2 , CH, etc. | ~30°-1500° | 10^{14} - 10^{17} | Operational | 19-21 |
| Rayleigh Scattering | All | NA | 10^{14} - 10^{20} | Semi-Operational | 22-23 |
| Raman Scattering | N_2 , CO, CO_2 , O_2 , H_2 , --- | ~30°-3000° | 10^{17} - 10^{20} | Semi-Operational | 24-25 |
| Hi-Res IR Spectroscopy | CO, HF, Cl, CO_2 , --- | ~30°-3000° | 10^{15} - 10^{18} | Developmental | 27-29 |
| E-Beam Fluorescence | N_2 , H_2 | ~30°-1500° | 10^{13} - 10^{16} | Operational | 30-31 |
| Resonance Fluorescence | C_2 , OH, Na | Unknown | 10^{15} - 10^{18} | Developmental | 32-33 |

The emission and absorption of infrared radiation by the principal products of combustion of conventional liquid propellants, H_2O and CO_2 , provides a means of measurement of temperature and the partial pressure of H_2O and CO_2 in the exhaust of rocket engines. The IR E/A technique is based upon the band model radiative transfer concept¹³ and has been used on a number of applications to rocket testing. (See, for example, Reference 14.) Two of the most recent applications are given in References 15 and 16, where it is shown that small changes in propellant injector configurations are detectable using the technique. In one application,¹⁵ the results of applying the technique have been used to make a preliminary assessment of liquid engine performance computer codes. Current effort on the technique is being devoted to improvements in instrumentation and data treatment with the goal being to provide higher confidence in the data through better uncertainty analysis.¹⁷ Current testing efforts are devoted to extensions of the performance code evaluation as described in Reference 16 in order to provide validation for the latest performance codes.¹⁸

3.1.1.2 Resonance Absorption (Appendix B-2).

The ultraviolet (UV) resonance absorption method is applicable to minor diatomic species and free radicals such as NO, OH, NH, CN, and CH. Application to rocket combustion flows has not been made, but results of several measurements in turbojet engine exhausts have been published.¹⁸⁻²⁰ Laboratory equipment has so far been employed for this technique. However, design of a dedicated system would not be difficult. Estimates of uncertainty (± 15 percent) are probably conservative, and a thorough analysis has not been done. No need for application to rocket exhaust flows is anticipated at this time.

3.1.1.3 Rayleigh/Raman Scattering (Appendices B-3 and B-4).

Rayleigh scattering as a measure of gas density²² and Raman scattering as a measurement technique for temperature and species concentration²⁴ have received much attention in the past few years.

Rayleigh and Raman scattering data from a rocket exhaust were first obtained during an AFRPL sponsored test program²³ in 1974-75. The program served as a feasibility demonstration, and temperature and species concentration data were successfully obtained. Many problems (background interference, fluorescence, plume fluctuations, etc.) were encountered in the test, and the experience gained was used in designing apparatus for use of Raman spectroscopy in a subsequent test program.²⁵ In the latter test, the objective was to measure instantaneous temperature and number density of N_2 in a turbulent mixing zone between external air flow (Mach number 2 and 3) and a rocket plume. A laser pulse width of about 20 nanoseconds was used at a repetition rate of 12 pulses per minute using a Q-switched ruby laser. Data uncertainty was about ± 8 percent; fluctuations in temperature up to ± 20 percent were measured. The limitations imposed in both tests were mainly economic in that better data requires either much more instrumentation or much longer test times. It is concluded that the Raman scattering technique can be used to gather most data required in gaseous combustion flows, provided funds are available. Emphasis is currently being placed on improvements in equipment, such as the use of image intensifiers to obtain profile data and Fabry-Perot etalons for higher throughput than can be obtained using spectrometers.

Nonlinear Raman excitation techniques, such as Coherent Anti-Stokes Raman Spectroscopy (CARS),²⁶ are still in the development stage and were not considered in this assessment.

3.1.1.4 High Resolution Spectroscopy (Appendix B-5).

Molecules which have a well defined vibrational-rotational line structure, such as CO or HF, are approachable either in emission or absorption by analysis of the resolved line structure. HF has been used successfully as a tracer gas for mixing studies by absorption spectroscopy.²⁷ The application to rocket gases using conventional high resolution spectroscopy is discussed in Reference 28, where a high resolution CO spectrum from a rocket

exhaust is shown, and the criteria for diagnostics of CO are defined. The application of tunable lasers to make high resolution absorption measurements in flames is also a very attractive technique.²⁹ The difficulty with the high resolution method is increased over the IR band model method by the necessity to solve the inversion problem for the radiative transfer on a line by line basis. However, the end result using resolved lines will have a higher confidence level than for the band model because the physics is much better defined. The conventional spectroscopy is straightforward, and no substantial barriers to application are anticipated for molecules having a resolvable line structure.

3.1.1.5 Electron Beam Fluorescence (Appendix B-6).

Electron-beam excitation of fluorescent radiation can be used to provide a measure of the distribution function for several molecules and atoms of interest in far field rocket plumes under high altitude simulation conditions. The technique is useful in a direct sense for gas number densities of about 10^{13} cm^{-3} (the signal sensitivity limit) to about 10^{16} cm^{-3} (upper limit governed by quenching collisions). A typical example is given by the application to chemical laser type flows³⁰ in which species concentration measurements in the mixing region between adjacent jets were made. The latter measurements also demonstrated the problems which can arise when proper attention is not given to the complex energy transfer and quenching reactions that may occur. The technique has been used with considerable success in low density expansions of gases in which the condensation properties were being studied.³¹

3.1.1.6 Resonance Fluorescence (Appendix B-7).

In the resonance absorption technique, the transmittance of source radiation tuned to the resonance of the absorbing media is measured. The source may be a gas discharge tube containing the same gas for which absorption measurements are desired, or it may be a tunable laser. The excited state which

results from absorption of a photon will either relax by emission of a photon (fluorescence) or by collision with other atoms or molecules (quenching). If the quenching rate is low, the emitted radiation may be analyzed in much the same way as E-beam excited fluorescence. However, the cross section for E-beam excitation is larger than for fluorescence so that no advantage is generally gained by using fluorescence in the density range below which quenching is a problem. However, it was recently pointed out by Daily³² that in the limit of a large amount of quenching, the need for detailed knowledge of quenching cross section disappears, and the technique may be used for several species including the alkali metals. The method, which employs a tunable laser in the UV or Visible, is then known as "saturated fluorescence." A successful extension of the method as outlined by Daily was made to C_2 in flames in which saturation could not be obtained, by noting the linear dependence of the fluorescence on the source power.³³ The technique appears to have potential for use in rocket combustion flows containing a considerable amount of free carbon.

3.1.2 Assessment of Gas Phase Only Diagnostics.

From consideration of the "needs" for liquid propellant rocket combustion flow measurements (Section 2.1) and the techniques that are available to make such measurements (Table 2), it is concluded that:

- (1) Existing techniques are adequate, in principle, to meet currently anticipated measurement needs.
- (2) Refinements in hardware, data handling software, and uncertainty analysis will continue to require attention.

In other words, it is concluded that basic research on new techniques for gas (only) flows is not required, while continued development is required to make measurements more economical either from the hardware or test complexity standpoint, and to improve sensitivity, accuracy and confidence level of the measurements.

A discussion of the cost of making a measurement seems to be in order. A rough attempt to classify the techniques according to the cost of making one radial profile measurement of the density and temperature of a specie at nozzle exit conditions is given in Table 3. Note, however, that there is little overlap in species which can be measured by more than one technique; i.e., H_2O can only be measured by IR E/A, CO_2 can be measured by IR E/A or Raman, CO can be measured by either Raman or high resolution, N_2 can only be measured by Raman, etc. Thus, total reliance on only one technique for an application is not always possible.

3.2 Techniques for Gas/Particle Flows.

3.2.1 Assessment of Gas/Particle Flow Diagnostics.

A survey of diagnostic applications to the gas/particle flows produced by solid propellant combustion revealed no successful application of either particle or gas phase techniques. Much research on particle diagnostics by optical methods in simpler flow regimes (flames, wind tunnels, etc.) is in progress, but the only attempts at application to solid rocket plumes have been unsuccessful. Such attempts include Laser Doppler Velocimetry for velocity³⁶ and holography for particle size.³⁷ Attempts at using the IR E/A technique for gas phase diagnostics at the exit of a solid propellant motor nozzle likewise met with failure,³⁸ and interpretation of spectral emission data in terms of particle temperature has also been unsuccessful.³⁸ Therefore, it can be concluded from the outset that existing techniques are inadequate to meet the needs for measurements in the gas/particle flows of solid rocket motors.

Interest in gas/particle flows does not arise solely from solid propellant rockets but also from problems encountered with such processes as coal fired turbine and magnetohydrodynamic power generation.³⁻⁵ However, no actual diagnostic measurements have been reported--only studies to identify approaches. It is instructive to list the approaches utilized to date for in situ particle diagnostic measurements as given in Table 4. The most

TABLE 3. COST ANALYSIS FOR GAS PHASE COMBUSTION DIAGNOSTIC TECHNIQUES.

| <u>TECHNIQUE</u> | <u>SPECIES</u> | <u>TEMPERATURE</u> | <u>HARDWARE COST \$K</u> | <u>NUMBER OF 60 SECOND FIRINGS</u> |
|----------------------------------|---|--------------------|--------------------------|------------------------------------|
| IR Emission/Absorption | H ₂ O, CO ₂ | Yes | 12** | 1 |
| UV Resonance Absorption | OH, NO, CH, CN | No | 6** | 1 |
| Saturated Resonance Fluorescence | OH, K, Na, C ₂ | No | 60 | 10* |
| Raman Scattering | N ₂ , O ₂ , CO, CO ₂ , HF, HCl | Yes | 75 | 10* |
| High Resolution Spectroscopy | CO, HF, HCl | Yes | 50-100*** | 5-10*** |

*Use of imaging techniques can reduce the number of firings to a single firing but with about 15K increase in hardware cost.

**Use of multielement detector arrays can reduce the 60 second firings to less than 10 seconds but with increased hardware cost by approximately the number of detectors times the base cost.

***Cost and number of firings depends upon whether a tunable laser or a high resolution spectrometer is used.

TABLE 4. OPTICAL DIAGNOSTIC TECHNIQUES FOR PARTICLE MEASUREMENTS.

| <u>TECHNIQUE</u> | <u>MEASUREMENTS POSSIBLE</u> | <u>RANGES OF APPLICATION</u> | <u>REFERENCES</u> |
|--------------------------------------|-------------------------------|---|-------------------|
| Holography | Size distribution Velocity | $d > 2\mu\text{m}$ $v < 200 \text{ m/sec}$ | 39-41 |
| Laser-Doppler Velocimetry | Size distribution Velocity | $0.5\mu\text{m} < d < 15\mu\text{m}$ | 42-45 |
| Diffusion Correlated Spectroscopy | Average size | $d < 1\mu\text{m}$ | 46-50 |
| Mie Angular Scattering | Size distribution | $0.2\mu\text{m} < d < 10\mu\text{m}$ | 51-52 |

significant result of examining this list is that of the six properties of particles listed as "needed" in 2.2., only two (velocity and size distribution) are measurable by the optical scattering or interference techniques under development. The fact is that optical scattering techniques can give only size and velocity information since the scattering of an optical beam is influenced only by the scattering cross section (size) and the Doppler frequency shift (velocity). Other principles of physics must be employed to obtain information on composition, mass, and physical state. Moreover, the size range and the velocities expected in rocket exhausts are not fully addressed by the optical techniques. Thus, research is required to develop the particle diagnostics needed for rocket combustion flows. The research needed is a re-examination of the optical scattering techniques for geometrical size and velocity and an investigation of new approaches for mass, composition, physical state, and thermal properties.

3.2.2 Assessment of Optical Techniques for Particle Diagnostics.

Many investigators are currently engaged in development of laser scattering diagnostics for particle measurements, and it would be presumptuous of the writer to attempt to survey all this work. It will suffice here to make some appropriate comments regarding application of the various techniques to rocket flow problems. The basic principles of the methods are again outlined in Appendix B.

3.2.2.1 Holography (Appendix B-8).

In the strictest sense, holography does not meet the criteria laid out in Section 1 for a diagnostic -- it is a direct measurement. But, because it is a very useful in situ tool with wide application to combustion measurements, discussion of the technique is included here. What is listed in Table 4 as limitations on size and velocity represent approximate limits on optical resolution via the Rayleigh criteria,^{5,39,40} practical limits on particle identification for a 1 μ sec laser pulse separation, respectively.

The laser pulse width also has the effect of blurring the particle; for a 2μ particle moving at 200 m/sec a pulse width less than 10 nanosec is required to "freeze" the particle. These theoretical limits have been approached recently in a system being constructed for application to combustion bomb type experiments.⁴¹ Extension of holography to the velocities (μ -3000 m/sec) expected in the near field of rocket plumes and to particles having dimension less than $2\mu\text{m}$ is not likely. However, application to combustion studies and to the secondary smoke region (see Figure 1) of tactical missile plumes can provide very useful information.

3.2.2.2 Laser Doppler Velocimetry (LDV) (Appendix B-9).

In the most recent approaches to LDV measurements, velocity and particle size are obtained by interpreting the fine structure of the scattered heterodyne signal from the interference pattern of a probe volume formed by two intersecting laser beams (see Appendix B-9). The velocity is determined by the frequency of the scattering signal and the particle size by the "visibility" or shape of the wave pattern.⁴²⁻⁴⁴ Two serious limitations arise in application of LDV to rocket exhausts. First, electronic signal processors are limited to frequencies less than about 100 MHz, which, in turn, places an upper limit of about 1.5 km/sec on velocity⁴³ (see Appendix B-9). Nozzle exit and near field rocket exhaust velocities range up to about 3 km/sec. (Frequency detection to much higher frequencies is possible using Fabry-Perot interferometers, but the practical difficulties associated with use of these devices and inherent resolution limits negates their use.⁴³) Second, the large particle loading of solid propellant motor exhausts makes penetration of the flow field difficult, thus seriously reducing the number of usable scattering events for particle sizing and velocity measurement. The ultimate lower limit of measurable particle size using this technique is reached when the "visibility" (integral of the pulse shape) does not change appreciably with decrease of particle size. A practical lower limit of about the wavelength of the illuminating laser results from this criteria.⁴⁵ The upper limit on size is governed by the double

value of the Fraunhofer diffraction function; for a typical system, the upper limit is about 15 μm . Other limitations of the technique are due to distortion of the signal pattern by nonhomogeneous particle velocity vectors and multiple scattering events. These limitations lead to the conclusion that LDV measurements in solid propellant combustion applications are restricted to phenomenological laboratory studies and far field smoke studies.

3.2.2.3 Diffusion Correlated Spectroscopy (Appendix B-10).

A technique that has been recognized by only a few investigators⁴⁶⁻⁴⁸ makes use of the influence on the homodyne scattering spectrum from an LDV system of the correlation of positions of particles undergoing Brownian motion in a gas. The technique has been identified as "Laser Doppler Spectroscopy" by Hinds and Reist,⁴⁶ but use of this name is misleading since it is not the Doppler effect which determines the line shape but the fluctuation in the scattered signal received on a detector caused by changes in the phase factor with time as a particle moves via its Brownian motion. The combination of all the scattering signals received by the detector from the illuminated field results in a cancellation from noncorrelated, independent particles, but signals from the same particle are correlated and thus give a finite correlation function. If the illuminated field is uniform and use is made of the probability of finding a particle whose motion is governed by diffusion at some position, then the resulting homodyne power spectrum will be given by a Lorentzian line shape. If the illumination field is not uniform, then the signal will be convoluted with the intensity variation across the field; for a Gaussian distribution of intensity (i.e., the usual distribution for a single mode gaseous laser beam), the result of the convolution will be a Voigt profile.⁴⁸ The result of a measurement of the line profile halfwidth in a monodisperse aerosol medium is to determine the diffusion coefficient, which is then uniquely related to particle size. For a polydisperse aerosol, the halfwidth measurement gives an "average" particle size. It appears that the theory can be manipulated to give a

distribution of particle sizes from multiple measurements at several angles, but no serious effort has yet been made to accomplish this.

The potential of this technique has only been scratched, with measurements reported only for laboratory flames.⁴⁷ The lack of application of the technique probably stems from a lack of understanding of the principles involved since, by the above discussion and the literature cited, it is clear that the mathematical physics leading to the final result is quite complex. Nevertheless, the experiment is very straightforward (see Appendix B-10) and yields much information. Some work conducted recently⁴⁹ has contributed to more confidence in the method in that comparison of the average particle size determined from the homodyne power spectral halfwidth with that obtained from electron microscope photographs of samples from an acetylene flame were in reasonable agreement.

The major limitation of the method for rocket exhausts appears to be imposed by the velocity; that is, a particle must remain in the illuminated field long enough for the correlation to be established. Penner, Bernard, and Chang⁵⁰ have estimated this minimum time to be about 10^{-5} sec; thus, for a stream velocity of 1000 m/sec, the diameter of the illumination beam should be about 1 cm. In turn, this sort of requirement necessitates very high power lasers in order to obtain good signal-to-noise ratio.

From the above discussion, it is concluded that additional research on the Diffusion Correlated Spectroscopic Technique is warranted in order to determine its usefulness in rocket propulsion applications.

3.2.2.4 Mie Angular Scattering (Appendix B-11).

The dependence of the measured scattering intensity at a given azimuth, with respect to the direction of an incident laser beam on particle size and index of refraction of the medium, is used in this technique. Measurements are made at a number of scattering angles to form a measurement vector. The measurement vector can be equated to a matrix of angle and size dependent

scattering function times a size vector. The inversion of the scattering matrix then yields a particle size distribution if the index of refraction is known.⁵¹⁻⁵² Presumably, the technique can also yield effective indices of refraction if some other measurement, say polarization ratio, is also measured. The technique has not been thoroughly demonstrated with experimental data, but since it is based upon first principle physics, it should be a very powerful technique. Limitations for rocket flows include

- (1) Lack of index of refraction data for particles at the temperatures of interest; bulk material data is not adequate.
- (2) Lack of sensitivity of the angular dependence of the Mie scattering function on particle size d in both the lower ($d < 0.25\lambda$) and upper ($d > 10\lambda$) size ranges, where λ is the wavelength of the incident laser beam.
- (3) Only single scattering data can be inverted successfully so that the technique is limited to flows with particle loadings sufficiently small that multiple scattering effects are negligible. A quantitative value of particle density which bounds this limitation is not available.

3.2.3 Assessment of Gas Phase Diagnostics in Gas/Particle Flows.

Very little can be said about the success or the limitations of the spectroscopic techniques discussed in 3.1 (for clean gas flows) when applied to gas/particle flows. Clearly, if the radiation, absorption, and/or scattering by particles does not appreciably distort the emitted, transmitted, and/or scattered radiation from the gas species, then the techniques discussed in 3.1 may be applied. This situation may exist for flows with low particle loading such as may be found in the exhausts of "smokeless" type solid rocket propellants, but experiments to determine the extent of the interference for such propellants have not yet been

carried out. Some possible sources of interference between gas phase diagnostics and particles that can be foreseen are listed as follows:

- (1) Radiation from hot gases may be much smaller than from particles so that gas radiation cannot be detected. (This situation was encountered at the exit of a highly aluminized, second stage rocket motor.)³⁸
- (2) Absorption and scattering by particles may be so great that no source radiation is transmitted through the gas/particle flow, i.e., total extinction.³⁸
- (3) The scattered radiation from a laser beam may be multiply scattered so that the integrity of the signal at the detector is lost; i.e., the detector receives contributions due to scattering by particles all along the beam so that the source of the detected radiation is not localized.
- (4) An incident laser beam may be absorbed by the particles, raising their temperature and producing thermal radiation which contributes to the background noise for Raman or fluorescence detection. (This is the situation reported by Eckberth for Raman measurements in sooty flames.)⁴

The above list of possible problems is not exhaustive, but it seems clear that not enough is currently known about how to avoid or account for the interferences of signal detection due to particles to make gas diagnostic measurements in highly loaded gas/particle flows with any degree of confidence. Experimental investigation in simulated gas/particle flows is warranted. Such investigation should at least include determination of particle loading and size bounds under which the various gas diagnostics will not be affected by interference caused by particle effects.

4. ADVANCED TECHNIQUES.

This section is devoted to examination of techniques having the inherent capability for measurement of those properties of combustion products for which no measurement techniques currently exist, such as particle composition, mass, state, and temperature. Since optical scattering can at the most give particle size, velocity, and index of refraction information, it is concluded that other physical principles must be exploited to provide the other particle properties. For gas phase properties, the spectroscopic methods discussed in 3.1 contain the necessary information, but distortions of the spectral data due to multiple scattering and particle radiation and absorption may destroy the integrity of the methods. Approaches to both the problems of particle and gas phase diagnostics will be discussed in the following paragraphs.

4.1 Particle Composition and Mass, X-Ray Methods.

The specificity of X-ray spectroscopy in identifying and counting atoms in the solid state is immediately obvious from the inherent X-ray physics.⁵³⁻⁵⁴ An incident X-ray beam at energy e_i into a field of particles containing atoms having an absorption edge with energy $e_j^!$ less than e_i will be absorbed by those atoms and some of them will re-emit (fluoresce) at an energy e_j just less than the absorption edge energy. The energy $e_j^!$ or e_j (or wavelengths $\lambda_j^!$ and λ_j) identifies the atom, and the number of X-ray photons emitted (or absorbed) is a measure of the number density of j-type atoms, n_j (see Figure 4). Thus, in principle, a method has been identified for particle composition and mass measurement. However, the feasibility of actually utilizing such a method requires considerable investigation. The results of a paper study on the feasibility of the use of X-ray spectroscopy for gas/particle flow diagnostics is reported elsewhere.⁵⁵

Three possible X-ray measurement approaches are:

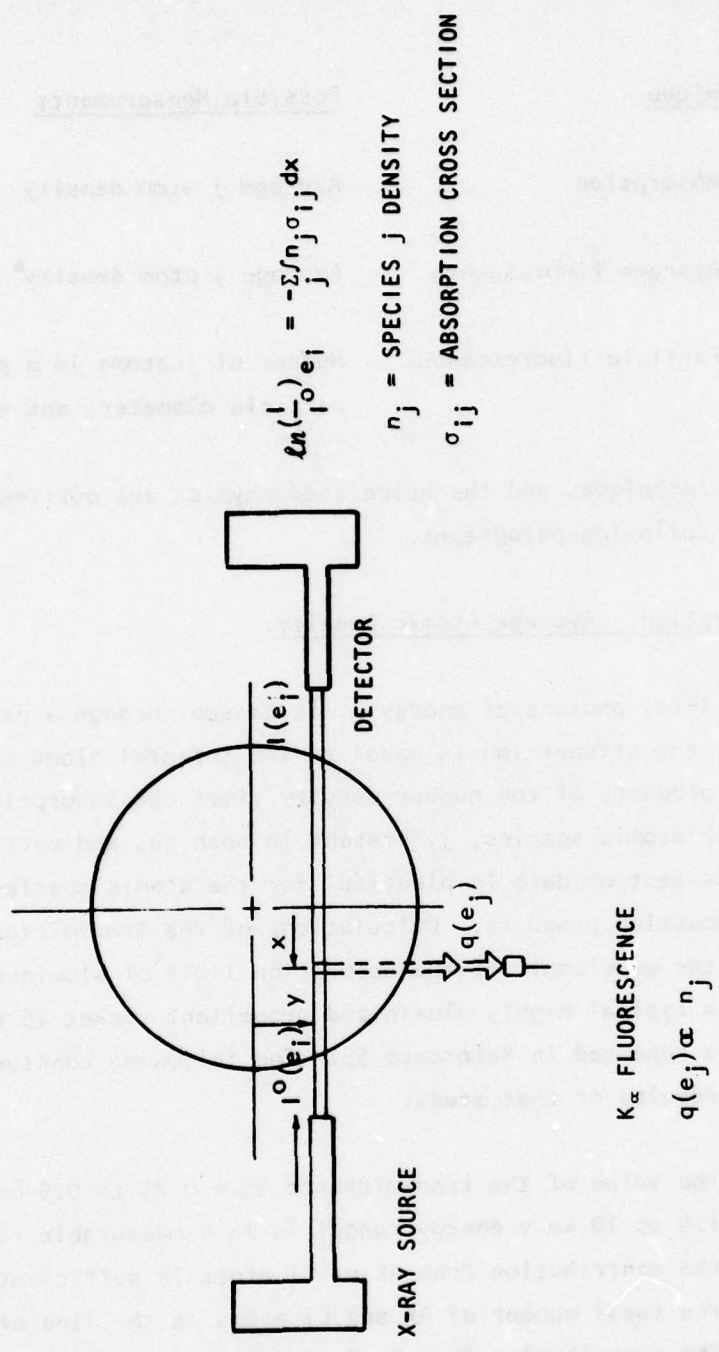


Figure 4. Illustration of X-Ray Spectroscopic Technique.

| <u>Technique</u> | <u>Possible Measurements</u> |
|--------------------------|--|
| 1. Absorption | Average j atom density |
| 2. Average fluorescence | Average j atom density |
| 3. Particle fluorescence | Number of j atoms in a particle, particle diameter, and velocity |

The envisioned techniques and the associated physics are outlined very briefly in the following paragraphs.

4.1.1 Absorption - Average Atomic Density.

When a beam of X-ray photons of energy e_j is passed through a particle-laden gas flow, the attenuation is equal to the integral along the path of the sum of the products of the number density times the absorption cross section for each atomic species, j, present in both gas and particles. Absorption cross section data is plentiful for the atomic species of interest in combustion products. Calculations of the transmittance of radiation near the wavelength of the absorption limit of aluminum through the exhaust of a typical highly aluminized propellant rocket (5 cm dia nozzle exit) are reported in Reference 55. The following conclusions were drawn from the results of that study.

- (1) The value of the transmittance ($\tau = 0.25$ to 0.9 over the 1.4 to 10 ke v energy range) is in a measurable range, and the contribution from Al or Cl atoms is sufficient to measure the total number of Al and Cl atoms in the line of sight. The contribution from C, N, and O elements to the absorption must be known, however, in order to uniquely determine the Al and Cl content; or sufficient measurements at different wavelengths must be made to invert the matrix and thus determine the number density of each contributing atom.

- (2) The contribution to the absorptance by O and N atoms makes it necessary that the X-ray path external to the rocket flow be purged by some low absorption gas, say helium.
- (3) The Beer's law form of the equation for the X-ray absorption is amenable to Abel inversion so that local, average density can be determined for axisymmetric flows from the measured transmittance profiles. The three-dimensional inversion techniques for X-ray absorption as used by the medical profession⁵² also appear to be adaptable for nonaxisymmetric cases.

The above conclusions drawn from Reference 51 provide sufficient justification to conduct an experimental demonstration study of the X-ray absorption techniques with consideration of available equipment and definition of rocket test scenarios. It should be emphasized that this technique can only yield an average atomic density, not direct information about particles. However, if the Al is contained in the Al_2O_3 particles as believed by most combustion experts, then a measure of the local average density distribution can yield much information about the validity of the gas-dynamic treatment of two-phase flows and the assumed particle size distributions which are input to the models.

4.1.2 Time Averaged Fluorescence - Space Averaged Atomic Density.

Many of the problems associated with the X-ray absorption measurement (i.e., interferences from other elements, inversion to obtain local values, etc.) are avoided if the characteristic fluorescent radiation at the $K\alpha$ energy of the specie of interest can be measured. An array of detectors tuned to the energy e_j can then be used to obtain local values of the atomic number density. The main problems with the fluorescence measurements are the determination of the local beam intensity and the absorption in the path between the X-ray beam and the detectors. The rates of Al and Cl K_α photon

emission at the axis of a typical rocket and the absorption along the path to the detector were calculated and are given in Reference 55. It was shown that the fluorescence measurement can be accomplished provided that X-ray sources having a flux on the order of 10^{12} photons/sec cm^2 are provided. Again, the theoretical calculations show sufficient merit that laboratory demonstration experiments are justified.

4.1.3 Particle Fluorescence - Number of Atoms in Particle, Velocity, Size.

The maximum yield of information about particles using X-ray fluorescence would come from the pulse of photons produced as a particle moves through the X-ray beam. Conceptually, the fluorescent event could yield information on the kind and number of atoms in the particle, the mass, the velocity, and the geometrical dimension (see Figure 5). However, the same sort of problems that are encountered in optical scattering (multiple scattering, finite illuminated volume, etc.) are encountered here, as well as the same absorption problem that accompanies the interpretation of average X-ray fluorescence measurements (4.1.2). The total possible number of $\text{Al K}\alpha$ photons emitted by a $1\mu \text{ Al}_2\text{O}_3$ particle traveling at 1000 m/sec during the crossing of a 1 mm wide X-ray beam (~ 1 m/sec) of X-ray photons at an energy just larger than the absorption edge is estimated to be 10^{-17} times the incident X-ray photon flux rate.⁵⁵ Some 30 percent of these will be absorbed in the path to the detector in the typical tactical rocket exhaust flow. The questions to be answered by a feasibility study are then, "Does there exist a source of X-rays of sufficient intensity to produce about 100 photons from the particle in the one more time interval?" "What are the detector requirements to record a pulse shape (or, less desirably, the integral over the pulse)?" "Does such a detector exist, and, if not, is such a detector possible?" Again, the potential of this method is sufficient great that laboratory investigation is justified.

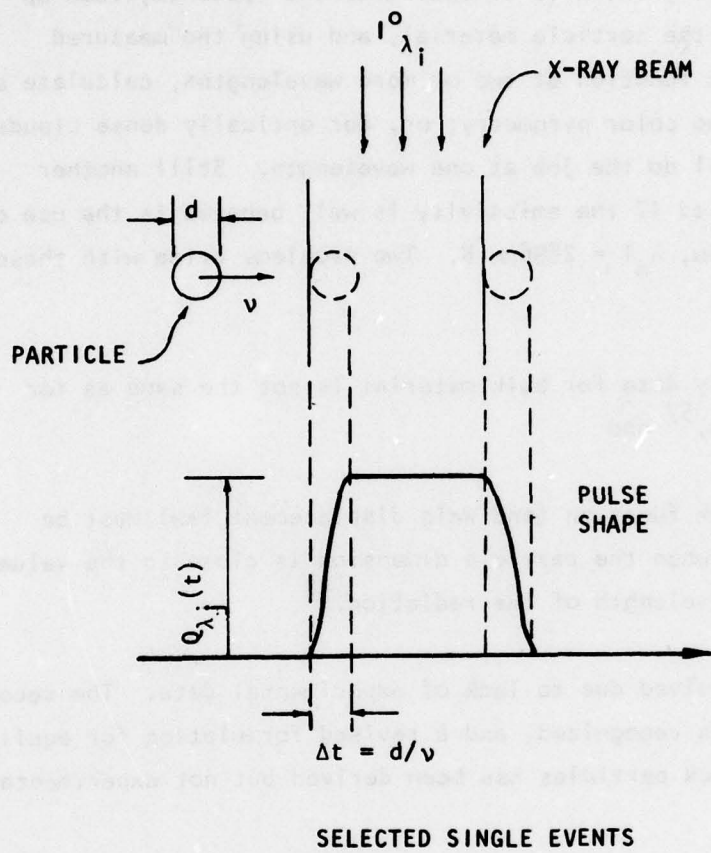


Figure 5. Scattering Event Chronology for a Particle Passing Through an X-Ray Beam.

4.2 Particle Temperature - Radiation/Absorption Properties.

The usual approach to the measurement of the temperature of a particle cloud that is not optically thick is to determine the spectrum, look up an emissivity value for the particle material, and using the measured radiation and the Planck function at two or more wavelengths, calculate a temperature. This is two color pyrometry; or, for optically dense clouds, an optical pyrometer will do the job at one wavelength. Still another approach which can be used if the emissivity is well behaved is the use of the Wein displacement law, $\lambda_m T = 2898 \mu\text{m}^\circ\text{K}$. Two problems arise with these approaches:

- (1) Emissivity data for bulk material is not the same as for particles,⁵⁷ and
- (2) the Planck function (and Wein displacement law) must be modified when the particle dimension is close to the value of the wavelength of the radiation.⁵⁸

The first problem is unsolved due to lack of experimental data. The second problem has recently been recognized, and a revised formulation for equilibrium radiation from black particles has been derived but not experimentally verified.⁵⁹

Thus, two very important areas of research are identified, and measurement of particle temperature must await solution of these problems.

Stated very briefly, the revision of the Planck Black Body Law for particles of dimension close to the wavelength of interest can be expressed (to first order) in the form of a correction term. For spherical particles, the revised function $N_{bb}(\lambda, T, d)$ is dependent upon wavelength λ , temperature T , and the particle diameter d , and is related to the Planck function $N_{BB}(\lambda, T)$ through the expression⁵⁹

$$\frac{N_{bb}(\lambda, T, d)}{N_{BB}(\lambda, T)} = \left(1 - \frac{\lambda^2}{2\pi^2 d^2}\right)$$

where λ cannot be greater than $\sqrt{2} \pi d$. Figure 6 gives a typical result for 1000°K particles over a range of particle sizes. The result is quite striking and obviously affects the determination of temperature from the spectral shape of the radiation from particles or the Wein displacement law. The portion of the spectrum at wavelengths less than about the diameter of the particle are not appreciably altered, however, and the temperature of the particles may then still be obtained by the Planck function. Experimental verification of the revised radiation law is sorely needed.

The work by Dowling and Randall⁵⁷ addresses the measurement of small particle radiation, but results have not yet been forthcoming. In their experiment, the radiation from a single particle trapped in the focal region of two laser beams is sought. The validity of the revised radiation expressions can be tested by the dependence of the radiation spectrum on different size particles using their experiment. A prerequisite to measurement of temperature of particles is resolution of the particle radiation law and the emissivity problems. If the experiment by Randall, et. al., does not yield information, then experiments using particle clouds with all the incumbent problems of particle coagulation are necessary in order to develop an in situ measurement technique for particle temperature.

4.3 Particle State - Liquid or Solid.

Evidence exists to show that Al_2O_3 particles are in the liquid state over at least a part of their trajectory in a rocket motor.⁶⁰ This conclusion can be drawn in two ways. First, the temperature within the motor and through the initial expansion in the nozzle is much greater than the melting temperature of Al_2O_3 (i.e., about 2200°K). Second, experimental evidence in the residue on nozzle walls and in the construction of the larger particles that are collected after a firing points to a prior liquid state.

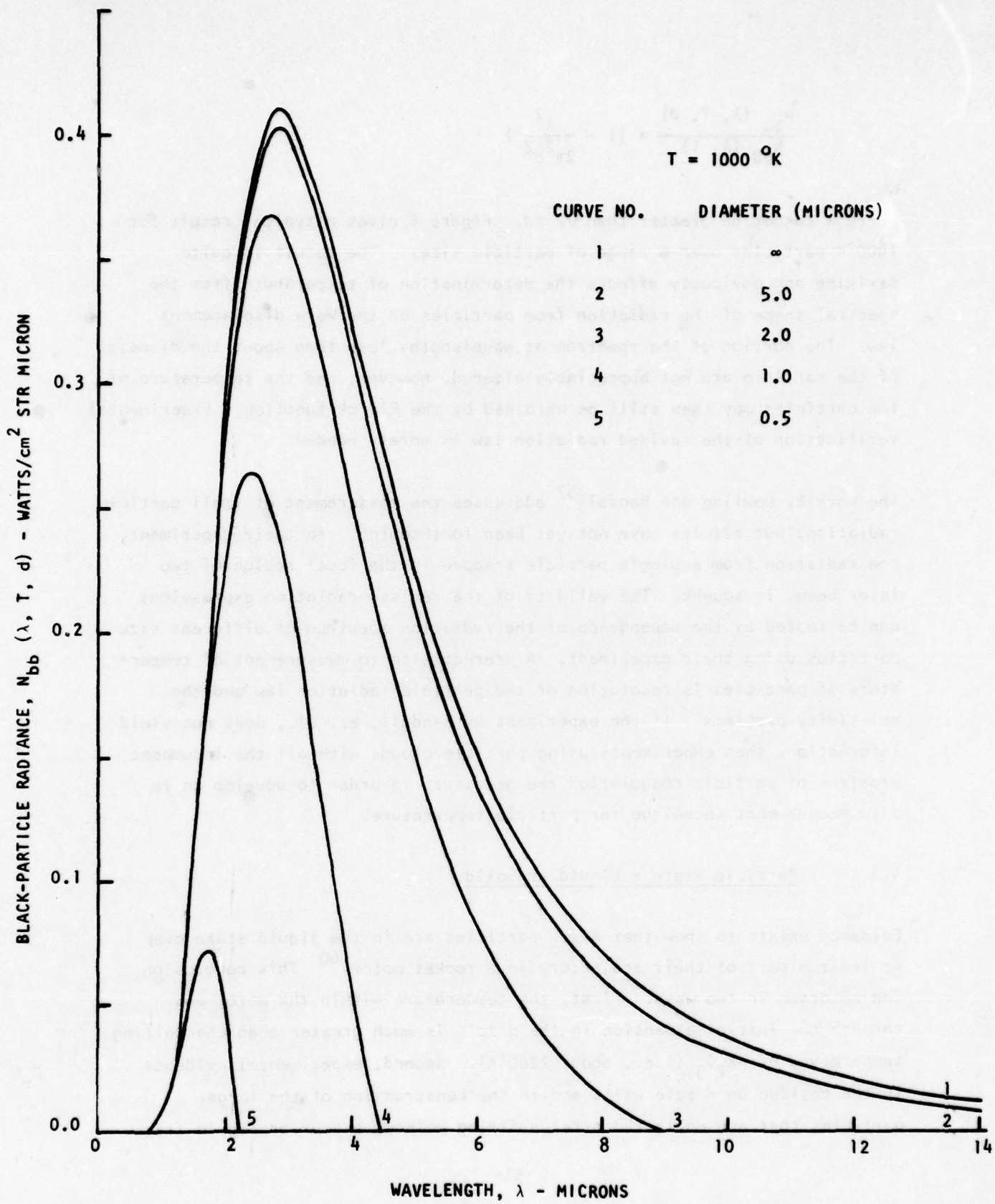


Figure 6. Spectral Radiance of Particles.

But the information sought for use in performance models is the location in the nozzle where the state change takes place. If a diagnostic were available, the information could presumably be obtained by a series of tests using different nozzle expansion ratios.

One principle that can be cited as a possible diagnostic is the expected change of refractive index as the particle changes state, which should be evidenced in the spectral radiation characteristics through the apparent emissivity or in the Mie scattering characteristics. In either case, insufficient information exists to propose a diagnostic, and, again, research is needed on the radiation characteristics of particulate matter.

4.4 Gas Properties - Spectroscopic Methods.

All the techniques discussed in 3.1 have the potential of being successful in gas/particle flows under particle loading conditions in which the effect of particles on the gas induced radiation are minimal. It remains to determine the conditions under which a given technique can be used, by both modeling the process and conducting laboratory experiments. A suggested research plan is then very straightforward:

- (1) Model the radiation-particle interaction to predict the effects of scattering and particle radiation and absorption on the emitted, transmitted, or scattered radiation of interest.
- (2) Under controlled conditions of both gas and particle properties, conduct experiments to provide confidence in the model predictions and to obtain experience with the interferences on signals resulting from particles in the flow.
- (3) From the results of steps 1 and 2, determine optimum diagnostic techniques to use for different types of particulates and different size and density ranges.

It is recognized that the recommended approach presented above is not a very glamorous one, but no devious schemes to avoid particle interferences have so far come to mind. Perhaps the straightforward attack suggested will serve to inspire ingenuity.

Considering the spectroscopic methods available, the following specific comments can be made.

- (1) The low signal levels encountered in Raman scattering make this technique very susceptible to background emission. Mie scattering from particles is several orders of magnitude greater than Raman scattering from molecules and presents a serious background problem. Also, the experience of Eckberth et. al.,⁴ with laser heating of the particles tends to make the technique even more questionable for hot gas/particle flows. Eckberth⁴ concluded that resonant enhanced methods such as Coherent Antistokes Raman Scattering (CARS) in which much larger signal levels can be expected, should be used. However, the nonlinear dependence on both beam intensity and molecular density have discouraged this writer from serious consideration of CARS for solid rocket propulsion applications (see also Reference 61).
- (2) Methods which require absorption measurement are susceptible to error in that the particle contribution to absorption and scattering must be taken into account. Moreover, beam definition becomes problematical for high particle laden flows.
- (3) Saturated fluorescence methods appear promising, with the main problem being that of localizing the observation point to reduce effects of multiple scattering.

- (4) Most solid propellants contain traces of sodium and potassium impurities. Because of the low ionization potential of these alkali atoms, ionization and emission of radiation from upper excited electronic status occur. If the spectra from the upper excited states of alkali metals is observable, the temperature, the electron concentration, and the alkali atom density can be determined from emission measurements.

5. CONCLUSIONS.

The study reported herein has considered the needs for measurement of properties of combustion products in rocket motors and exhaust plumes.

The conclusions reached during the study are listed as follows:

- (1) The needed measurements for rocket combustion serve mostly as inputs and validation data for propulsion system performance evaluation, internal models of combustion and nozzle expansion processes, and prediction models for plume observables (e.g., IR radiation, plume visibility, radar cross sections). The desired measurements include gas temperature and major species concentration, and the temperature, size, mass, composition, state and velocity of particles in flows ranging from 3500°K - 40 atm rocket chamber conditions to the low density high altitude plumes at ambient temperature and densities.
- (2) For the case of purely gaseous flows from modern liquid propellant rockets, the currently existing spectroscopic techniques of measurement (including high and low resolution spectroscopy, resonance absorption, fluorescence, electron beam fluorescence, and laser Raman scattering) were found to be adequate, in principle, to meet rocket propulsion system needs. Refinements in the form of instrumentation improvement, data treatment, and sensitivity and uncertainty analysis will be required on a continuous basis to meet increased accuracies required in the validation of models, and the need for more accurate fundamental data on molecular parameter, cross section, etc., is ever present.
- (3) For the case of the combined gas/particle flows from solid propellant combustion, current techniques for measurement of particle properties were found to be inadequate, and

techniques for measurement of gas properties in the presence of particles were found to be largely untried. Optical techniques for particle diagnostics address only the particle size and velocity problems, and other principles must be employed to measure composition, mass, state and temperature. Gas phase methods suffer from interferences caused by background emission from particles, multiple scattering which destroys the geometrical integrity of the data, and severe attenuation and dispersion of source beams.

- (4) X-ray spectroscopy appears promising for measurement of particle composition and mass properties. Absorption and/or average fluorescence are feasible for measurement of Al or Cl local atomic densities and possibly can provide measurement of O, N, and C densities. From these measurements and a suitable model, particle mass distributions can be inferred. Individual particle fluorescent scattering events are a possibility for direct measurement of particle atom content and velocity. Further feasibility analysis on all X-ray methods to define instrumentation requirements and data analysis is required, to be followed by proof of principle experiments.
- (5) Only emitted or absorbed spectrally-resolved radiation can be used to measure the temperature of particles. The emissivity and radiation law for particles is dependent upon the particle size when the size is near that of the wavelength of the radiation. Expressions derived for "black particle" radiation based upon calculation of the eigenstate density for small particles and employing Bose-Einstein quantum statistics must be validated by experiment, and particle emissivities for the materials of interest must be measured before further progress can be made toward particle temperature measurement.

(6) A systematic modeling and experimental program is required to investigate spectroscopic techniques for gas property measurement in the presence of particles. The methods of fluorescent scattering and alkali metal emission appear to offer the best possibilities and should be investigated first.

REFERENCES

1. Goulard, R., Mellor, A. M., and Bilger, R. W., "Combustion Measurements in Air Breathing Propulsion Engines. Survey and Research Needs," Combustion Science and Technology, Vol. 14, pp. 195-219, 1976.
2. Goulard, R., "Optical Measurement of Thermodynamic Properties in Flow Fields," AGARD-CP-193 on Applications of Non-Intrusive Instrumentation in Fluid Flow Research, May 1976.
3. Self, S. A. and Kruger, C. H., "Diagnostic Methods in Combustion MHD Flows," Journal of Energy, Vol. 1, pp. 25-43, 1977.
4. Eckberth, A. C., Bonczyk, P. A., and Verdick, J. F., "Review of Laser Raman and Fluorescence Techniques for Practical Combustion Diagnostics," United Technologies Research Center R77-952665-6, Feb. 1977.
5. Coleman, H. W., Hardesty, D. R., et al, "Diagnostics Assessment for Advanced Power Systems," Sandia-Livermore Laboratories 77-8216, Mar. 1977.
6. Briel, S. A., Ed., Proceedings of TTCP Rocket Plume Technology Working Group Meeting, Naval Weapons Center, China Lake, CA, Mar. 1972.
7. Stewart, J. D., AFRPL/OSR Workshop on Rocket Related Diagnostics, SAMSO Hdq., El Segundo, CA, Mar. 1976.
8. Zinn, B. T., Ed., "Experimental Diagnostics in Gas Phase Combustion Systems," Progress in Astronautics and Aeronautics, Vol. 53, AIAA Press, 1977.
9. Hoshizaki, H., Chou, Y. S., Meyer, J. W., Wilson, K. H., and Thomas, P. D., "Plume Visibility Detection Study," JANNAF 10th Plume Technology Meeting, Naval Oceans Systems Center, San Diego, CA, 13-15 Sep. 1977.
10. Combs, L. P., "DER Computer Program Documentation and User's Guide-Vol. 1," Rocketdyne, a Div. of North American Rockwell Corp., Canoga Park, CA, 15 Dec 1971; Rev. 1, Jan. 1974.
11. Boynton, F. P., Ludwig, C. B., and Thompson, A., "Radiative Properties of Carbon Particles Produced by a Rocket Motor," AIAA Journal, Vol. 6, pp. 865-1968.
12. Dawborn, R. and Kinslow, M., "Studies of the Exhaust Products from Solid Propellant Rocket Motors," AEDC-TR-76-49, Arnold Engineering Development Center, TN, Sep. 1976.
13. Brewer, L. E. and Limbaugh, C. C., "Infrared Band Model Technique for Combustion Diagnostics," Applied Optics, Vol. 11, pp. 1200-1204, 1972.

REFERENCES

14. Nelius, M. A., Darlington, C. R., et al, "Exhaust Plume Gas Dynamic and Radiation Measurements on a 500 lb_f Thrust Liquid Rocket Engine at Simulated Flight Conditions," AEDC-TR-44, Arnold Engineering Development Center, TN, Dec. 1977.
15. McGregor, W. K., Brewer, L. E., Darlington, C. R., Kiech, E. L., and Nelius, M. A., "Rocket Engine Injector Induced Exit Plane Property Distribution Diagnosed by Infrared Emission/Absorption," JANNAF 10th Plume Technology Meeting, Naval Ocean Systems Center, San Diego, CA, 13-15 Sep. 1977.
16. McRae, T. G., Ring, L. R., and Byrd, M. C., "Evaluation of Combustion/Nozzle Flow Codes with Titan III Transtage Nozzle Exit Measurements," JANNAF 10th Plume Technology Meeting, Naval Ocean Systems Center, San Diego, CA, 13-15 Sep. 1977.
17. Limbaugh, C. C., "An Uncertainty Propagation Analysis for an Infrared Band Model Technique for Combustion Gas Diagnostics," AEDC-TR-76-155, Arnold Engineering Development Center, TN, Apr. 1977.
18. Ring, L. R., "Evaluation of Combustion/Nozzle Gas Dynamic Models for Liquid Rocket Engine Applications," AFRPL-TR-77-46, July 1977.
19. McGregor, W. K., Seiber, B. L., and Few, J. D., "Concentration of OH and NO in YJ93-GE-3 Engine Exhaust Measured In Situ by Narrow Line UV Absorption," Proceedings of the Second Conference on the Climatic Impact Assessment Program, Cambridge, MA, Nov. 1972.
20. Few, J. D., McGregor, W. K., and Glassman, H. N., "Comparison of UV Absorption Measurements with Probe Sampling Measurements of Nitric Oxide Concentration in a Jet Engine Combustor Exhaust," AEDC-TR-76-134, Arnold Engineering Development Center, TN, Sep. 1976, and "Resonance Absorption Measurements of NO Concentration in Combustor Exhaust," pp. 187-204, Ref. 8.
21. Neer, Me. E. and Drewry, J. E., "Supersonic Combustion Flowfield Studies Using Absorption Spectroscopy," pp. 227-242, Ref. 8.
22. Cattalica, R., Robben, F., and Talbot, L., "The Interpretation of the Spectral Structure of Rayleigh Scattered Light from Combustion Gases," pp. 575-588, Ref. 8.
23. Williams, W. D., Powell, H. M., et al, "Emitted Radiation from Special Engines (ERASE)-Vol. III: Determination of Temperature and Species Number Density in the Exhaust Plume Utilizing Laser-Raman/Rayleigh Scattering," AEDC-TR-76-121, Arnold Engineering Development Center, TN, 1977.

REFERENCES

24. Lapp, M. and Penney, C. M. (Eds.), Laser Raman Gas Diagnostics, Plenum Press, New York, 1974.
25. Williams, W. D., Powell, H. M., et al, "Laser-Raman Diagnostics of Temperature and Number Density in the Mixing Region of a Rocket Engine Exhaust Plume and a Coflowing Air Stream," JANNAF 10th Plume Technology Meeting, Naval Ocean Systems Center, San Diego, CA, 13-15 Sep. 1977.
26. Harvey, A. B. and Byer, R. L., "Coherent Anti-Stokes Raman Spectroscopy," Applied Physics Letters, Vol. 25, pp. 387-390, Oct. 1974.
27. Malte, P. C. and Nicholls, J. A., "Turbulent Mixing in Invert and Combusting Flows Visualized by HF Tracer Absorption," Comb. Science and Technology, Vol. 5, pp. 299-311, 1972.
28. Krakow, B., Kiech, E. L., McAdoo, H. A., "Isolated CO Lines for Use in Combustion Diagnostics," AEDC-TR-77-11, Arnold Engineering Development Center, TN, Sep, 1977.
29. Hanson, R. K., Kuntz, P. A., and Kruger, C. H., "High-Resolution Spectroscopy of Combustion Gases Using a Tunable IR Diode Laser," Applied Optics, Vol. 16, pp. 2045-2048, 1977.
30. Whitfield, D. L., Lewis, J. W. L., and Williams, W. D., "Specie Number Density, Pitot Pressure, and Flow Visualization in the Near Field of Two Supersonic Nozzle Banks Used for Chemical Laser Systems," AEDC-TR-73-11, Arnold Engineering Development Center, TN, May 1973.
31. Lewis, J. W. L., Williams, W. D., Price, L. L., and Powell, H. M., "Nitrogen Condensation in a Sonic Orifice Expansion Flow," AEDC-TR-74-36, Arnold Engineering Development Center, TN, July 1974.
32. Daily, J. W., "Saturation Effects in Laser Induced Fluorescence Spectroscopy," Applied Optics, Vol. 16, pp. 568-571, 1977.
33. Baronavski, A. P., and McDonald, J. R., "Measurement of C₂ Concentrations in an Oxygen-Acetylene Flame: An Application of Saturation Spectroscopy," Jou. Chem Phys, Vol. 66, pp. 3300-3301, 1977.
34. Mazumber, M. K. and Kirsch, K. J., "Flow Tracing Fidelity of Scattering Aerosol in Laser Doppler Velocimetry," Applied Optics, Vol. 14, pp. 894-901, April 1975.
35. Hsieh, T., "Analysis of Velocity Measurements about a Hemisphere - Cylinder Using a Laser Velocimeter," Jou. of Spacecraft and Rockets, Vol. 14, pp. 280-283, May 1977.

REFERENCES

36. Morse, H. L., Barclay, J. T., Siefert, H. S., and Babcock, W., "Development of a Laser-Doppler Particle Sensor for the Measurement of Velocities in Rocket Exhausts," AIAA Paper No. 68-723, AIAA Fluid and Plasma Dynamics Conference, Los Angeles, CA, June 24-26, 1968.
37. Trollinger, J. D., Spectron Development Co., Costa Mesa, CA, 1977, Private Communication.
38. Brewer, L. E., Staats, G. E., and McGregor, W. K., "Exhaust Plume Spectral Radiance Measurements from Full-Scale Solid-Propellant and Model Gaseous-Propellant Rocket Motors," AEDC-TR-75-152, Arnold Engineering Development Center, TN, January 1976.
39. Trollinger, J. D., "Laser Instrumentation for Flow Field Diagnostics," AGARDograph No. 186, March 1974.
40. Vienot, C. J., "Holography," Laser Handbook-Vol. 2, North Holland Pub. Co., New York, p. 1487-1543, 1972.
41. Wuerker, R., Briones, R., and George, D. "Holography of Solid Propellant Combustion," AIAA Paper No. 77-977, AIAA/SAE 13th Propulsion Conference, Orlando, FL, July 11-13, 1977.
42. Farmer, W. M., "Measurements of Particle Size, Number Density, and Velocity Using a Laser Interferometer," Applied Optics, Vol. 11, p. 2603, 1972.
43. Stevenson, W. H., "Principles of Laser Velocimetry," Progress in Astronautics and Aeronautics, Vol. 53, Ed. B. T. Zinn, AIAA Press, p. 307, Ref. 8.
44. Duraao, D.F.G., and Whitelaw, J.H., "Critical Review of Laser Anemometry Measurements in Combusting Flows," Progress in Astronautics and Aeronautics, Vol. 53, Ed. B.T. Zinn, AIAA Press, p.357.
45. Bently, H. T., and Bomar, B. W., "Development of a Laser Velocimeter System for Flame Studies," AEDC-TR-76-150, Arnold Engineering Development Center, TN, June 1977.
46. Hinds, W., and Reist, P. C., "Aerosol Measurement by Laser Doppler Spectroscopy-I Theory and Results for Homogeneous Aerosols," Aerosol Science, Vol. 3, pp. 501-514, 1972; "II-Operational Limits, Effects of Polydispersity, and Application," Aerosol Science, Vol. 3, pp. 515-527, 1972.
47. Bernard, J.M., and Penner, S. S., "Determination of Particle Sizes in Flames from Scattered Laser Power Spectra," in AIAA Progress in Astronautics and Aeronautics, Vol. 53, Experimental Diagnostics in Gas Phase Combustion Systems, AIAA Press, pp. 411-420, 1977.
48. Penner, S. S., Bernard, J. M., and Jerskey, T., "Power Spectra Observed in Laser Scattering from Moving, Polydisperse Particle Systems in Flames-I. Theory," Acta Astronautica, Vol. 3. pp. 69-91, 1976.

REFERENCES

49. Driscoll, J. F., "Submicron Particle Size Measurements in Acetylene-Oxygen and Aluminum-Oxygen Flames," OSR Summer Faculty Research Program, Final Report, 26 Aug. 1977.
50. Penner, S. S., Bernard, J. M., and Chang, P. "Determination of Particle-Sizes (or Temperatures) Using the Power Spectra of Scattered Radiation from Pulsed Lasers," submitted to Acta Astronautica, Apr. 1977.
51. Chow, L. C. and Tien, C. L., "Inversion Techniques for Determining the Droplet Size Distribution in Clouds: Numerical Examination," Applied Optics, Vol. 15, pp. 378-383.
52. Lewis, J. W. L., Curry, B. P., and Weaver, D. P., "Determination of the Size Distribution Function for Particles in a Hypersonic Flowfield," AEDC-TR-77- , (to be published).
53. Bertin, E. P., Principles and Practices of X-Ray Spectrometric Analysis, Plenum Press, New York, 1971.
54. Woldseth, R., X-Ray Energy Spectrometry, Kevex Corp., Burlingame, CA, 1973.
55. McGregor, W. K., "X-Ray Spectroscopy as a Diagnostic Tool in Solid Propellant Combustion Flows," AFRPL-TR-78-61, May 1979.
56. Swindell, W., and Barrett, H. H., "Computerized Tomography: Taking Sectional X-Rays," Physics Today, Vol. 30, pp. 32-41, Dec. 1977.
57. Dowling, J. M. and Randall, C. M., "Infrared Emissivities of Micron-Sized Particles of C, MgO, Al₂O₃ and Zr O₂," AFRPL-TR-77-14 (Aerospace Corp. Contract Effort), Apr. 1977.
58. Baltes, H. P., "Planck's Radiation Law for Finite Cavities and Related Problems," Infrared Physics, Vol. 16, pp. 1-8, 1976.
59. McGregor, W. K., "On the Radiation From Small Particles," JQSRT, (to be published).
60. Geisler, R., Private Communication, Aug. 1977.
61. Tolles, W. M. and Turner, R. D., "A Comparative Analysis of the Analytical Capabilities of Coherent Anti-Stokes Raman Spectroscopy (CARS) Relative to Raman Scattering and Absorption Spectroscopy," Applied Spectroscopy, Vol. 31, pp. 96-103, 1977.

APPENDIX A. EQUILIBRIUM PROPERTIES OF COMBUSTION PRODUCTS FOR
SEVERAL TYPICAL ROCKET PROPELLANT COMBINATIONS.

This appendix contains results of one-dimensional, equilibrium calculations of rocket motor performance and species concentrations for propellants that are typical for propulsion systems for which measurements may be required. The computer code used was an unpublished code used by the AFRPL and is similar to that presented in CPIA publication #246, "JANNAF Rocket Engine Performance Prediction and Evaluation," April 1975.

TABLE A-1. O_2/H_2 .

| Expansion Ratio | <u>Chamber</u> | <u>6:1</u> | <u>25:1</u> | <u>40:1</u> |
|-----------------------------|----------------|----------------|-------------|-------------|
| I_{sp} (Sec) | 0.0 | 407.9 | 446.3 | 455.0 |
| Temperature ($^{\circ}K$) | 3107 | 1678 | 1109 | 959 |
| Species | | Mole Fractions | | |
| H | 0.024 | - | - | - |
| HO | 0.011 | - | - | - |
| H_2 | 0.419 | 0.433 | 0.433 | 0.433 |
| H_2O | 0.545 | 0.567 | 0.567 | 0.567 |

TABLE A-2. $LO_2/RP-1$.

| Expansion Ratio | <u>Chamber</u> | <u>6:1</u> | <u>25:1</u> | <u>40:1</u> |
|-----------------------------|----------------|----------------|-------------|-------------|
| I_{sp} (Sec) | | 310.2 | 342.7 | 350.5 |
| Temperature ($^{\circ}K$) | 3484 | 2170 | 1541 | 1378 |
| Species | | Mole Fractions | | |
| CO | 0.374 | 0.355 | 0.321 | 0.304 |
| CO | 0.109 | 0.151 | 0.187 | 0.204 |
| H | 0.035 | - | - | - |
| HO | 0.038 | 0.002 | - | - |
| H_2 | 0.130 | 0.154 | 0.190 | 0.207 |
| H_2O | 0.302 | 0.337 | 0.302 | 0.285 |
| O_2 | 0.006 | - | - | - |
| O | 0.006 | - | - | - |

TABLE A-3. N_2O_4/MMH .

| Expansion Ratio | Chamber | 6:1 | 25:1 | 40:1 |
|-----------------------------|----------------|-------|-------|-------|
| I_{sp} (Sec) | - | 273.3 | 328.5 | |
| Temperature ($^{\circ}K$) | 3241 | 1816 | 1241 | |
| Species | Mole Fractions | | | |
| CO | 0.110 | 0.098 | 0.071 | 0.067 |
| CO ₂ | 0.646 | 0.071 | 0.099 | 0.107 |
| H | 0.019 | - | - | - |
| OH | 0.022 | - | - | - |
| H ₂ | 0.120 | 0.134 | 9.162 | 0.177 |
| H ₂ O | 0.355 | 0.374 | 0.345 | 0.326 |
| NO | 0.013 | - | - | - |
| N ₂ | 0.313 | 0.323 | 0.323 | 0.323 |
| O ₂ | 0.002 | - | - | - |

TABLE A-4. $\text{ClF}_3/\text{B}_5\text{H}_9$.

| Expansion Ratio | <u>Chamber</u> | <u>6:1</u> | <u>25:1</u> | <u>40:1</u> |
|------------------------------------|----------------|------------|-------------|-------------|
| I_{sp} (Sec) | | 295.4 | 331.1 | 340.4 |
| Temperature ($^{\circ}\text{K}$) | 4320 | 3028 | 2618 | 2509 |
| Species | Mole Fractions | | | |
| BCL | .005 | .003 | .003 | .002 |
| BCLF | .008 | .006 | .004 | .004 |
| BCLF ₂ | .005 | .012 | .017 | .018 |
| BCL ₂ | .001 | - | - | - |
| BCL ₂ F | - | .001 | .002 | .002 |
| BF | .092 | .076 | .070 | .068 |
| BF ₂ | .180 | .190 | .188 | .173 |
| BF ₂ H | .002 | .002 | .002 | .002 |
| BF ₃ | .031 | .080 | .122 | .137 |
| CL | .160 | .100 | .066 | .057 |
| CLH | .111 | .212 | .255 | .281 |
| CL ₂ | .001 | - | - | - |
| F | .021 | .001 | - | - |
| FH | .287 | .271 | .239 | .228 |
| H | .096 | .043 | .032 | .028 |

TABLE A-5. $\text{ClF}_3/\text{AZ-50}$.

| Expansion Ratio | Chamber | 6:1 | 25:1 | 40:1 |
|------------------------------------|---------|--------|--------|--------|
| I_{sp} (Sec) | | 310.72 | 326.96 | 333.41 |
| Temperature ($^{\circ}\text{K}$) | 3527 | 1815 | 1359 | 1159 |

| Species | Mole Fractions | | | |
|------------------------|----------------|------|------|------|
| CLN | .001 | - | - | - |
| CF | .001 | - | - | - |
| CHN | .029 | - | - | - |
| CN | .003 | - | - | - |
| C_2H | .009 | - | - | - |
| C_2HCL | .011 | - | - | - |
| C_2H_2 | .008 | - | - | - |
| C_2N | .002 | - | - | - |
| LL | .051 | - | - | - |
| CLH | .131 | .179 | .179 | .179 |
| F | .004 | - | - | - |
| FH | .542 | .536 | .536 | .536 |
| H | .019 | - | - | - |
| H_2 | .032 | .037 | .037 | .037 |
| N_2 | .133 | .146 | .146 | .146 |
| C (Graphite) | .024 | .102 | .102 | .102 |

TABLE A-6. MINIMUM SMOKE SOLID.

| Expansion Ratio | Chamber | 1:1 | 3.7:1 |
|-----------------------------|----------------|-------|-------|
| I_{sp} (Sec) | | 98.5 | 201.3 |
| Temperature ($^{\circ}$ K) | 2323 | 2068 | 1240 |
| Pressure (Psia) | 1000 | 555 | 44.2 |
| Species | Mole Fractions | | |
| CO | 0.458 | 0.452 | 0.402 |
| CO ₂ | 0.083 | 0.089 | 0.138 |
| H ₂ | 0.175 | 0.181 | 0.231 |
| H ₂ O | 0.176 | 0.170 | 0.120 |
| N ₂ | 0.108 | 0.108 | 0.108 |

TABLE A-7. ALUMINIZED (18 PERCENT) SOLID.

| Expansion Ratio | <u>Chamber</u> | <u>1:1</u> | <u>7:1</u> | <u>15:1</u> | <u>23:1</u> |
|--------------------------------|----------------|------------|------------|-------------|-------------|
| I_{sp} (Sec) | - | 106.4 | 250.8 | 274.4 | 284.8 |
| Temperature ($^{\circ}$ K) | 3394 | 3175 | 2178 | 1849 | 1689 |
| Pressure (Psia) | 1750 | 1004 | 40.2 | 14.7 | 8.6 |
| Species | Mole Fractions | | | | |
| CO | 0.240 | 0.241 | 0.239 | 0.236 | 0.233 |
| CO ₂ | 0.013 | 0.013 | 0.0176 | 0.022 | 0.024 |
| H | 0.022 | 0.017 | - | - | - |
| H ₂ | 0.294 | 0.299 | 0.317 | 0.317 | 0.320 |
| H ₂ O | 0.125 | 0.124 | 0.120 | 0.115 | 0.112 |
| OH | 0.004 | 0.003 | - | - | - |
| N ₂ | 0.077 | 0.076 | 0.079 | 0.079 | 0.079 |
| Cl | 0.007 | 0.005 | 0.001 | - | - |
| HCl | 0.135 | 0.140 | 0.151 | 0.152 | 0.152 |
| AlCl ₂ | 0.002 | 0.001 | - | - | - |
| Al ₂ O ₃ | 0.073 | 0.075 | 0.076 | 0.076 | 0.076 |

APPENDIX B. BRIEF DESCRIPTION OF EXISTING DIAGNOSTIC TECHNIQUES
APPLICABLE TO ROCKET COMBUSTION AND PLUME MEASUREMENTS.

Introduction

The purpose of this appendix is to present in the briefest way the essential principles, assumptions, hardware, restrictions and limitations, and uncertainty estimates for the techniques that have been employed either for combustion related diagnostics or in similar fields. This material is included in the report for completeness and to support statements made in the main text. An example result of an application is given where possible. The examples given are either of test-oriented rocket applications or as closely related to the rocket measurement as possible. The choice of examples was somewhat arbitrarily made to illustrate the status of equipment development and the sophistication of the techniques according to published material, and the reader may have knowledge of better examples. References were chosen which, in the author's judgement, best describe the technique.

The principles of each technique are expressed mathematically wherever possible, calling attention to "first principle" determination of the desired properties from the measured variables. The equations have been condensed as much as deemed possible, and the reader is referred to the references for extensive detail. The restrictions and weaknesses listed stress the fundamental physics in most cases, believing that hardware development is mostly a matter of time and money.

The principal, descriptive reference for each technique is called out in the title of each section, with other supporting references introduced as needed. Some references are repeated here from the main text in order that each description might stand alone. Again, only the references deemed sufficient to describe the technique are listed, and no attempt was made to be exhaustive.

APPENDIX B-1. IR BAND MODEL EMISSION/ABSORPTION
(REFERENCES B-5 AND B-6).

Principle

Emission and absorption spectroscopy can be applied to gas flow diagnostics most straightforwardly by dealing with resolved spectral lines (see Appendix B-5). If the liner of a band system cannot be resolved, but the molecular species has a well defined structure, then line by line calculations can be performed (see Appendix B-2). However, for many species (H_2O and CO_2 , for example) the structure of the band systems have not been defined, and the line spacing is such that many lines may fall within a practical instrument bandpass. For such cases an artifice called a "band model" is employed (References B-1 and B-2), in which the ordinary laws of radiative transfer are applied to a fictitious line by line model which is designed to approximate the radiance and transmittance of the actual molecular radiance and transmittance measured at a specified temperature, partial pressure, and gas density. Such models have been shown to simulate the actual radiative transfer quite well within the accuracy of the empirical data available (Reference B-2). Since H_2O and CO_2 are the principle products of combustion in most practical rockets and both have accessible infrared (IR) emission/absorption bands with extensive band model data (References B-3 and B-4), a diagnostic technique has been developed around the radiative transfer equations using the band model theory for these molecules (References B-5 and B-6).

The first element in the diagnostic technique is the correct expression for the radiative transfer. Considering a path through a nonhomogeneous gas stream made up of many small isothermal, isobaric zones of constant composition, the radiance $N_{\Delta\lambda}$ emitted at the edge of the path in a finite band increment $\Delta\lambda$ is given by (see Figure B-1 1)

$$N_{\Delta\lambda} = \sum_j \sum_{i=1}^m N_B (T_{i\Delta\lambda}) [\tau_{i-1} (T_i, P_{ij}, P_i) - \tau_i (T_i, P_{ij}, P_i)] \quad (B-1 1)$$

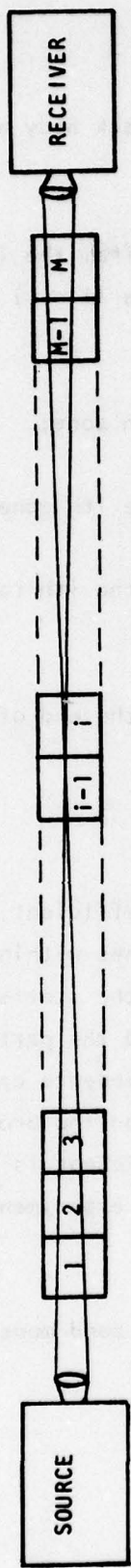


Figure B-1 1. Illustration of Radiative Transfer Through Nonhomogeneous Radiating and Absorbing Path Made up of Isothermal, Isobaric Zones.

where $N_B(\tau_i)$ is the radiance of a black body at temperature T_i within the wavelength increment $\Delta\lambda$;

$\tau_{i-1, i}$ are the transmittances from the initial edge ($i = 1$) to the beginning of the i th zone ($i = 1$) and to the end of the i th zone (i), respectively;

T_i is the temperature in the i th zone;

P_i is the static pressure in the i th zone; and

P_{ij} is the partial pressure of the i th radiating species in the i th zone.

The transmittance from the edge $i = 1$ to the end of the i th zone is given by

$$\ln(\tau_i) = \sum_{h=1}^i (k_h)_{\Delta\lambda} \Delta\lambda \quad (\text{B-1 2})$$

where $(k_h)_{\Delta\lambda}$ represents the absorption coefficient of the i th zone made up of contributions from all the spectral lines within the wavelength interval $\Delta\lambda$, and depends upon the temperature T_h , the static pressure P_h , the partial pressure of the absorbing species P_{hj} , and the partial pressure of all other species that goes to make up P_h . The dependence upon other species comes about through foreign gas contributions to line broadening. The complicated, unknown character of the absorption coefficient is circumscribed through the artifice of the band model and associated experimentally-determined band model parameters.

In the nomenclature of Reference B-3, the band model expression for τ for a homogeneous path is

$$\ln(\tau)_{\Delta\lambda} = -2\pi \left(\frac{Y}{D}\right) f(x) \quad (\text{B-1 3})$$

where γ is the half width (width at half maximum intensity) of the lines within the wavelength increment and depends upon the static pressure, the composition, and the temperature of the gas within the homogeneous increment ℓ ;

d is the spacing between the lines;

$f(x)$ is a function of the parameter

$$x = \frac{\ell}{2\pi} \left(\frac{S/d}{\gamma/d} \right) \quad (\text{B-1 4})$$

which depends upon the form of the band model being used, including the line shape function;

ℓ is the length of path over which the temperature, composition, pressure, and partial pressure of the absorbing species are constant; and

S is the line strength, defined for single lines as

$$S = \int_0^{\infty} k_{\nu} d\nu \quad (\text{B-1 5})$$

Now, the τ_i and τ_{i-1} of Equation (B-1 1) are made up of contributions from each zone along some nonhomogeneous path between $i = 1$ and i (or $i-1$), while the transmittance expressed by Equation (B-1 3) applies only to a homogeneous path. A second artifice must be used to relate the defined, homogeneous band model parameters to the integrated path transmittance. One approach is referred to as the Curtis-Godson approximation (References B-3 and B-7), which states that "there is some homogeneous gas with band model parameters (S/d) and (γ/d) which has the same transmittance as the inhomogeneous gas having individual zone parameters $(S/d)_h$ and $(\gamma/d)_h$." The result of the approximation is

$$\overline{\left(\frac{S}{d}\right)} L = \sum_h \left(\frac{S}{d}\right)_h \ell_h \quad (\text{B-1 6})$$

$$\overline{\left(\frac{S}{d}\right)} \overline{\left(\frac{Y}{d}\right)} L = \sum_h \left(\frac{S}{d}\right)_h \left(\frac{Y}{d}\right)_h \ell_h \quad (\text{B-1 7})$$

where L is the total path length composed of the sum of the individual zonal path lengths, ℓ_h . Young (Reference B-4) discusses the limitations of the Curtis-Godson approximation and introduces alternatives, which have the effect of changing the form of $f(x)$.

The key to the use of the band model approach to radiative transfer is an adequate expression $f(x)$, which will satisfy experimental data over a sufficiently large range of temperature and pressure. Full discussion of the current forms for $f(x)$ under all conditions of temperature and pressure and for different species is beyond the scope of this brief discussion, and the references must be consulted (see References B-3, B-4, B-7, B-8, and B-9). The recommended function for use with H_2O (25-26 μm) and CO_2 (4.35-4.4 μm) is that reported by Young (Reference B-10) which is based upon an exponential-tailed line strength distribution with combined collisional and pressure broadening.

The second part of the diagnostic approach using the band model radiative transfer equations is the necessary inversion procedure to determine local values of temperature and species partial pressure from the integrated radiance and transmittance measurements. The procedure developed by Brewer and Limbaugh (Reference B-5) for cylindrically symmetric flows is illustrated in Figure B-1 2. The symmetric flow is divided into concentric zones in which the temperature, static pressure, and species partial pressure are assumed constant. If there are M such zones and M measurements of transmittance and radiance are made as shown in Figure B-1 2, and the local composition and static pressure are known a priori, then sufficient information is available to determine zonal temperatures and partial pressures. The procedure is to

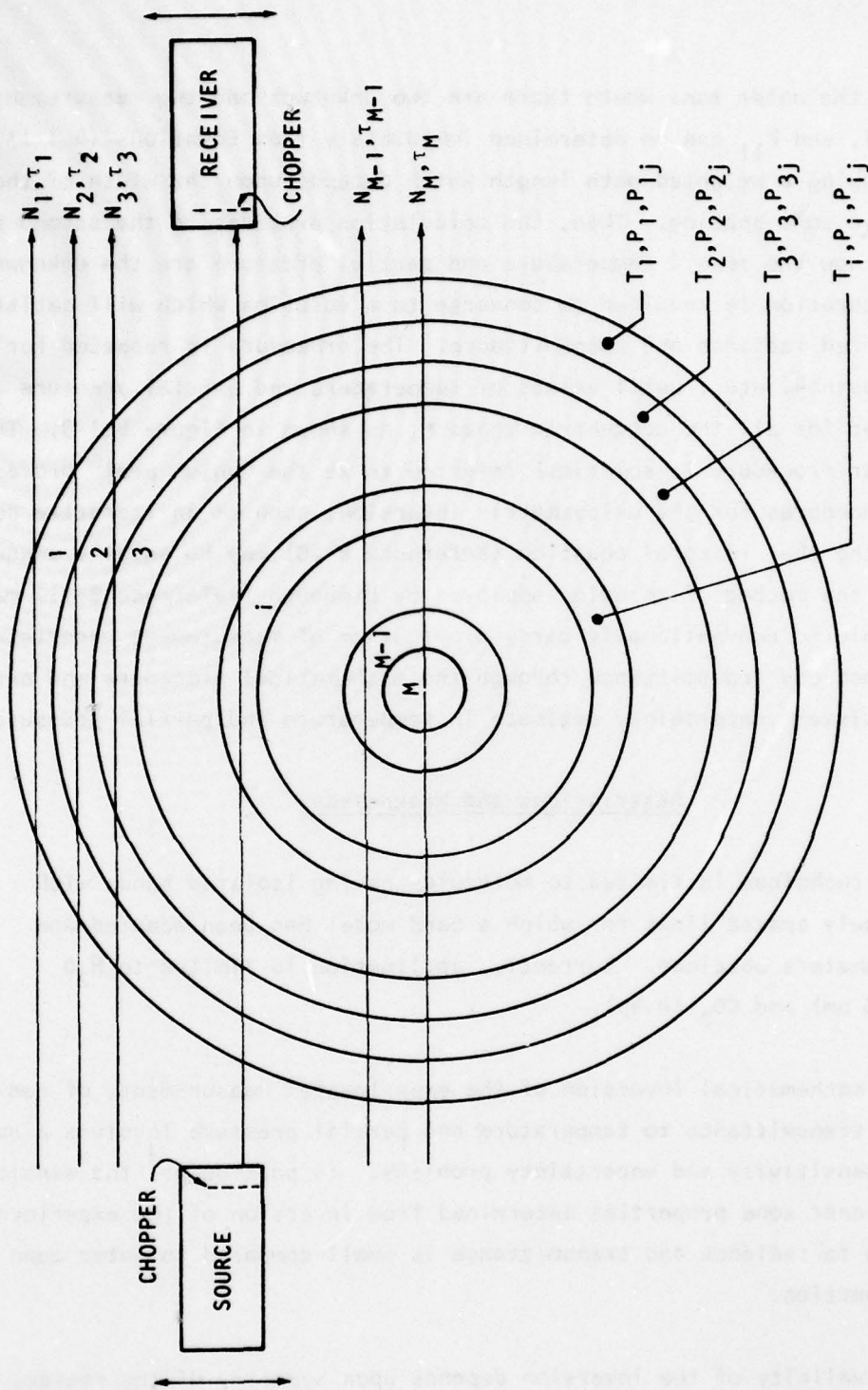


Figure B-1 2. Schematic of Orientation of Symmetric Zones for Emission/Absorption Technique.

begin at the outer zone where there are two unknowns and two measurements and the T , and P_{11} can be determined immediately from Equations (B-1 1) and (B-1 2) using a weighted path length which depends upon the width of the concentric zone spacing. Then, the calculation proceeds to the second path in which now the zone 2 temperature and partial pressure are the unknowns and an iteration is required to converge to a solution which will satisfy the measured radiance and transmittance. The procedure is repeated for path 3, path 4, etc., until values of temperature and partial pressure are determined for all the concentric zones M , as shown in Figure B-1 3. This particular procedure is sometimes referred to as the "onion peel" process. Other procedures for the axisymmetric inversion, such as an iterative solution of the Abel integral equation (Reference B-10) may be equally adequate. However, the method of solution employed by Limbaugh (Reference B-11) makes it possible to conventionally carry propagation of measurement uncertainty in radiance and transmittance through the mathematical procedure and arrive at a consistent uncertainty estimate in temperature and partial pressure.

Restrictions and Weaknesses

1. The technique is limited to molecules having isolated bands with closely spaced lines for which a band model has been adapted and parameters obtained. Currently, application is limited to H_2O ($2.5 \mu m$) and CO_2 (4.4μ).
2. The mathematical inversion of the experimental measurements of radiance and transmittance to temperature and partial pressure involves a number of sensitivity and uncertainty problems. In particular, the sensitivity of inner zone properties determined from inversion of the experimental data to radiance and transmittance is small compared to outer zone properties.
3. The validity of the inversion depends upon symmetry of the source, so that applications are limited.

N - RADIANCE
 τ - TRANSMITTANCE

T - TEMPERATURE
 P - SPECIES PARTIAL PRESSURE

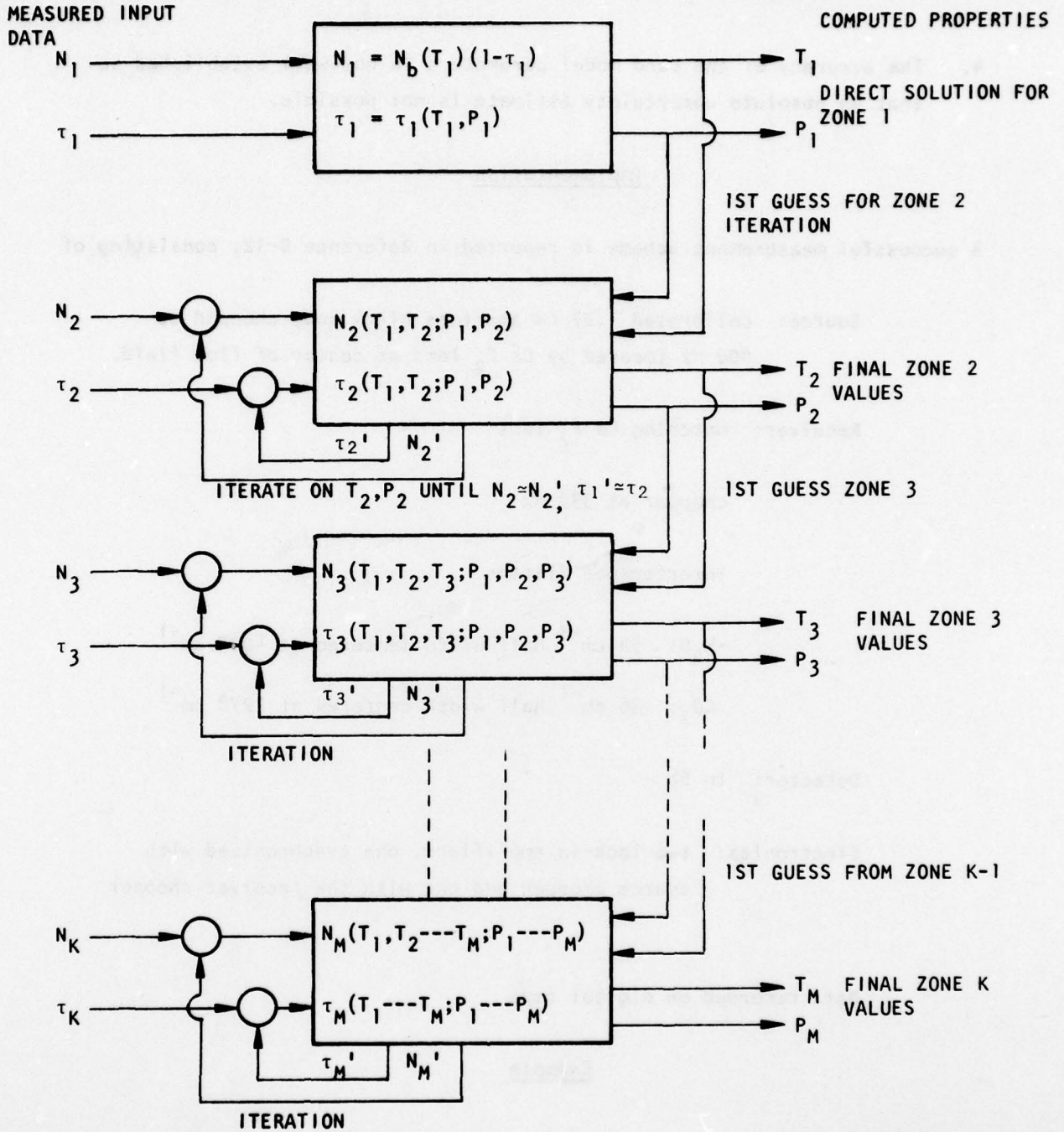


Figure B-1 3. Computational Flow Chart for AEDC IR Emission/Absorption Inversion Method.

4. The accuracy of the band model parameters is not well established so that an absolute uncertainty estimate is not possible.

Implementation

A successful measurement scheme is reported in Reference B-12, consisting of

Source: calibrated 1.27 cm aperture black body chopped at
400 Hz focused by Ca F₂ lens at center of flow field.

Receiver: matching Ca F₂ lens

chopper at 333 Hz

interference filters

-H₂O: 54 cm⁻¹ half width centered at 4005 cm⁻¹

CO₂: 36 cm⁻¹ half width centered at 2278 cm⁻¹

Detector: In Sb

Electronics: two lock-in amplifiers, one synchronized with
source chopper and one with the receiver chopper

Data recorded on digital tape

Example

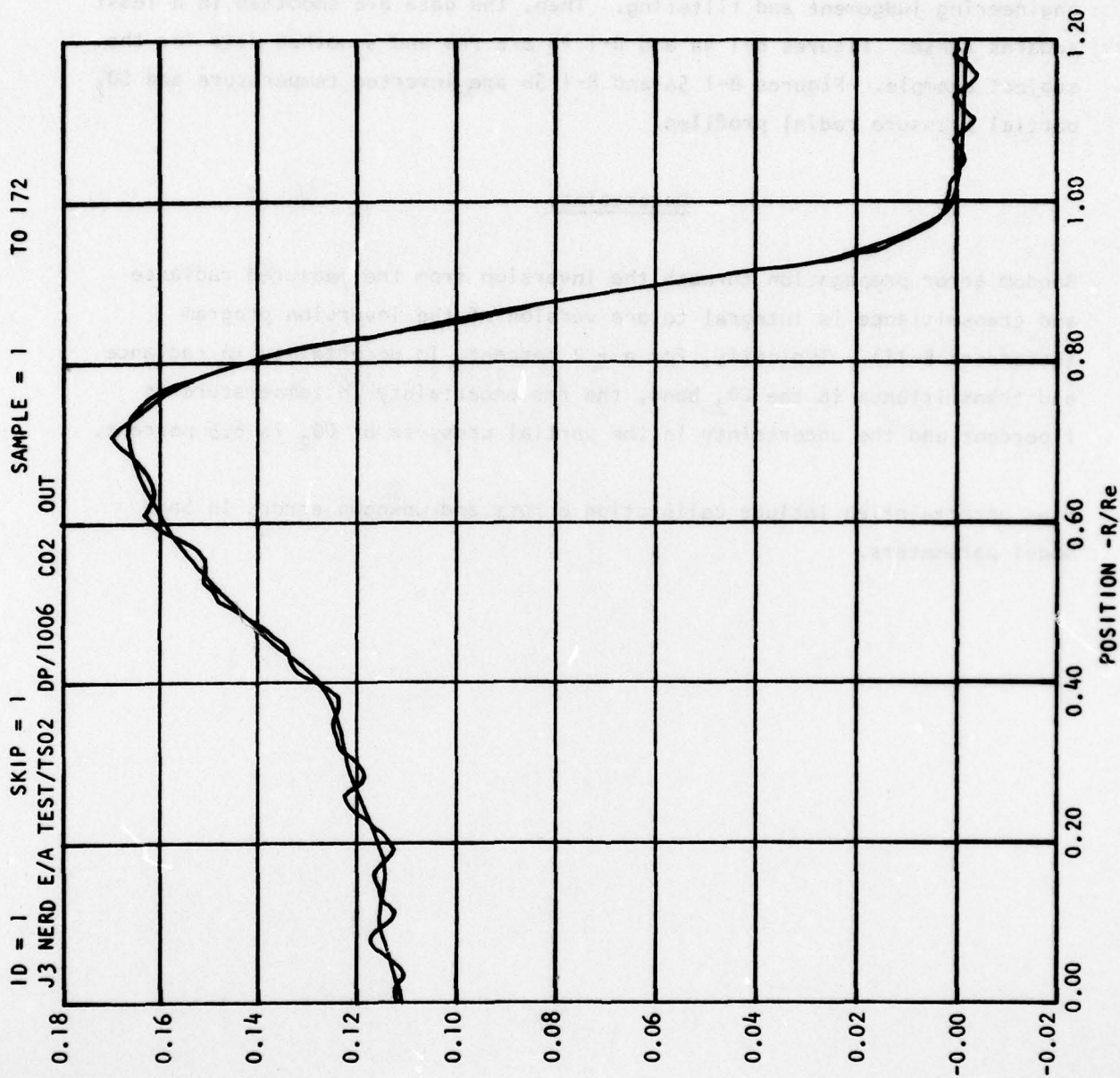
T and [CO₂] profiles were obtained from the exit plane of a Transtage Engine (Reference B-12). The engine had a 040 expansion ratio bell nozzle and delivered 8000 lb_f with storable propellants N₂O₄/AZ-50. Raw radiance

and transmittance data must be smoothed in order to accomplish the inversion. Deterministic noise (instrumentation fluctuations) must be first removed by engineering judgement and filtering. Then, the data are smoothed in a least squares sense. Figures B-1 4a and B-1 4b are raw and smoothed data for the subject example. Figures B-1 5a and B-1 5b are inverted temperature and CO₂ partial pressure radial profiles.

Uncertainty

Random error propagation through the inversion from the measured radiance and transmittance is integral to one version of the inversion program (Reference B-11). Typically, for a ± 2 percent, 1σ uncertainty in radiance and transmittance in the CO₂ band, the rms uncertainty in temperature is 1 percent and the uncertainty in the partial pressure of CO₂ is 6.5 percent.

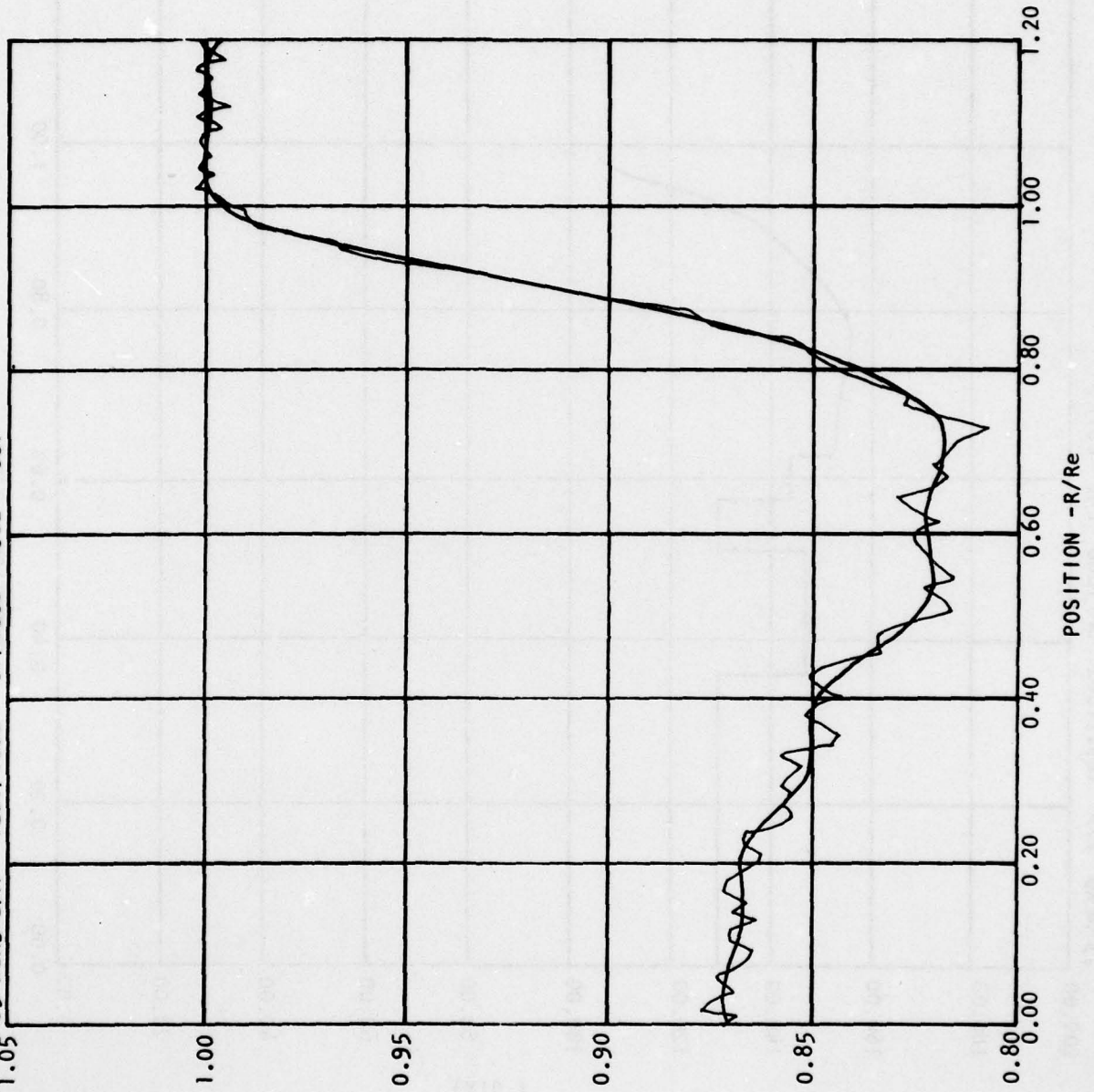
Bias uncertainties include calibration errors and unknown errors in band model parameters.



RADIANCE
RADIANCE

Figure B-1 4a. Raw and Smoothed Data from Transtage Engine Exit Plane - Radiance.

ID = 1 SKIP = 1 SAMPLE = 1 TO 172
J3 NERD E/A TEST/TS02 DP/1006 C02 OUT



TRANS.
TRANS.

Figure B-1 4b. Raw and Smoothered Data from Transtage Engine Exit Plane - Transmittance.

ID = 1 SKIP = 1 SAMPLE = 7 TO 38
J3 NERD E/A TEST/TS02 DP/1006 C02 OUT

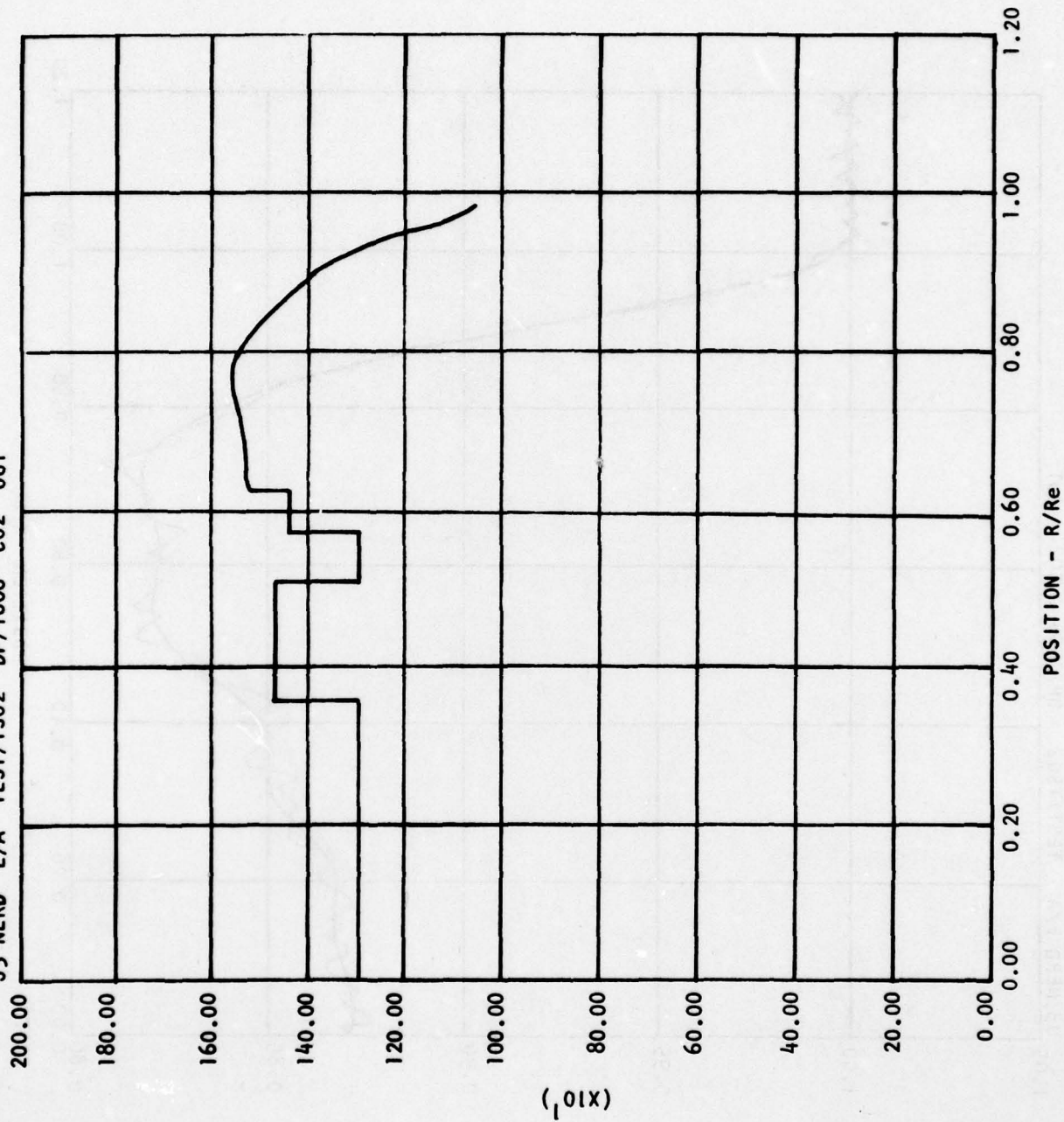


Figure B-1 5a. Inverted Data from IR Emission/Absorption Technique Applied to Transtage Engine Exit Plane Radiance and Transmittance - Temperature.

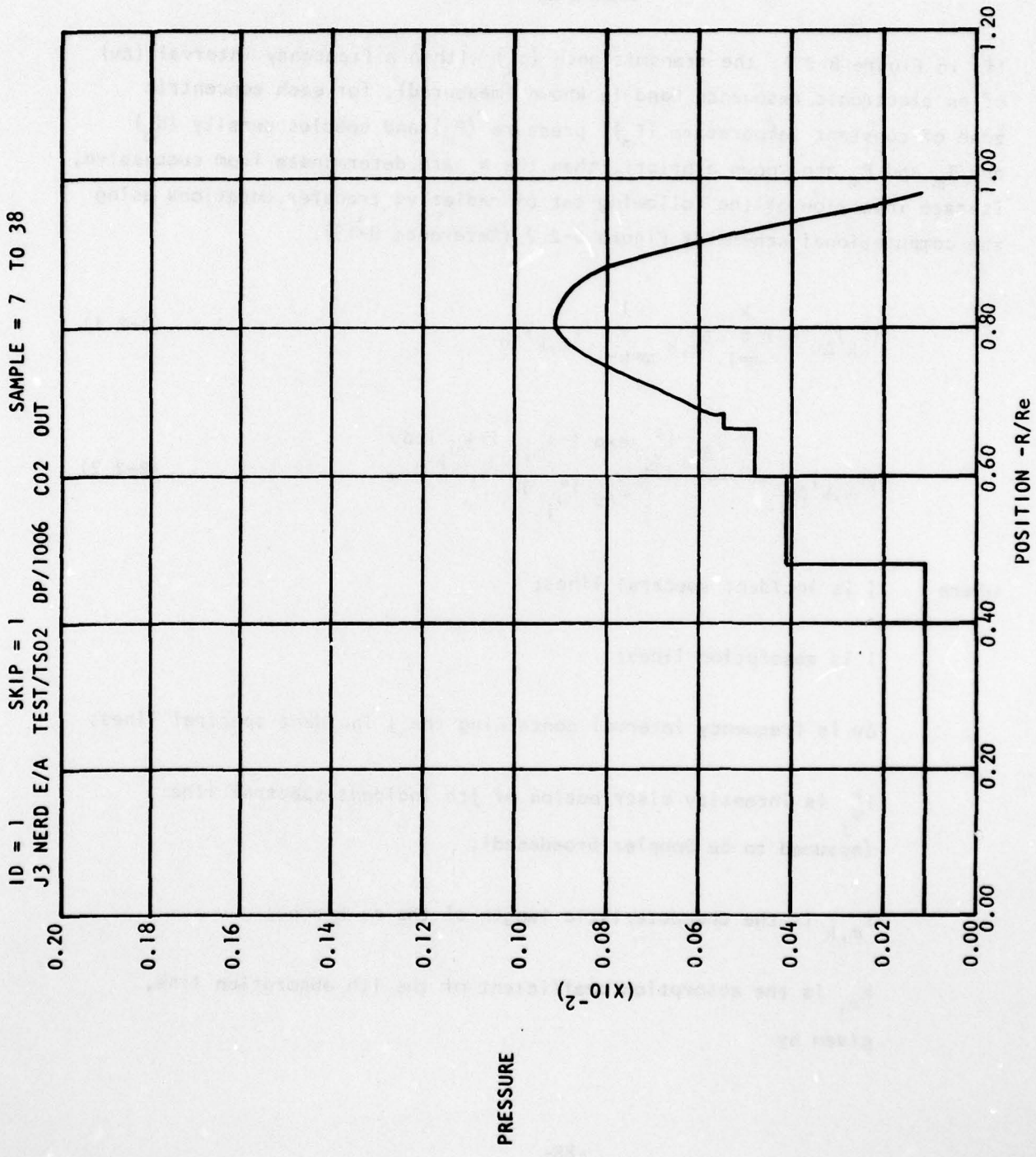


Figure 8-1 5b. Inverted Data from IR Emission/Absorption Technique Applied to Transtage Engine Exit Plane Radiance and Transmittance - CO₂ Partial Pressure.

APPENDIX B-2. UV RESONANCE ABSORPTION (REFERENCE B-12).

Principle

If, in Figure B-2 1, the transmittance (τ_k) within a frequency interval ($\Delta\nu$) of an electronic resonance band is known (measured), for each concentric zone of constant temperature (T_m), pressure (P_m) and species density (N_m) and T_m and P_m are known a priori, then the N_m are determinate from successive, iterate inversion of the following set of radiative transfer equations using the computational scheme of Figure B-2 2 (Reference B-13).

$$(\tau_k)_{\Delta\nu} = \left(\prod_{m=1}^k \tau_{m,k} \right)_{\Delta\nu} \quad (B-2 1)$$

$$(\tau_{m,k})_{\Delta\nu} = \frac{\sum_j \int_{\Delta\nu} I_{\nu_j}^{\circ} \exp(-\ell_{m,k} \sum_i k_{\nu_i}) d\nu}{\sum_j \int_{\Delta\nu} I_{\nu_j}^{\circ} d\nu} \quad (B-2 2)$$

where j is incident spectral lines;

i is absorption lines;

$\Delta\nu$ is frequency interval containing the j incident spectral lines;

$I_{\nu_j}^{\circ}$ is intensity distribution of j th incident spectral line
(assumed to be Doppler broadened);

$\ell_{m,k}$ is the characteristic length of the m, k zone;

k_{ν_i} is the absorption coefficient of the i th absorption line,
given by

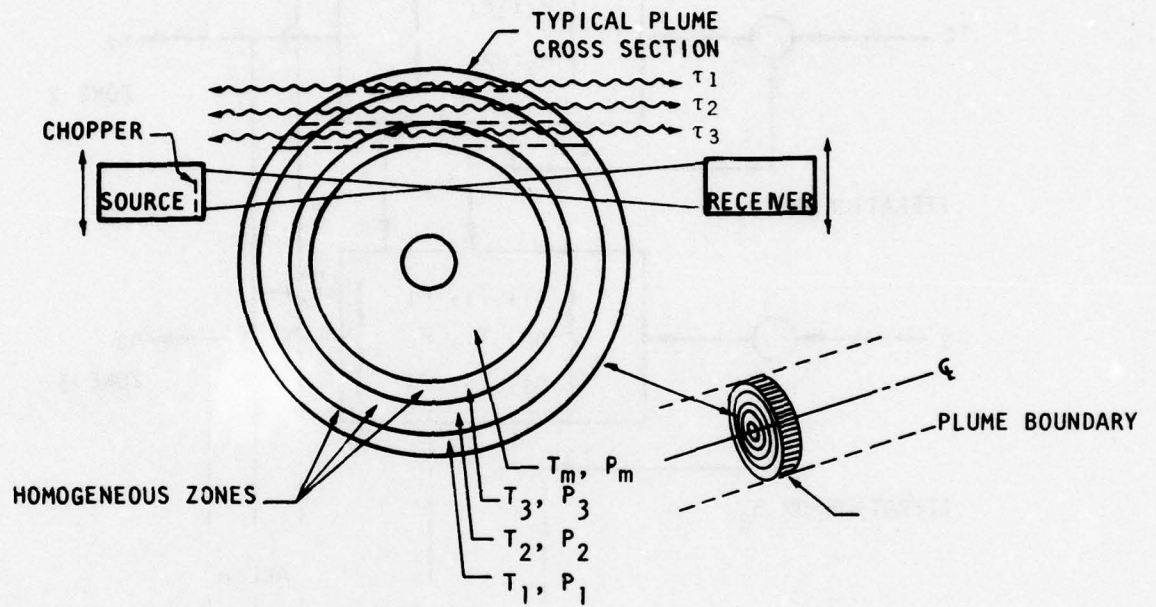
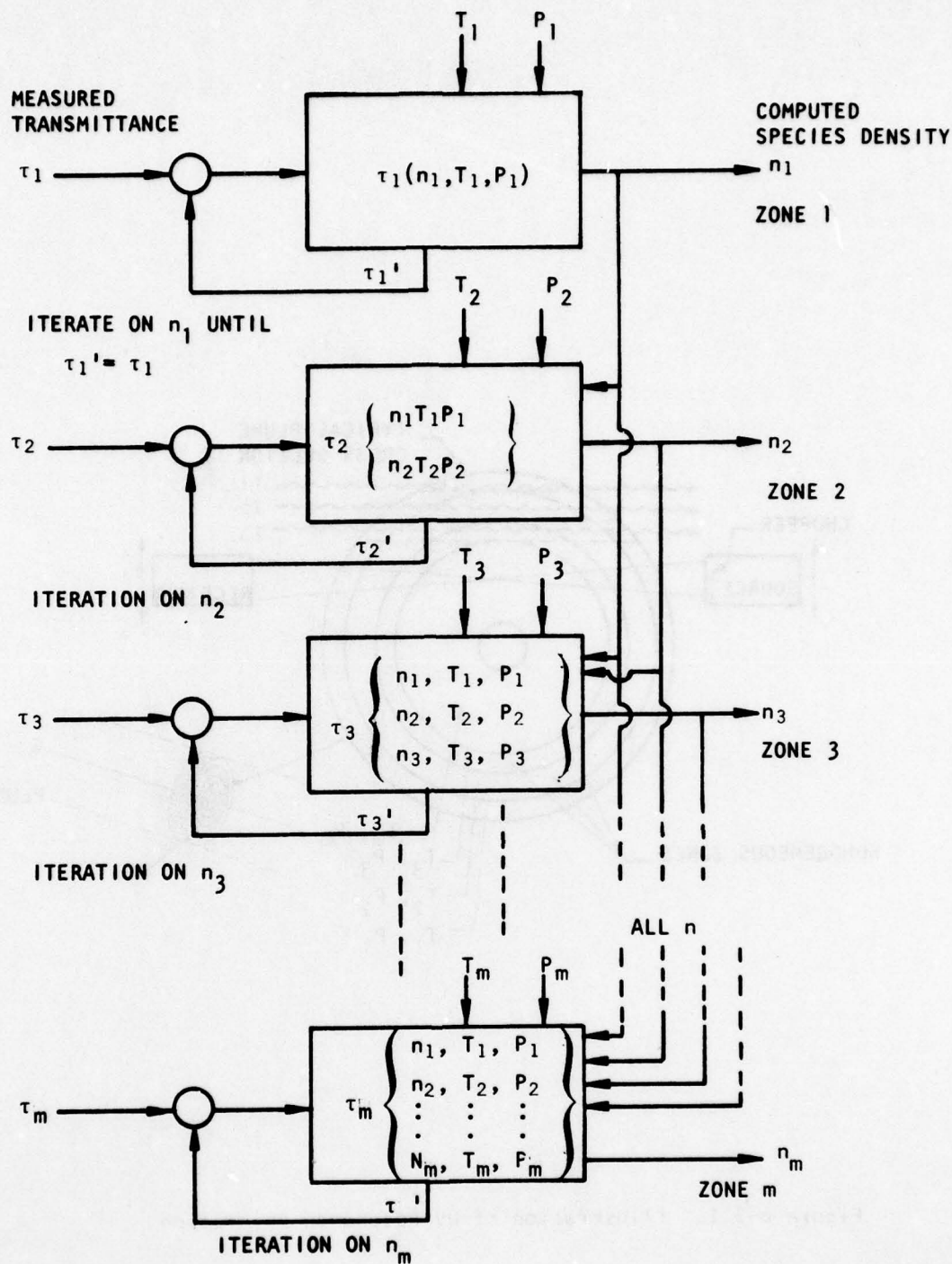


Figure B-2 1. Illustration of UV Resonance Absorption



τ - TRANSMITTANCE (MEASURED)
 T - TEMPERATURE (INPUT)

P - STATIC PRESSURE (INPUT)
 n - NUMBER DENSITY (COMPUTED)

Figure B-2 2. Computational Flow Chart for AEDC UV Resonance Absorption Inversion Method.

$$k_{v_i} = k_{v_i^0} \frac{1}{\pi} \int_{-\infty}^{\infty} \frac{a \exp(-y^2)}{a^2 + (\omega_i - y)^2} dy \quad ; \quad (\text{B-2 3})$$

a is the ratio of collisional and Doppler line half widths, given by

$$a = C P_m / T_m ; C = \text{exp. constant} \quad (\text{B-2 4})$$

ω_i is the Doppler frequency function, given by

$$\omega_i = \frac{2 \sqrt{\ln 2} (v_i - v_i^0)}{(\Delta v_i)_D}$$

v_i^0 is the frequency at line center;

$(\Delta v_i)_D$ is the Doppler half width of absorber line i , given by

$$(\Delta v_i)_D = 2 v_i^0 \sqrt{\frac{2 \ln 2 \chi T_m}{M c^2}} \quad ;$$

χ is Boltzmann's constant;

c is velocity of light;

M is mass of absorbing molecule;

$k_{v_i^0}$ is absorption coefficient at line center, given by

$$k_{v_i^0} = \frac{2 \sqrt{\pi \ln 2} e^2}{M c^2 (\Delta v_i)_D} N_{j'' i'} \quad ;$$

e is electronic charge;

$N_{J''}$ is density of absorbing molecules in J'' quantum state; for equilibrium,

$$N_{J''} = N_0 \frac{g_{J''} \exp(-E_{J''}/\chi T)}{(pf)}$$

N_0 is total density of absorbing molecules;

$g_{J''}$ is statistical weight of J'' th quantum state;

$E_{J''}$ is energy of J'' th quantum state;

(pf) is partition function for absorbing molecules; and

f_i is oscillator strength for the i th absorption line.

Example

NO number density profiles (Figure B-2 3) were obtained using absorption of λ -bands ($\gamma=226\text{nm}$) (Figure B-2 4) through exhaust of turbojet engine combustor (Reference B-14). Temperature and pressure were measured separately by probes. Also shown are results of probe measurements of NO concentration, indicating a well documented discrepancy (References B-14 and B-15).

Restrictions and Weaknesses

1. The technique is limited to those molecules and atoms which have a resonance transition in an accessible spectral range. The species present in combustion gases which have an accessible resonance absorption are:

AD-A073 520

AIR FORCE ROCKET PROPULSION LAB EDWARDS AFB CA
ASSESSMENT OF IN SITU DIAGNOSTICS FOR APPLICATION TO ROCKET PRO--ETC(U)
JUN 79 W K MCGREGOR

F/G 21/2

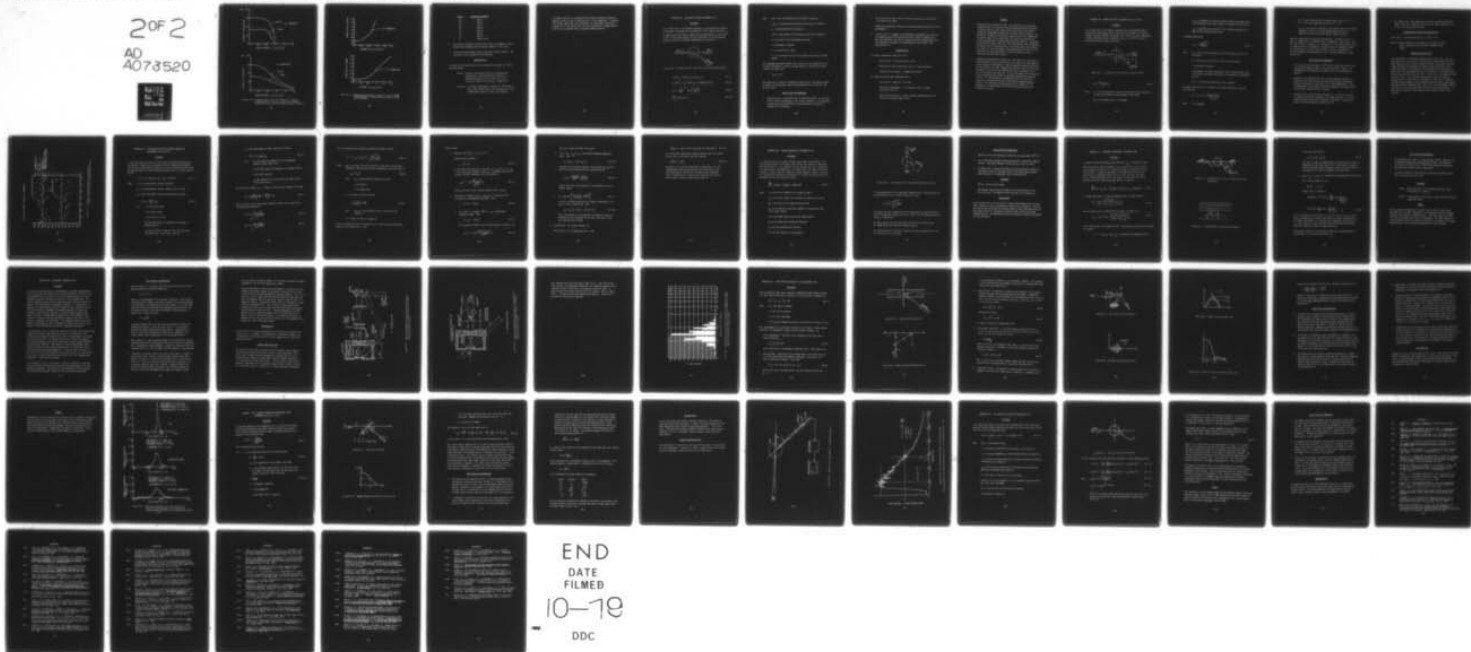
UNCLASSIFIED

AFRPL-TR-78-62

NL

2 OF 2

AD
A073520



END
DATE
FILMED
10-79
DDC



MICROCOPY RESOLUTION TEST CHART
NATIONAL BUREAU OF STANDARDS-1963-A

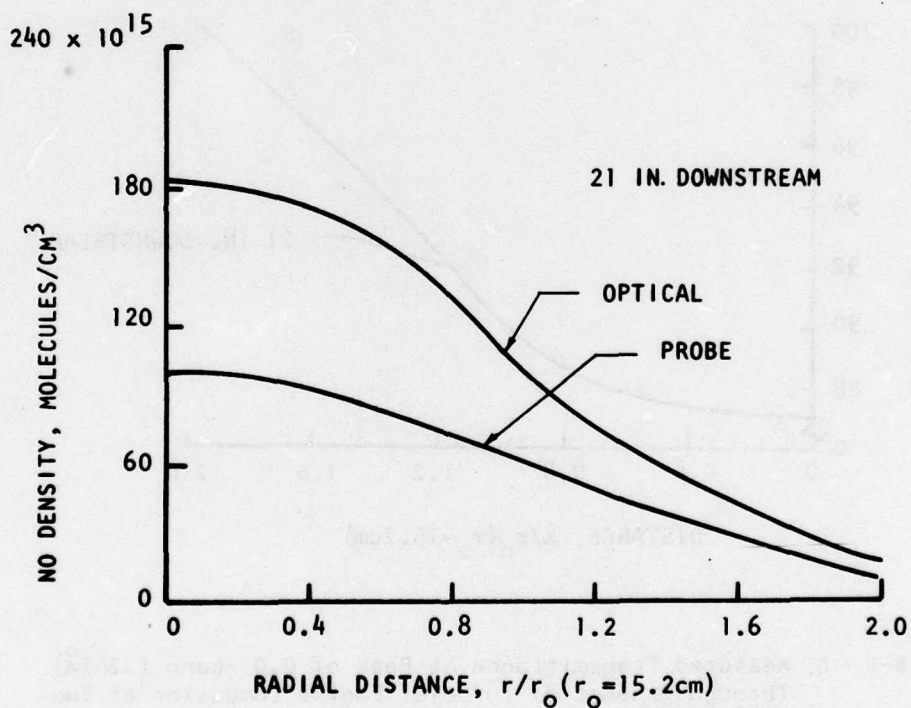
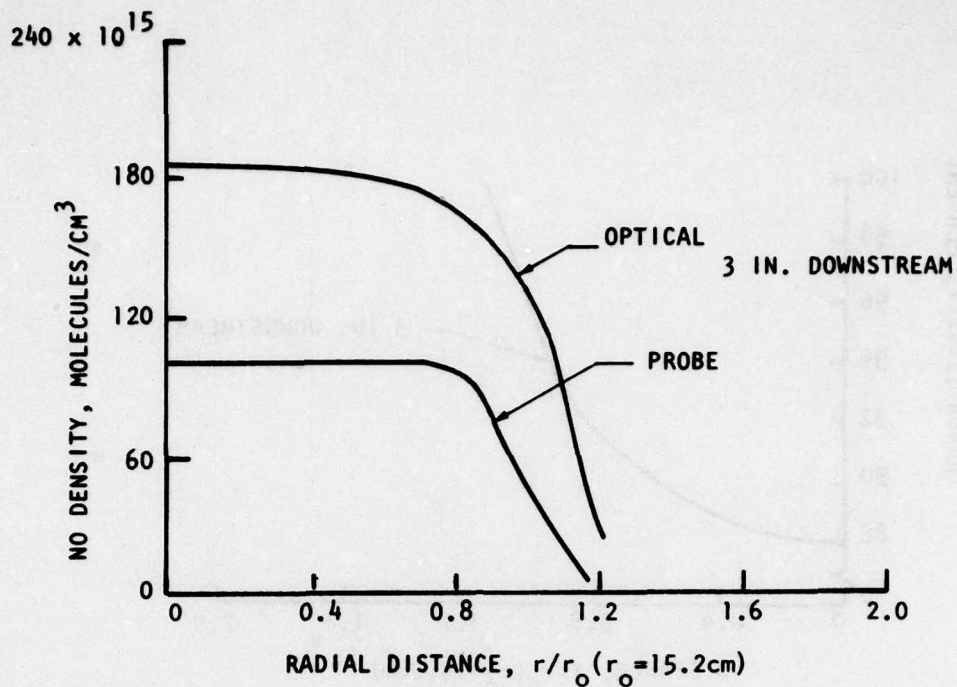


Figure B-2 3. NO Number Density Profiles in Exhaust of Turbojet Engine Combustor at Two Axial Locations as Measured by Sampling Probes and UV Resonance Absorption Techniques.

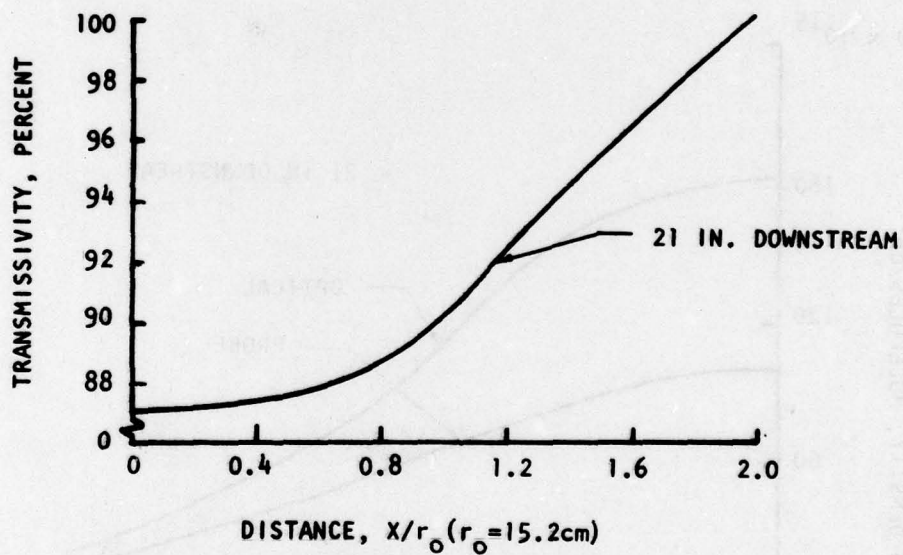
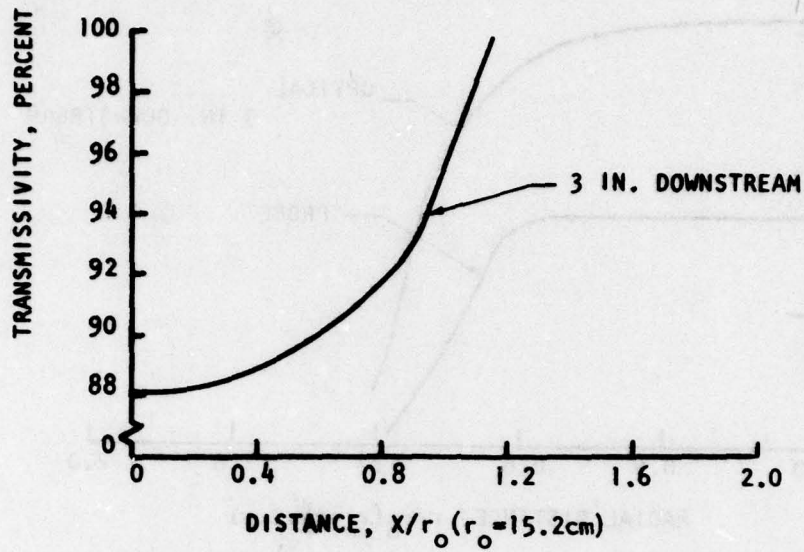


Figure B-2 4. Measured Transmittance at Peak of 0,0 -band (2262\AA) Through Exhaust of Turbojet Engine Combustor at Two Axial Locations.

| <u>Specie</u> | <u>Resonance Wavelength</u> |
|----------------|-----------------------------|
| NO | 226 nm |
| OH | 306 nm |
| NH | 337 nm |
| CN | 390 nm |
| CH | 432 nm |
| C ₂ | 514 nm |
| N _a | 589 nm |
| K | 766.5, 770 nm |

2. The required inversion to obtain local values of temperature and/or number density depends upon cylindrical symmetry of the source.
3. The model described above contains many experimental constants. The technique is only as good as those constants.

Implementation

The technique has been used mainly with laboratory equipment, as follows (Reference B-16),

Source: specially constructed capillary discharge tube operating at a specified potential (3000 vdc), a Specified pressure (6 Torr), and with a 12:3:1 mixture by volume of A, N₂ and O₂, respectively.

Receiver: 1/2 M Ebert spectrometer operated at 1.6^o bandpass, with an RCA 1P28 PM tube: data recording was usually accomplished using strip chart type recorders.

A systematic analysis of uncertainty has not been conducted, although an approach similar to that of Reference B-11 is quite adaptable. A conservative estimate based upon trial calculation for measurement uncertainty of 5 percent 1σ in the γ -band of NO, the total uncertainty in number density of NO will be no greater than ± 15 percent (Reference B-16).

APPENDIX B-3. RAYLEIGH SCATTERING (REFERENCE B-17).

Principle

If, in Figure B-3 1, the radiation spectrum (I_ν), scattered at an angle θ by molecules illuminated with a monochromatic laser beam of intensity I_{ν_0} is measured, and the relative species mole concentrations (C_i) are known a priori, then the gas density (N) and temperature (T) can be obtained through the following relations (References B-17 and B-18):

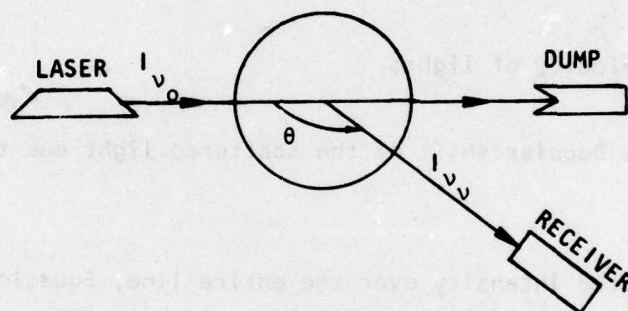


Figure B-3 1. Configuration for Laser Rayleigh Scattering Measurements

$$I_\nu(\theta)/I_{\nu_0} = K(\theta)N \sum_i C_i \sigma_i(\nu_0) \alpha_i f_i(\nu) \quad (\text{B-3 1})$$

$$I_{\Delta\nu}(\theta)/I_{\nu_0} = \int_{\Delta\nu} I_\nu(\theta)/I_{\nu_0} d\nu = K(\theta)N \sum_i C_i \sigma_i(\nu_0) \alpha_i \quad (\text{B-3 2})$$

$$f(\nu) = \frac{M_i}{2\pi\chi T}^{1/2} \exp\left(-\frac{M_i \nu^2}{2\chi T}\right) \quad (\text{B-3 3})$$

$$\frac{\nu - \nu_0}{\nu_0} = \frac{2\nu}{c} \sin \theta/2 \quad (\text{B-3 4})$$

where $K(\theta)$ is an instrumentation and orientation constant;

$\sigma_i(v_0)$ is the Rayleigh scattering cross section for species i ;

α_i is the polarizability of species i ;

$f_i(v)$ is the velocity (v) distribution function for species i ;

M_i is the mass of the i th molecular species;

χ is Boltzmann's constant;

c is the velocity of light;

$v-v_0$ is the Doppler shift of the scattered light due to thermal motion.

The integrated scattered intensity over the entire line, Equation (B-3 2), is easily calibrated in terms of the gas density if the relative concentrations are known; then

$$I_{\Delta v} / I_{v_0} = CN.$$

The temperature is found by iterating on velocity until the spectral shape of measured and calculated spectra (from Equations (B-3 1), (B-3 3), and (B-3 4)) match.

Restrictions and Weaknesses

1. Rayleigh theory is valid only when the scattering center is much, much smaller than the wavelength of the incident radiation. Thus, presence of particulate matter destroys the technique, and Mie scattering (Appendix B-11) dominates.

2. The concentration (mole fraction or partial pressure) of each species in the gas must be known.
3. Temperature measurement requires very high resolution (order of 0.01 cm^{-1}) measurements.
4. A density limit is imposed on the temperature measurement by virtue of the changing nature of the scattering from a Doppler broadening to a Brillouin broadening, the latter resulting when the molecular mean free path becomes of the order of the wavelength of the incident light (Reference B-17).

Implementation

For Density Measurement (Reference B-19):

Laser source: 1 Joule pulsed ruby laser

Narrow band ($\sim 1\text{\AA}$) interference filter at laser wavelength

Photomultiplier detector: standard electronics

For Temperature Measurement (Reference B-17):

Laser source: argon ion, 1W or more

Fabry-Perot spectrometer: 2 cm spacing, 0.25 cm^{-1} range,
resolution 0.014 cm^{-1}

Detector and Electronics: photon counting grade photomultiplier tube with minicomputer data system

Examples

1. Relative Density (Reference B-19). The scattering at the incident wavelength from a pulsed ruby laser beam passing through the exhaust of 500 and 1000 lb_f thrust model rocket engines burning storable propellants (N₂O₄/MMH) was measured at several radial stations. The assumption was made that the species composition did not change over the radial extent of the plume; then the relative gas density was directly proportional to the Rayleigh scattered intensity. Knowledge of the relative species densities was also assumed so that the absolute gas density profile was determined. Particulate matter was evidently very scarce in the plume because the measured densities were not very different from those calculated so that contributions from Mie scattering must have been minimum.
2. Temperature (References B-17 and B-20). The spectral line profile of the Rayleigh and Brillion scattering from an argon laser beam (488 nm) passing through a hydrogen-air flame was measured at several positions. At the center of the flame, temperatures measured from the line profile matched well the equilibrium temperature, and no influence of Mie or Brillion scattering was observed. At the flame edge the Mie scattering from entrained particles from the atmosphere rendered the technique invalid. In the high density precombustion region the Brillion scattering introduced distortion of the Doppler broadened Gaussian profile. The experiment provides opportunity to observe all the phenomena to be encountered in the use of Rayleigh scattering for diagnostics purposes.

APPENDIX B-4. RAMAN SCATTERING (REFERENCES B-21 and B-22).

Principle

If, in Figure B-4 1, the number of photons within a wavelength range $\Delta\lambda$ scattered per second ($Q_{\Delta\lambda}$) from a laser beam at wavelength λ_i traveling through a medium containing the species s at a density n_s and a temperature T , due to the Raman effect is measured, then $n_s(r)$ and $T(r)$ can be determined from the following relations:

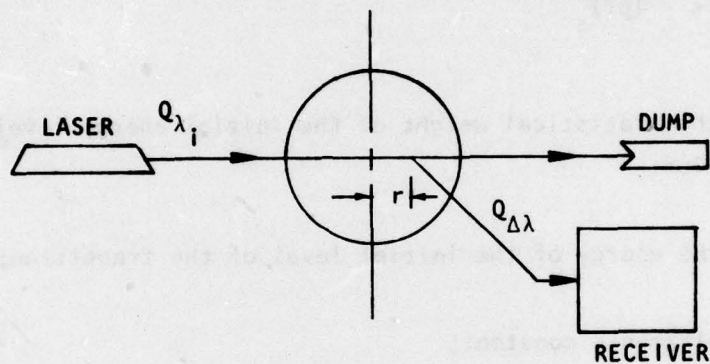


Figure B-4 1. Illustration of Laser Raman Scattering System

$$Q_{\Delta\lambda} = K Q_{\lambda_i} \sum_{s_j} n_{s_j} \sigma_{s_j} \quad (\text{B-4 1})$$

where K is the instrumentation constant which depends upon the geometry, collection efficiency, and wavelength of the system;

Q_{λ_i} is the photon current in the beam;

n_{sj} is the number of s species molecules producing spectral lines j at wavelengths within the interval $\Delta\lambda$ accepted by the receiver;

σ_{sj} is the Raman cross section for the s species molecules for each of the j spectral transitions.

At thermal equilibrium

$$n_{sj} = n_s \frac{g_j e^{-E_j/\chi T}}{(pf)_s} \quad (B-4 2)$$

where g_j is the statistical weight of the initial energy level of the transition;

E_j is the energy of the initial level of the transition;

χ is Boltzman's constant;

j corresponds to a given vibrational state ν and rotational state J (for purely rotational transitions j corresponds to a rotational state J);

$(pf)_s$ is the partition function for the s molecule.

The Raman cross section for a specific vibrational-rotational transition can be written

$$\sigma_j = \sigma_{\nu'J'} = C_{\nu'J'} \frac{g_{\nu'J'} S_{\nu'J'}}{\lambda_{\nu'J'}^4}$$

where C is a constant;

$g\nu\nu'$ is the vibrational band strength factor relative to $\nu' = 1$, $\nu'' = 0$ (for pure rotational spectra, $g\nu'\nu'' \equiv 1$);

$S_{j,j''}$ is the relative rotational line strength factor (for diatomic molecules, the $\Delta J = 0, \pm 2$ Hönl-London factors are given in Reference B-23 for the various angular momentum states).

Ideally, a Raman spectrum from only one molecule is radiated within $\Delta\lambda$ so that the summation in s of Equation (B-4 1) disappears. Also, ideally, only one line or band j of species s is included in $\Delta\lambda$. Unfortunately, the ideal is seldom met and so the diagnostic procedure contains a computer program for determination of n_s and T from a given set of $Q_{\Delta\lambda}$ measurement at several wavelengths (see Reference B-21 for a detailed procedure of Raman Diagnostics).

Restrictions and Weaknesses

1. Cross sections are very small ($\sim 10^{-31} \text{ cm}^2$) so that photon count rates are small, and therefore, signal to noise ratio (S/N) is small. The development of the technique is therefore mainly an instrumentation problem.
2. Because of the inherently poor S/N, spurious background radiation (typically from scattering off surfaces, laser excited fluorescence, radiation from gases or particles, etc.) limits applications. Also, the measurement time required to achieve acceptable S/N extends rocket firing times, increasing cost of testing.
3. Overlap of lines from different molecules ($s > 1$) within a practical $\Delta\lambda$ required to achieve a reasonable S/N frequently occurs. In rocket exhausts overlap of N_2 and CO rotational lines makes it necessary to measure the combined density (Reference B-23).

4. The species that can be measured are limited to those gases having a Raman transition. Generally, this means that atoms such as Na, K, O, H, etc., are inaccessible by Raman.

Implementation (Typical, Reference B-23)

Laser Source: Q-switched pulsed ruby, 1 Joule or more

Receiver: Double tandem 3/4 m spectrometer with photon counting quality photomultiplier tube and minicomputer data system

Example (Reference B-24)

The instantaneous (~ 20 nanosec) temperature and species ($N_2 + CO + O_2$) number densities on the axis (6 ft downstream) of the exhaust plume from a model (500 lb_f thrust), storable propellant rocket engine under simulated flight conditions was measured from Raman scattered radiation using a pulsed ruby laser. The purpose of the measurement was to determine the magnitude of the temperature and density fluctuations in the highly turbulent mixing of plume and external flow. Figure B-4 2 is an example of data obtained. Shown is the rotational temperature fluctuations about an average value, the total density fluctuations of ($N_2 + CO + O_2$) about an average value as measured in the rotational bands and the N_2 number density measured from the vibrational band. The $\Delta\lambda$ for this measurement situation was 0.9 nm. The firing rate of the laser was 12 pulses per minute. The uncertainties quoted are based upon the total number of photon counts received.

$M_\infty = 2.05$, ALTITUDE = 33,000, 6:1 CONTOURED

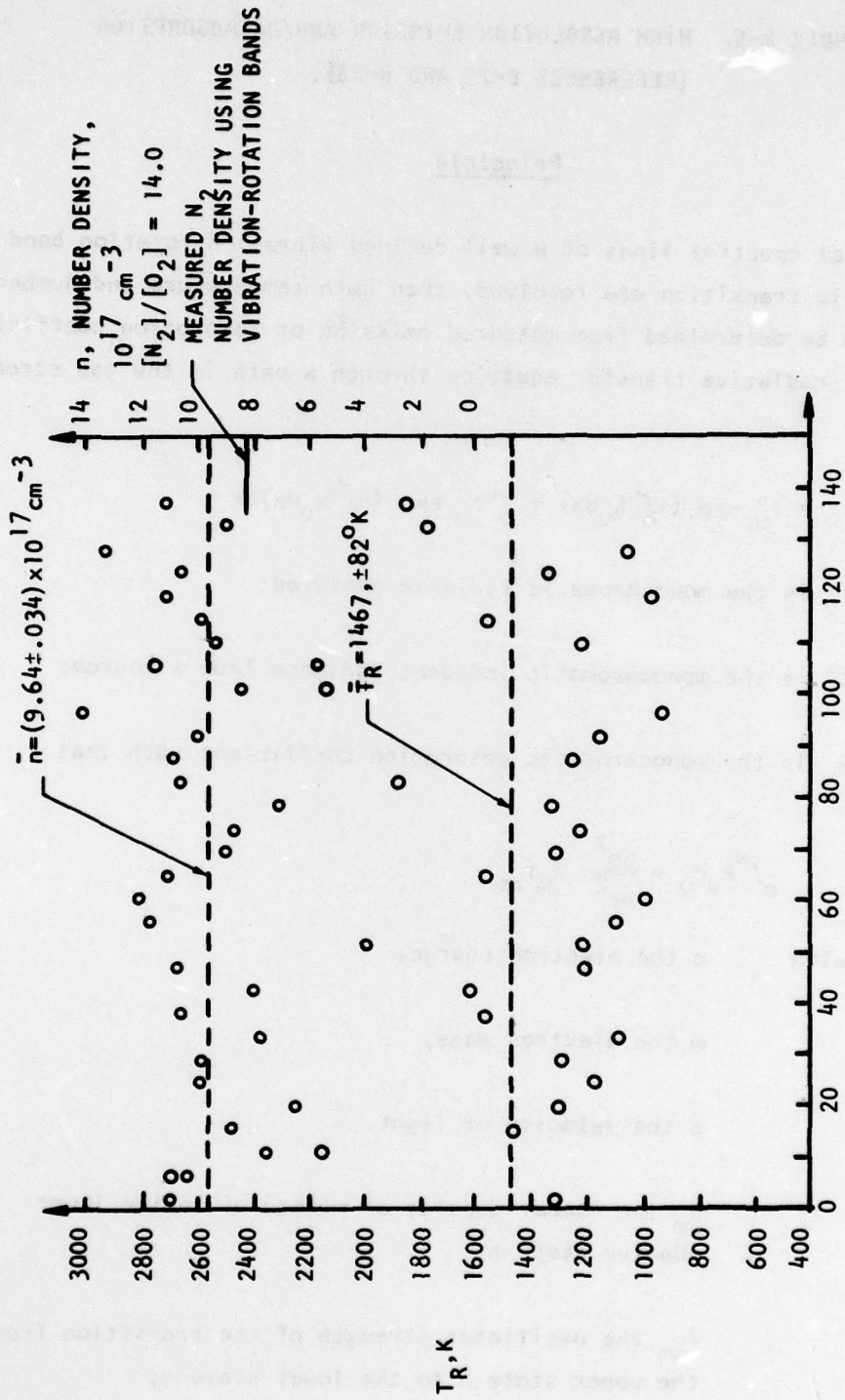


Figure B-4 2. Temperature and Number Density as a Function of Engine Time for a 500lbf N_2O_4 /MMH Rocket Engine.

APPENDIX B-5. HIGH RESOLUTION EMISSION AND/OR ABSORPTION
(REFERENCES B-25 AND B-26).

Principle

If individual spectral lines of a well defined vibration-rotation band or an electronic transition are resolved, then both temperature and number density can be determined from measured emission or absorption coefficients. The general radiative transfer equation through a path in the gas stream is written

$$I_{\nu} = I_{\nu}^{\circ} \exp(-\int_0^L k_{\nu} dx) + \int_0^L \epsilon_{\nu} \exp(-\int_0^L k_{\nu} dx) dx \quad (B-5 1)$$

where I_{ν} is the monochromatic radiance measured;

I_{ν}° is the monochromatic incident radiance from a source;

k_{ν} is the monochromatic absorption coefficient such that

$$\int_0^{\infty} k_{\nu} d\nu = \frac{\pi e^2}{mc^2} N_m f_{nm} \quad (B-5 2)$$

with e the electron charge,

m the electron mass,

c the velocity of light,

N_m the number density of molecules in the lower quantum state m ,

f_{nm} the oscillator strength of the transition from the upper state n to the lower state m ;

ϵ_{ν} is the monochromatic emission coefficient given by

$$\int_0^{\infty} \epsilon_{\nu} d\nu = A_{nm} N_n h \nu_{nm} \quad (\text{B-5 3})$$

with A_{nm} the transition probability for a spontaneous transition from state n to m,

N_n the number density of molecules in the upper state n,

h the Planck constant,

ν_{nm} the frequency of the transition from upper state n to the lower state m.

The oscillator strength f_{nm} is related to the transition probability through

$$f_{nm} = \frac{mc^4}{8\pi^2 e^2 \nu_{nm}^2} \frac{g_n}{g_m} \left(1 - \frac{g_m}{g_n} \frac{N_n}{N_m} \right) A_{nm} \quad (\text{B-5 4})$$

where g_m and g_n are the statistical weights of state m and n respectively. At equilibrium temperature T,

$$N_n = N_0 \frac{g_n e^{-E_n/kT}}{\sum_{\text{all } i} g_i e^{-E_i/kT}} \quad (\text{B-5 5})$$

$$N_m = N_0 \frac{g_m e^{-E_m/kT}}{\sum_{\text{all } i} g_i e^{-E_i/kT}} \quad (\text{B-5 6})$$

The line shapes may be, generally, expressed as Voigt profiles,

$$\epsilon_V, k_V = \epsilon_{V_{nm}}, k_{V_{nm}} \frac{1}{\pi} \int_{-\infty}^{\infty} \frac{a_{nm} e^{-y^2} dy}{a_{nm}^2 + (\omega - y)^2} \quad (\text{B-5 7})$$

where a_{nm} is the ratio of the half widths of lines due to collisional broadening alone and due to Doppler broadening alone, and given by

$$a_{nm} = C_{nm} \frac{p}{T} \quad (\text{B-5 8})$$

with C_{nm} an experimentally determined constant

p the pressure,

T the temperature;

ω is the Doppler function given by

$$\omega = \frac{\nu - \nu_{nm}}{(\Delta_a \nu)_{1/2}} 2 \sqrt{\ln 2} \quad (\text{B-5 9})$$

with $(\Delta_a \nu)_{1/2}$, the frequency width of the line at half intensity;

y is a dummy variable of integration.

This set of Equations (B-5 1) through (B-5 9) is sufficient to describe any spectral line transmission problem.

Special cases:

1. Optically Thin Case: $k_v = 0$, $I_v^0 = 0$

Equation (B-5 1) becomes

$$I_v = \int_0^L \epsilon_v dx \quad (\text{B-5 10})$$

If the total line intensity is measured, $I_v \rightarrow I_{nm}$, $\int_0^\infty \epsilon_v dv = \epsilon_{nm}$, in the cylindrically symmetric case ϵ_{nm} is obtained from the Abel integral transform (Reference B-27, for example)

$$\epsilon_{nm}(r) = -\frac{1}{\pi} \int_r^R \frac{dy}{\sqrt{y^2 - r^2}} \frac{d}{dy} I_{nm}(y) dy \quad (\text{B-5 11})$$

from ϵ_{nm} for two or more lines one obtains local T and N_0 .

2. Absorption of External Source: Right term in Equation (B-5 1) eliminated by instrumentation approach. Then

$$I_v = I_v^0 \exp(-\int_0^L k_v dx) \quad (\text{B-5 12})$$

- a. $I_v^0 = \text{const}$, I_v^0 ; measure $\int \frac{I_v}{I_v^0} dv \equiv \tau_{nm}$, transmittance (Reference B-28). Then

$$\ln \tau_{nm} = -\int k_{nm} dx \quad (\text{B-5 13})$$

For cylindrical symmetry, Abel inversion again is possible, and

$$k_{nm}(r) = -\frac{1}{\pi} \int_r^R \frac{dy}{\sqrt{y^2 - r^2}} \frac{d}{dy} [\ln \tau_{nm}(y)] dy \quad (\text{B-5 14})$$

Now local T and N_0 available from $k_{nm}(r)$.

- b. $I_v^o = \delta (I_v^o - I_{v_{nm}}^o)$, v_{nm} = line center frequency (Reference B-27). Then

$$\ln \tau(v_{nm}) = - \int_0^L k(v_{nm}) dx \quad (B-5 15)$$

and again for cylindrical symmetry local values of $k(v_{nm})$ and hence T and N_0 are determined from (Reference B-26)

$$k(v_{nm}) = \frac{2e^2 \sqrt{\pi} \ln 2}{MC^2} \frac{N_m f_{nm}}{(\Delta_a v)^{1/2}} \quad (B-5 16)$$

This is the "narrow line absorption" case amenable to use of tunable lasers.

c.
$$I_v^o = I_{nm}^o \exp \left[- \left(\frac{v - v_{nm}}{(\Delta_s v)^{1/2}} 2\sqrt{\ln 2} \right)^2 \right] \quad (B-5 17)$$

as from a resonance lamp where only Doppler broadening of the source lines is appreciable. Then

$$I_{\Delta v} = \int_{\Delta v} \int_0^L I_v^o \exp \left(- \int_x^L k_v dx \right) dx dv \quad (B-5 18)$$

This is equivalent to the resonance line absorption technique (Reference B-14) of Appendix B-2 and the "onion peel" inversion approach must be taken.

3. Line Reversal, $I_v^o = \text{Planck Function, } J_v^b$:

Vary J_v^b until $I_v = J_v^b$ (Reference B-30). Then

$$J_V^b(T_B) [1 - \exp(-\int_0^L k_V dx)] = \int_0^L \epsilon_V(T_G) \exp(-\int_0^L k_V dx) dx \quad (B-5 19)$$

For the constant temperature, constant density case, the integral on the right is the same as the left side and

$$J_V^b(T_B) = \epsilon_V(T_G)L \quad (B-5 20)$$

Therefore $T_B = T_G$ and the temperature is determined. For the nonhomogeneous case the equation must be solved directly and little advantage is served over the general case, Equations (B-5 1) through (B-5 9). Some sort of inversion must then be accomplished in order to obtain local properties.

APPENDIX B-6. E-BEAM FLUORESCENCE (REFERENCE B-32).

Principle

If a beam of electrons is passed through a gas, some of the species will be collisionally excited to electronic states which then radiate in some select band (Figure B-6 1). The radiation from the band may then yield information on species density and temperature. At steady state, the number of molecules excited to a state n per unit volume per second, dQ_n/dt , is equal to the number de-excited by radiation (fluorescence) to a state m plus those de-excited through collisions with molecular species,

$$\frac{dQ_n}{dt} = E\sigma_{en}N_o = \sum_n (\sum_m A_{nm}N_n - \sum_f N_n N_f \sigma_{nf} \bar{v}) \quad (B-6 1)$$

where E is the flux of electron flow through the beam;

σ_{en} is the cross section for excitation by electron collisions;

N_o is the density of the specie being excited;

A_{nm} is the radiative transition probability from excited state n to a lower state m ;

N_n is the steady state excited state number density;

N_f are the densities of quenching molecules;

σ_{nf} are the quenching cross sections;

\bar{v} is the mean velocity of the molecules.

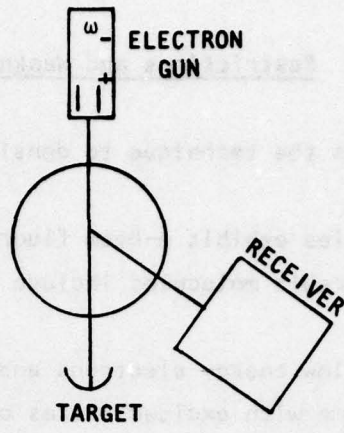


Figure B-6 1. Configuration for E-Beam Fluorescence Measurements

If the quenching term can be neglected, Equation (B-6 1) simplifies and the measured radiation from a single transition is just

$$I_{nm} = KA_{nm} \frac{g_n e^{-E_n/kT}}{\sum_i g_i e^{-E_i/kT}}$$

from whence the local temperature can be determined from the distribution. From the integrated intensity of all the lines in all the bands, emitted the local N_0 is determined.

The above assumes that the ground state rotational distribution does not change during the excitation-radiation process.

The technique can still be used if quenching cannot be neglected, but the N_f , $\bar{\nu}$ and σ_{nf} must all be known.

Restrictions and Weaknesses

1. Quenching limits the technique to densities less than about 10^{16} cm⁻³.
2. Only a few species exhibit e-beam fluorescence in accessible spectral regions. Applicable molecules include N₂, H₂, H, CO, O₂, and O.
3. Interaction of low energy electrons and excited metastable species in the sample volume with excited states of the species being studied poses problems yet incompletely solved (Reference B-33).

Equipment

Source: 15 keV electron beam.

Spectrometer with resolution capable of individual spectral lines (for N₂, the N₂⁺ 1st Negative System requires 0.2 Å resolution).

Applications

Direct application to the far field of vacuum plume expansions has not been made, although no severe implementation problems are contemplated. Relevant applications have been made to simulated reacting plumes (Reference B-35) and to mixing of flows in simulations of chemical laser mixing flow systems (Reference B-34). The quenching and other interaction problems are discussed in those references.

APPENDIX B-7. RESONANCE FLUORESCENCE (REFERENCE B-36)

Principle

If a beam of light at energy $h\nu_{\ell n}$ and intensity $I_{\nu_{\ell n}}^{\circ}$ is incident on a gas containing species having a resonance $\nu_{\ell n}$, (Figure B-7 1) then according to the diagram of Figure B-7 2, the rate of change of the density of the excited state n is equal to the number of I_n photons absorbed less the number lost by spontaneous radiation to all lower states m , plus those lost by induced radiation to all lower states m , plus those lost during molecular collisions with foreign gas species, as shown by,

$$\frac{dN_n}{dt} = N_{\ell} I_{\nu_{\ell n}}^{\circ} B_{\ell n} - \left[\sum_m A_{nm} N_n + \sum_m B_{nm} N_n I_{\nu_{nm}} + \sum_f N_f N_n \sigma_{nf} \bar{v} \right] \quad (\text{B-7 1})$$

At steady state $dN_n/dt = 0$ and the number density of excited states is

$$N_n = \frac{N_{\ell} I_{\nu_{\ell n}}^{\circ} B_{\ell n}}{\sum_m (A_{nm} + B_{nm} I_{\nu_{nm}}) + \sum_f N_f \sigma_{nf} \bar{v}} \quad (\text{B-7 2})$$

and the radiant emission coefficient for some n, k transition is

$$\epsilon_{\nu_{nk}} = A_{nk} N_n h\nu_{nk} = \frac{h\nu_{nk} A_{nk} I_{\nu_{\ell n}}^{\circ} B_{\ell n} N_{\ell}}{\sum_m (A_{nm} + B_{nm} I_{\nu_{nm}}) + Q} \quad (\text{B-7 3})$$

with Q substituted for the quenching term. Many special cases can be considered; for example,

1. $Q \ll (\sum_m A_{nm} + B_{nm} I_{\nu_{nm}})$, low density case (Reference B-37).

Principle

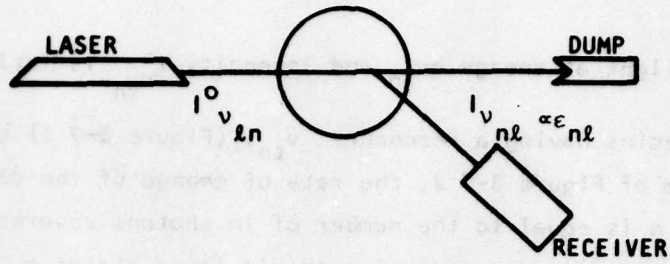


Figure B-7 1. Configuration for Laser Induced Fluorescence Measurements.

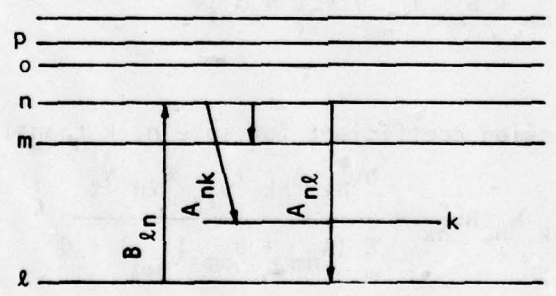


Figure B-7 2. State Diagram Illustrating Fluorescence.

For any one transition nk

$$\epsilon_{nk} \propto \nu_{nk} A_{nk} I_{\nu_{kn}}^{\circ} N_l \quad (\text{B-7 4})$$

This case is useful for measurement of N_l which can be related to temperature of the lower state l if l is one state in a ground vibration-rotation state distribution, and to the total density of the molecules for which the resonant transition occurs.

2. $\sum_m B_{nm} I_{\nu_{lm}}^{\circ} \gg \sum_m A_{nm} + Q$, saturation case (References B-36 and B-37).

For a 2-level system $m=l$, and

$$B_{nl} I_{\nu_{ln}}^{\circ} \gg A_{nl} + Q$$

Equation (B-7 3) reduces to

$$\epsilon_{nl} = A_{nl} N_l h \nu_{nl} = A_{nl} h \nu_{nl} \left(\frac{B_{ln}}{B_{nl}} \right) N_l \frac{1}{1 + \frac{A_{nl} + Q}{B_{nl} I_{\nu_{nl}}^{\circ}}}$$

$$\epsilon_{nl} \approx A_{nl} h \nu_{nl} \frac{g_l}{g_n} N_l \left[1 - \frac{A_{nl} + Q}{B_{nl} I_{\nu_{nl}}^{\circ}} + \dots \right] \quad (\text{B-7 5})$$

Now if the second term in brackets is much less than unity, the system is fully saturated, and the emission coefficient is directly proportional to the lower state density. If the term is not negligible, then a plot of ϵ_{nl} versus $1/I_{\nu_{nl}}^{\circ}$ will yield a straight line with intercept proportional to N_l and slope which yields the quenching rate, Q.

The measured intensity of the radiation scattered into some detector is proportional to the emission coefficient, ϵ_{nl} .

Restrictions and Weaknesses

1. The technique can be used in a lower and upper density range, but not in between because of the unknown quenching rate. The estimated limits are $N < 10^{16} \text{ cm}^{-3}$ or $N > 10^{19} \text{ cm}^{-3}$ corresponding to negligible and saturation quenching rates, respectively.
2. Limited to molecules or atoms having an electronic resonance transition: OH, CN, CH, C_2 , Na, K, etc.

Equipment

Source: tunable dye laser in the resonance wavelength range of the species of interest.

Receiver: spectrometer or interference filter with photomultiplier detection system.

Example

The only reported example akin to rocket flows is the C_2 concentration measurement by saturated fluorescence in an atmospheric pressure oxygen/acetylene flame reported in Reference B-37. The value found was $4.5 \times 10^{15} \text{ cm}^{-3}$ with an estimated uncertainty of 300 percent. The large uncertainty resulted mostly from lack of accurate calibration in the proof of principle experiment and is not considered representative of the technique.

APPENDIX B-8. HOLOGRAPHY (REFERENCE B-38)

Principle

If the undisturbed amplitude of a monochromatic, coherent electromagnetic field is mixed with the amplitude of a wave diffracted by an object in the same coherent field, the result will be a diffraction pattern, or interferogram, containing the Fourier transform of the disturbed wave. The Fourier transform, which contains three-dimensional information about the object, can be recorded on a photographic emulsion. If the emulsion is exposed in a linear portion of the film density versus intensity relation, then the film density represents an accurate recording of the Fourier transform. The inverse of the Fourier transform again represents the object field and is accomplished by exposing the interferogram to monochromatic, coherent light and reforming the image of the object. This process is referred to as holography. The literature describing the many aspects of holography is vast. Reference B-38 describes the use by holography in flow visualization and particle measurement application.

If the objective field is a particle cloud then an image of the reconstructed hologram can provide a magnified cross section of the particle field, yielding size and shape of each particle that is large enough to be imaged by the optical system. If a double pulsed laser is used, the movement of a particle between pulses can be measured by a double exposure hologram and the velocity obtained. The change in size and shape between pulses yields information on such things as growth rate in a condensing flow, or surface reaction rate during combustion. If the particle is moving very fast, then the film streak formed during a pulse interval (or a pulse chain) of the laser provides a measure of both velocity and size, although some degradation in resolution is suffered.

If the objective field is a variation in index of refraction, or density, then the illuminating beam may be mixed with a reference beam in an interferometer arrangement. The resulting interferogram may then be recorded as a hologram and analyzed in terms of flow field density variation.

Restrictions and Weaknesses

1. The particle size is limited by the ordinary diffraction limit of all optical systems to a smallest dimension R

$$R = 1.3 \lambda f$$

where λ is the wavelength of the incident light, and f is the ratio of the usable cone of light at the optical element (lens) to the distance from the object to the plane of the optical element. For a ruby laser and an f2 system, the best resolution attainable would be about 2 μm . The depth of field Z, over which the hologram is approximately in focus given by (Reference B-38)

$$Z = 100 \frac{d^2}{\lambda} ;$$

represents another limit such that the field cannot be defined well outside that interval. For a ruby laser and a $d = 2 \mu\text{m}$ particle, the depth of usable field would be about 600 μm . Imperfections in optics, noise from diffraction due to gas density gradients, etc., usually prevent these theoretical limits from being obtained.

2. Data reduction is a major problem because of the difficulty of placing quantitative criteria on focus quality and noise suitable for mechanization. Consequently, human judgement is generally required so that data reduction of a flow field with heavy particle loading is time consuming.
3. "Freezing" of particles require very short pulse lasers. In order to prevent blurring of particles the pulse width should be less than about $0.1 d/v$ where d is the particle diameter and v is the particle velocity. Thus for a 2μ particle traveling at only 200 m/sec, the pulse width should be less than 1 nanosec. Commercial lasers are currently limited to about 20 nanosec, thus limiting velocities at which 2 μm resolution holography can be applied to about 20 m/sec.

For this reason, holography appears to be limited to combustion chamber phenomena or the far field condensation problem.

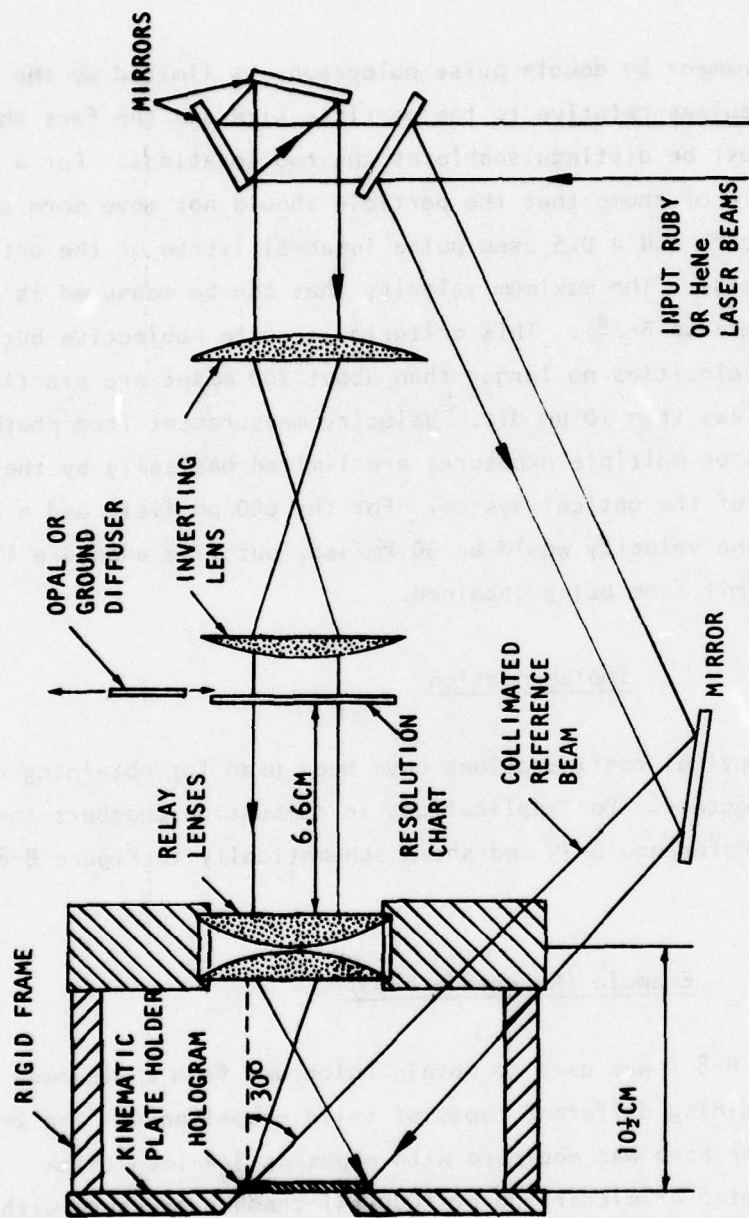
4. Velocity measurement by double pulse holography is limited by the time between laser pulses relative to the particle size and the fact that the particle must be distinguishable at the two locations. For a $10\ \mu\text{m}$ particle, a rule of thumb that the particle should not move more than about 10 diameters and a $0.5\ \mu\text{sec}$ pulse interval (state of the art of commercial lasers). The maximum velocity that can be measured is about 200 m/sec (Reference B-38). This criteria is quite subjective but suggests that velocities no larger than about 200 m/sec are practical for particles less than $10\ \mu\text{m}$ dia. Velocity measurement from photographic streaks or multiple exposures are limited basically by the depth of field of the optical system. For the $600\ \mu\text{m}$ field and a 2 nanosec pulse the velocity would be 30 km/sec, but film exposure limits prevent this limit from being obtained.

Implementation

A great variety of optical configurations have been used for obtaining and reconstructing holograms. For applications in combustion chambers the system described in Reference B-39 and shown schematically in Figure B-8 1 seems near optimum.

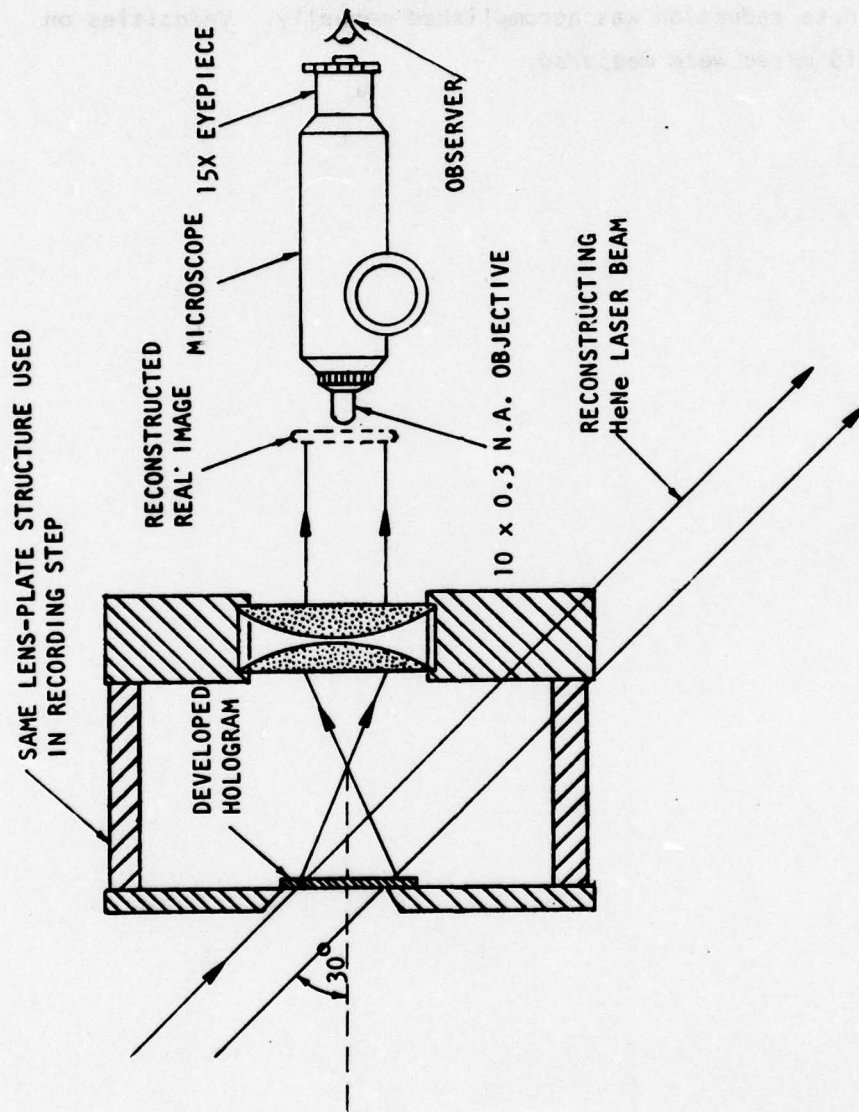
Example (Reference B-39)

The system of Figure B-8 1 was used to obtain holograms from a windowed combustion bomb containing different types of solid propellants. The 2-inch interval diameter bomb was equipped with opposing $3/4$ -inch thick windows and was operated at either 500 or 1000 psi chamber pressure with a firing duration of about 300 millisecc. The laser had a pulse width of about 50 to 80 nanosec with a separation between pulses of about $1.3\ \mu\text{sec}$. With the diffuser plate in Figure B-8 1 inserted, good quality holograms



A. RECORDING SYSTEM

Figure B-8 1. Optical Arrangement for Application of Holography to High Pressure Solid Propellant Combustion Studies (Reference B-39) (1 of 2)



B. RECONSTRUCTION SYSTEM

Figure B-8 1. Optical Arrangement for Application of Holography to High Pressure Solid Propellant Combustion Studies (Reference B-39) (2 of 2)

were recorded with resolution down to about $2.5 \mu\text{m}$. With the diffuser plate removed, the photographs showed only the refraction patterns due to changing indices of refraction in the gaseous combustion zones. A particle size distribution obtained with this system is shown in Figure B-8 2. The data reduction was accomplished manually. Velocities on the order of 10 m/sec were measured.

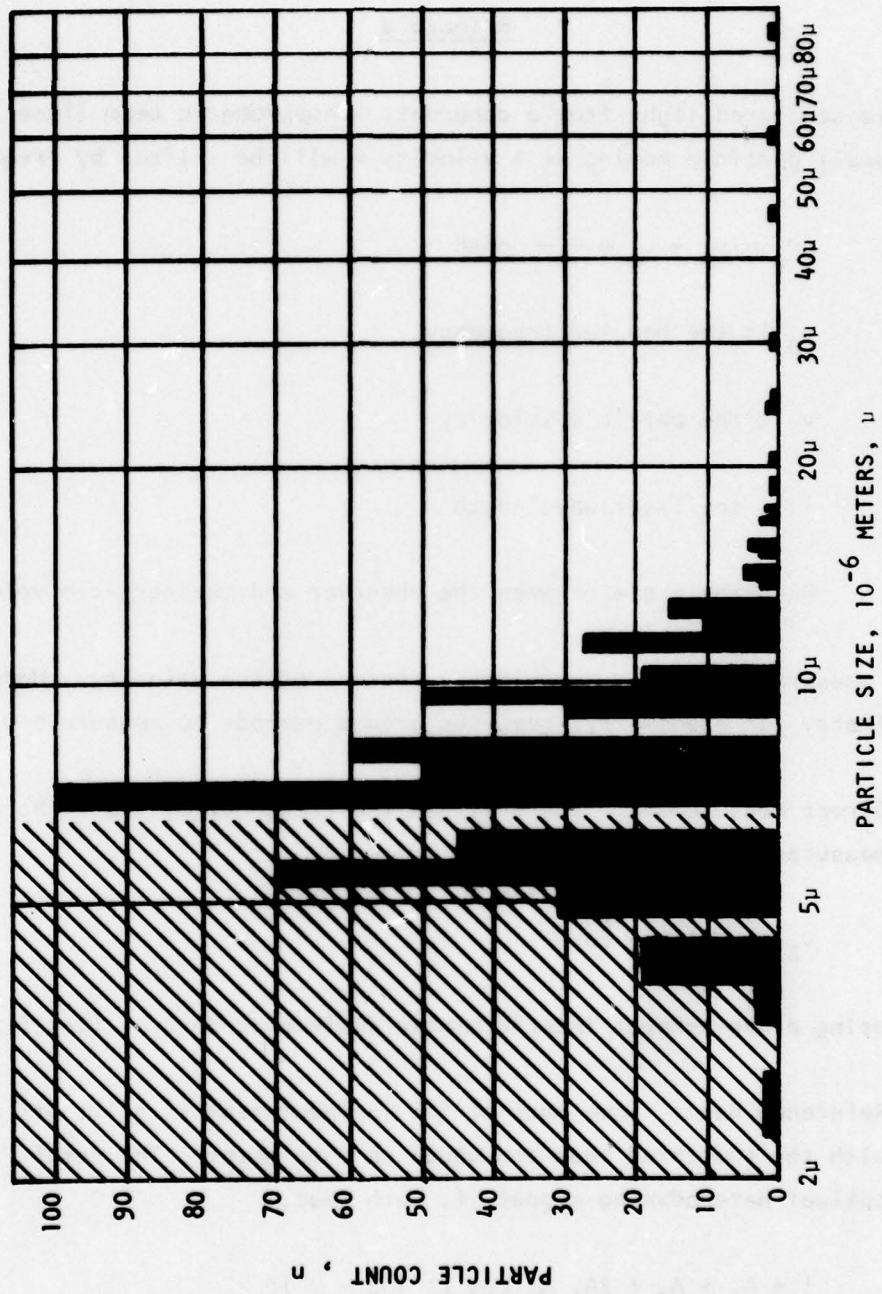


Figure B-8 2. Example Particle Size Distribution Data from Combustion Bomb Using Solid Propellant Sample at 500 psia, Obtained with Holo-system of Figure B-8 1 (Reference B-39).

APPENDIX B-9. LASER DOPPLER VELOCIMETRY (LDV) (REFERENCE B-38)

Principle

The Mie scattered light from a coherent, monochromatic beam (laser) incident on a small particle moving at a velocity v will be shifted by frequency by

$$\Delta v_D = v_D - v_o = \frac{v}{\lambda} \cos\theta \quad (\text{B-9 1})$$

where v_D is the Doppler frequency

v is the particle velocity

λ is the laser wavelength

θ is the angle between the observer and the particle velocity vector.

Thus, measurement of Δv_D provides a measure of the velocity. Modern Doppler velocimetry (or anemometry) revolves around methods to measure Δv_D .

1. Direct Measurement: The shift in the frequency of the light beam is measured directly,

$$v_D = v_o + \frac{v}{\lambda} \cos\theta \quad (\text{B-9 2})$$

using a Fabry-Perot interferometer (Reference B-40). (See Figure B-9 1.)

2. Reference Beam: Some part of the incident beam is split off and mixed with the scattered beam and added on a detector. The result is an optical heterodyning signal, I , such that,

$$I = A_1 + A_2 + 2A_1 A_2 \cos 2\pi (v_D - v_o)t \quad (\text{B-9 3})$$

where A_1 and A_2 are the amplitudes of the two scattered signals and

$$v_D - v_o$$

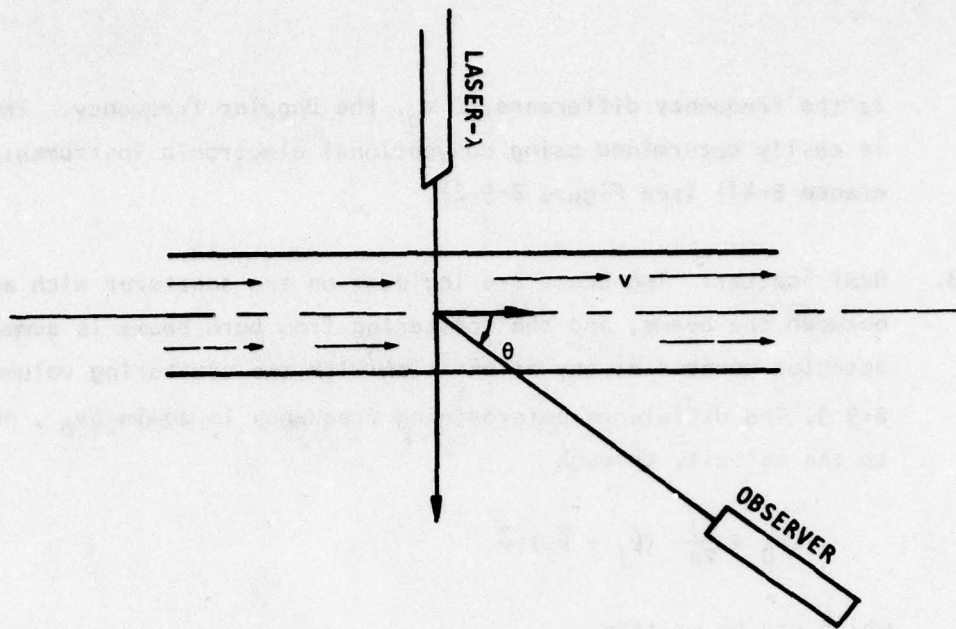


Figure B-9 1. Simplest LDV Configuration.

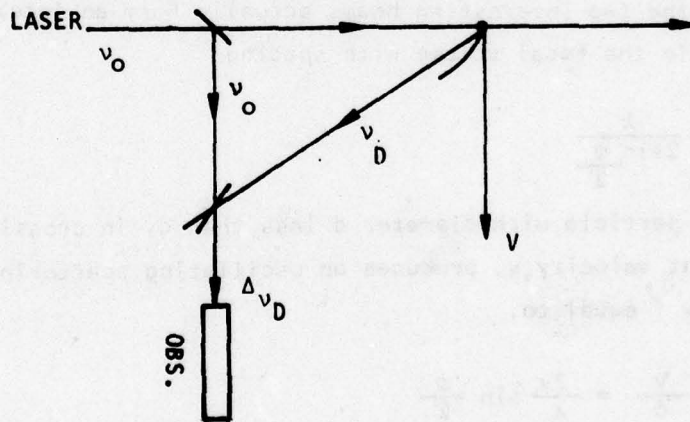


Figure B-9 2. Reference Beam LDV Configuration.

is the frequency difference, $\Delta \nu_D$, the Doppler frequency. The frequency is easily determined using conventional electronic instrumentation (Reference B-41) (see Figure B-9 2).

3. Dual Scatter: Two beams are incident on the scatterer with an angle ϕ between the beams, and the scattering from both beams is summed on a detector mounted at any orientation with the scattering volume. See Figure B-9 3. The difference heterodyning frequency is again $\Delta \nu_D$, now related to the velocity through

$$\Delta \nu_D = \frac{1}{2\pi} (\vec{k}_1 - \vec{k}_2) \cdot \vec{v} \quad (\text{B-9 4})$$

which can be written,

$$\Delta \nu_D = \frac{2v}{\lambda} \sin \frac{\phi}{2} \quad (\text{B-9 5})$$

as shown in Figure B-9 4 (Reference B-42).

4. Fringe Model (Velocity): In the dual scatter configuration (Figure B-9 5), the two intersecting beams actually form an interference fringe pattern in the focal volume with spacing

$$\delta = \frac{\lambda}{2 \sin \frac{\phi}{2}} \quad (\text{B-9 6})$$

Hence, a particle with diameter d less than δ , in crossing the fringe pattern at velocity v , produces an oscillating scattering signal with frequency f equal to,

$$f = \frac{v}{\delta} = \frac{2v}{\lambda} \sin \frac{\phi}{2} \quad (\text{B-9 7})$$

Now f is just $\Delta \nu_D$ of the dual scatter method, and thus the two interpretations of the configuration are equivalent (Reference B-43).

5. Fringe Model (Size): The shape of a scattering event as the particle of diameter d traverses the fringe pattern of spacing δ is related to the

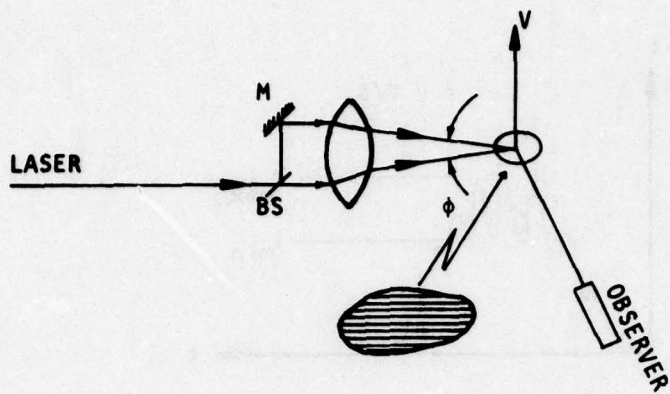


Figure B-9 3. Dual Scatter LDV Configuration.

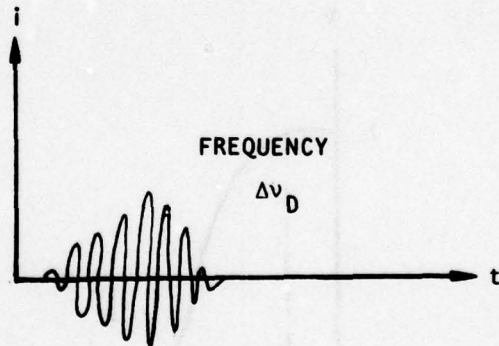


Figure B-9 4. AC Signal from Dual Scatter LDV.

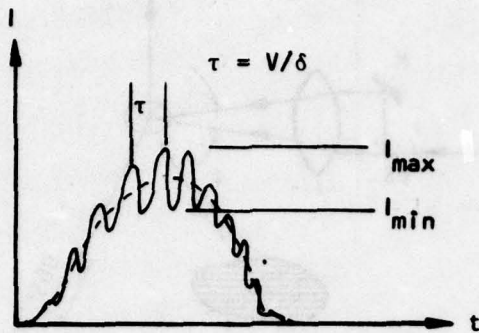


Figure B-9 5. Signal from Dual Scatter LDV.

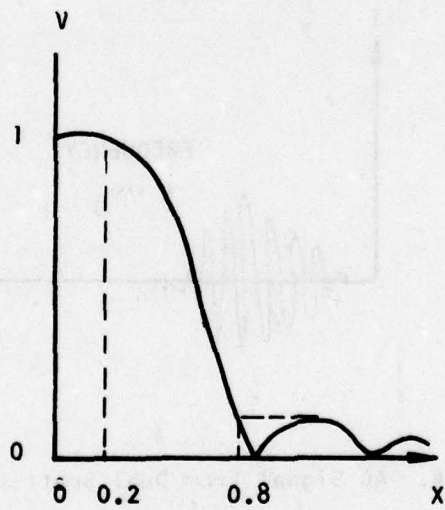


Figure B-9 6. Visibility Function for Dual Scatter LDV.

particle size through the "Visibility", defined by (Reference B-44)

$$v = \frac{I_{\max} - I_{\min}}{I_{\max} + I_{\min}} \propto \frac{2 J_1(x)}{x}$$

where x is d/δ and J_1 is a Bessel's function of the first kind. In practice, a calibration is required since the proportionality constant is not well known and depends upon the optical configuration (Reference B-45.)

Restrictions and Weaknesses

1. An upper limit on velocity using electronic processing is set by a practical upper frequency limit on electronic gear of about 10^8 Hz. This translates into upper velocity limits of a few hundred meters per second for the direct heterodying method, depending upon the angle of observation, and about 1.5 km/sec for the dual scatter (fringe) technique, depending upon the lower practical value of the angle between the intersecting beams (assumed 2° here) (Reference B-46).
2. Fabry-Perot interferometers permit measurements of frequency shifts corresponding to very high velocities, but a 10 MHz resolution limit translates into a resolution uncertainty in velocity of about 10 m/sec. The greatest weakness of this method of measuring the Doppler shift, however, is in the difficulty of maintaining optical stability under field conditions (Reference B-39).
3. LDV measures particle velocity; the desired measurement is usually gas velocity. Viscous drag may affect particle velocities, depending upon gas density and particle size, to an extent where particle velocity lags gas velocity. Thus, two phase flow theory must be applied to determine if this problem exists in any specific application (Reference B-47).

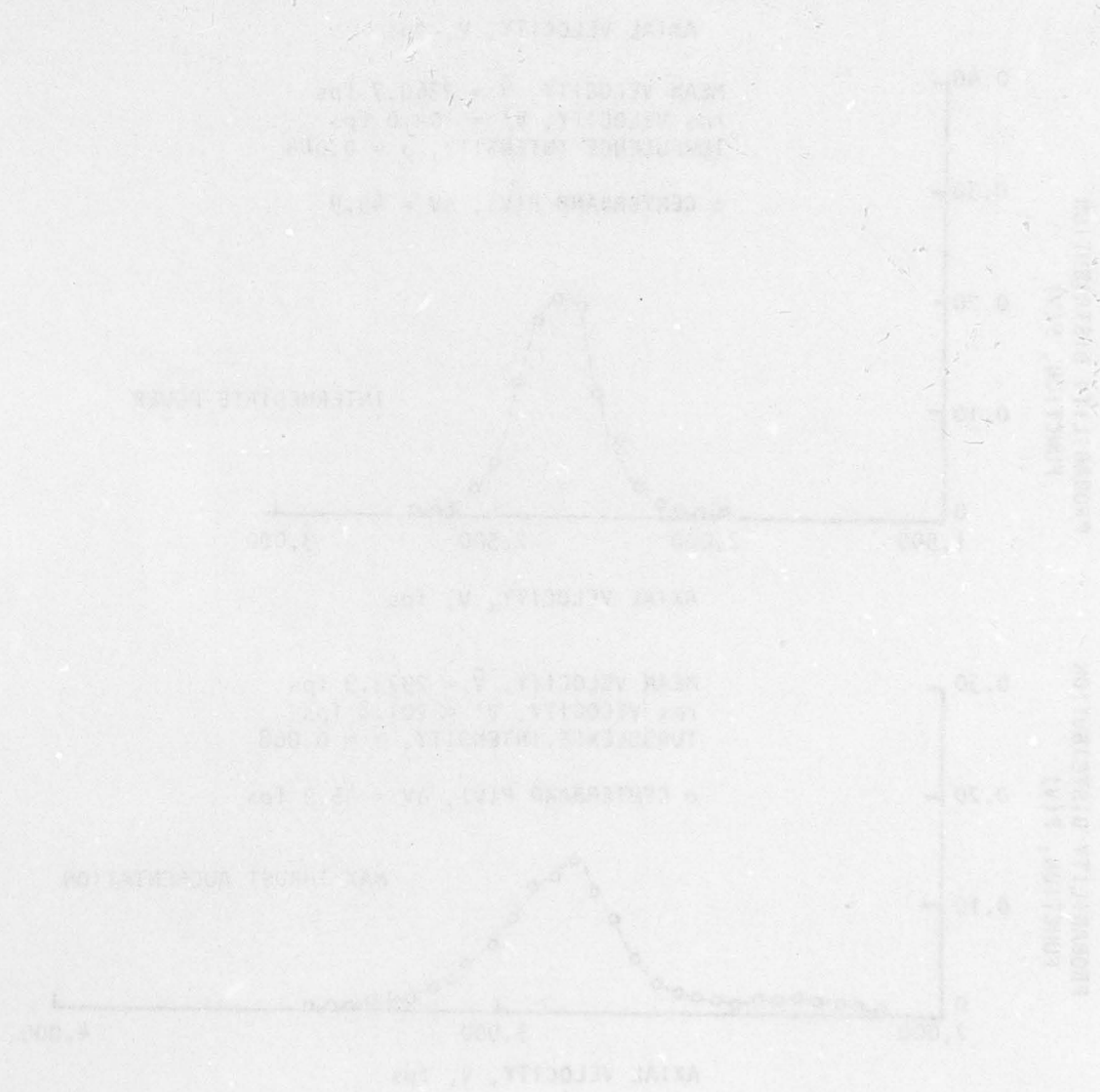
4. Measurements in turbulent flow take on their own characters and must be analyzed in terms of the statistical behavior of both the particle sampling and the turbulent structure (Reference B-47).
5. The range of particle sizes measurable by the shape of the fringe pattern is limited on the lower end by the asymptotic behavior of the visibility at about $d/\delta = 0.2$ (see Figure B-9 6); that is, $d = 0.1\lambda / \sin\phi/2$, which for $\phi =$ about 12° as a maximum gives a minimum value of about $d = \lambda$ (Reference B-48). The maximum value is set at about the value of d/δ at which the visibility becomes double valued (see Figure B-9 6); for spherical particles this limit is about $d/\delta = 0.8$, which for the $\phi = 12^\circ$ system with an argon laser places an upper limit of about $2.5 \mu\text{m}$ on the size. Thus, for a fixed system the range of sizes measurable is not large (i.e., $0.5 < d < 2.5 \mu\text{m}$ for a 12° argon laser system; $3 < d < 12 \mu\text{m}$ for a 1° system).
6. Interpretation of the scattering burst pattern is required to determine whether the particle is traversing the fringe pattern perpendicular to the fringe pattern or at an angle, to determine if more than one particle is in the scattering volume at a time, and to determine any number of other eventualities. This places very stringent requirements on the signal processor, and the data reduction and weakens the technique (Reference B-48).

Implementation

Equipment used in LDV systems takes on many forms. A particularly successful system is described in Reference B-48, which was used for both velocity and particle size measurements inside a diesel engine combustion chamber. A system designed for high velocity measurements in turbojet engine exhausts is described in Reference B-49.

Example

Measurement of the axial velocity distribution, the rms turbulent fluctuations, and the turbulent intensity made in the exhaust of an F101-GE-100 turbofan engine are described in Reference B-49. The dual scatter system utilized the fringe crossing principal and analyzed individual scattering events to obtain the measurements. Example data are shown in Figure B-9 7. The system had a maximum velocity limit of about 4500 ft/sec (1370 m/sec).



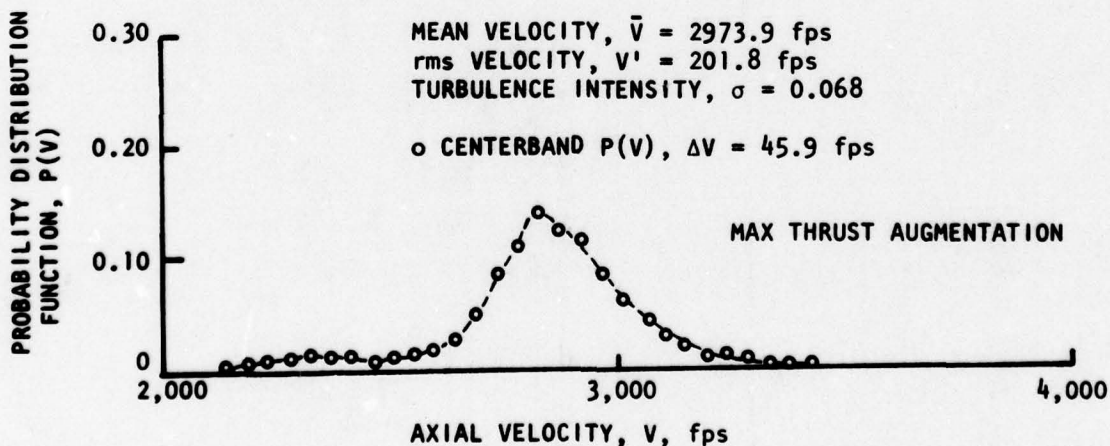
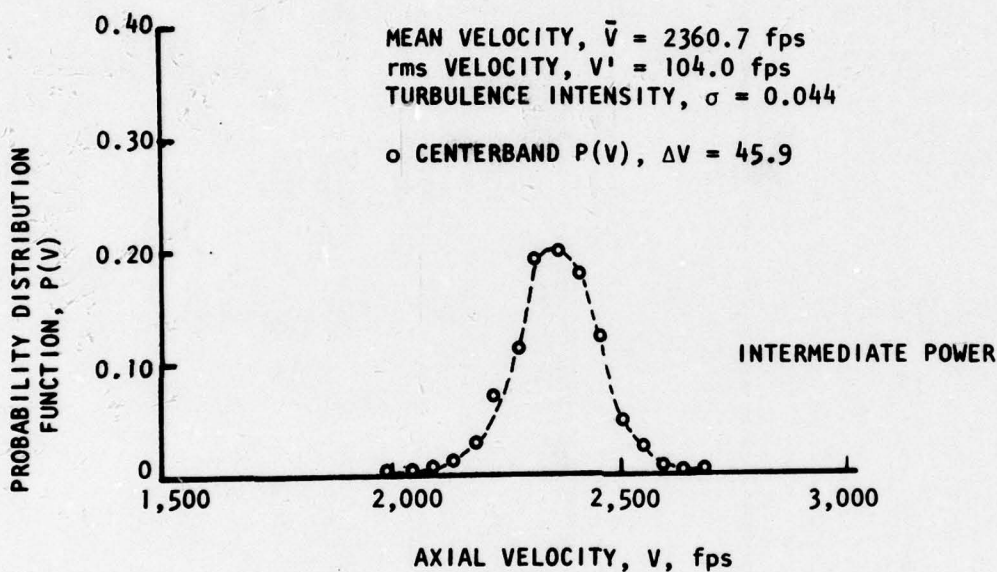
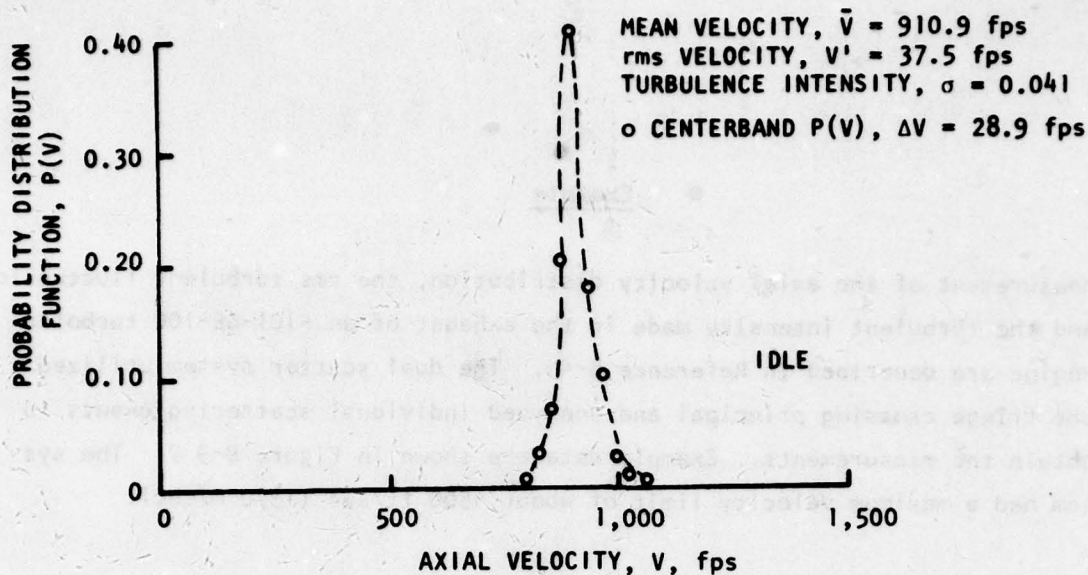


Figure B-9 7. Velocity Histograms of the Axial Velocity at Nozzle Exit of the Exhaust of an F101-GE-100 Turbofan Engine Obtained by Laser Doppler Velocimetry.

APPENDIX B-10. DIFFUSION CORRELATED SPECTROSCOPY (DCS)
(REFERENCES B-50, B-51, B-52)

Principle

If the power spectrum at low frequency ($\omega = 0$ to ~ 20 kHz) of the light scattered by monodisperse particles in Brownian motion at an angle ϕ from a uniform illumination source (laser) is measured (Figure B-10 1), spectrum of the Lorentzian form

$$P_s(\omega) = I_s \frac{K^2 D / \pi}{\left(\frac{K^2 D}{\pi}\right)^2 + \omega^2} \quad (\text{B-10 1})$$

will be observed (Figure B-10 2),

where K is the absolute value of the scattering vector

$$K = \frac{4\pi}{\lambda_0} \sin \phi/2; \quad (\text{B-10 2})$$

λ_0 is the wavelength of the incident laser beam;

D is the diffusion coefficient of the particles, which for Stokes flow (molecular mean free path small with respect to particle size) is given by

$$D = \frac{k T c}{3\pi\eta d} \quad (\text{B-10 3})$$

k is Boltzmann's constant;

T is the temperature;

η is the coefficient of viscosity;

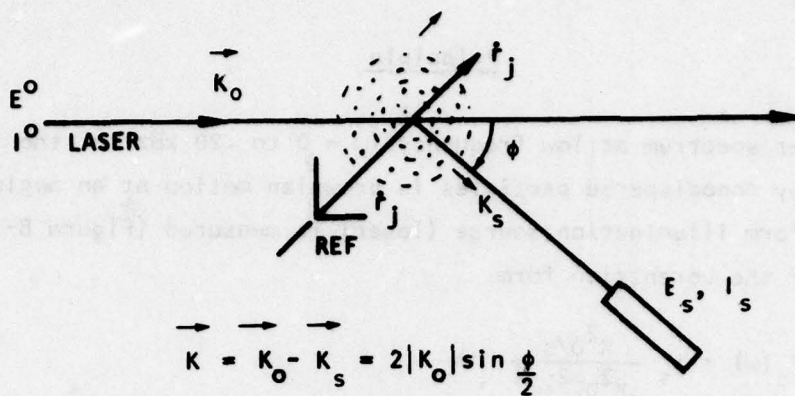


Figure B-10 1. Orientation for DCS.

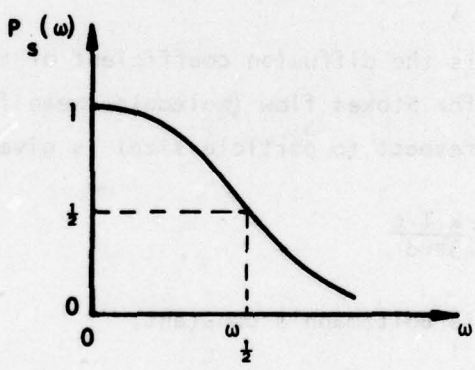


Figure B-10 2. Homodyne Spectrum from Particle Scattering.

C is a slip flow correction factor (for a molecular mean free path small compared to the particle size, $C_c \rightarrow 1$);

d is the particle diameter.

The frequency in Hz at the half power point is

$$W_{1/2} = \frac{kD^2}{\pi} = 16\pi \frac{D}{\lambda^2} \sin^2 \frac{\phi}{2} = \frac{16}{3} \frac{k}{\lambda^2 \eta} \sin^2 \frac{\phi}{2} \frac{T}{d} \quad (\text{B-10 4})$$

so that either T or d may be determined from the measured half width.

This result makes a powerful tool of a rather simple measurement scenario. The result is based upon an involved theoretical analysis of the scattering from randomly spaced particles in Brownian motion (given completely in Reference B-53 and in considerable detail in Reference B-53 and B-54). If the illumination field is not uniform, then the intensity distribution along the path of observation must be convoluted with the phase function produced by the Brownian motion, and a power spectrum of Voigt form results when the distribution is Gaussian. The latter should be avoided by proper experimental arrangement, if possible, and further consideration of that case (treated in References B-51 and B-54) will not be given here.

Restrictions and Weaknesses

1. The technique is considered to be still in the developmental stage. Two important extensions that must be made are (1) development of the mathematical model to invert a set of measurements made at different angular orientation to the parameters of a polydisperse distribution of sizes, and (2) introduction of a more adequate particle drag law to handle lower density flows where the Stokes law is not applicable.
2. A fundamental limitation on the particle size range measurable at any given velocity exists because of a limitation on observation time. One way of looking at this limitation is to say that sufficient

observation time must exist for the random Brownian motion to assert itself; in a similar manner, a time interval (or a sufficient number of observations) is required in the classical oil drop experiment to establish the Gaussian distribution for Brownian motion. Penner, Bernard, and Chany (Reference B-55) have considered this problem and have determined the effect of including a finite observation time \bar{T} . Their result can be stated: the Lorentzian spectral function will not be perturbed appreciably if,

$$\frac{K^2 D}{\pi} \geq 0.2 \left(\frac{3.7}{\bar{T}} \right)$$

or, where $\bar{T} = \Delta z/v$, where Δz is the diameter of the laser beam, this criteria can be written

$$vd \leq 0.9 \frac{kT}{\lambda^2 \mu} \Delta z$$

with μ the viscosity, k Boltzmann's constant, and T the temperature. For a flame at 2000° K, a He-Ne laser ($\lambda = 0.6328 \mu\text{m}$) and $\mu = 8 \times 10^{-4}$ poise,

$$vd \leq 0.08 \Delta z$$

A few representative values follow for illustration.

| $d(\mu\text{m})$ | $v(\text{m/sec})$ | $\Delta z(\text{cm})$ |
|------------------|-------------------|-----------------------|
| 0.1 | 1 | 0.0125 |
| 0.1 | 10 | .125 |
| 0.1 | 100 | 1.25 |
| 0.1 | 1000 | 12.5 |
| 1 | 10 | 1.25 |
| .01 | 100 | 0.125 |

Thus, as velocity increases the illumination volume must be increased, which introduces spatial resolution limitations and requires larger power lasers to retain signal to noise ratio.

Implementation

Figure B-10 3 shows the essential equipment required for the diffusion correlated spectroscopy technique. A typical experiment conducted at the AFRPL (Reference B-56) utilized the following equipment : 75 mw He-Ne laser, 1.6Å bandwidth centered at 6328Å, RCA 4832 PM tube, tape recorder (bandwidth -25 KHz fm systems), Spectral Dynamics spectrum analyzer Model 360-65.

Example (Reference B-56)

The system shown in Figure B-10 4 was used to obtain data in an acetylene/air flat flame burner. A spectrum is shown in Figure B-10 4 with the data reduction indicated, giving a particle size of about 312 nm.

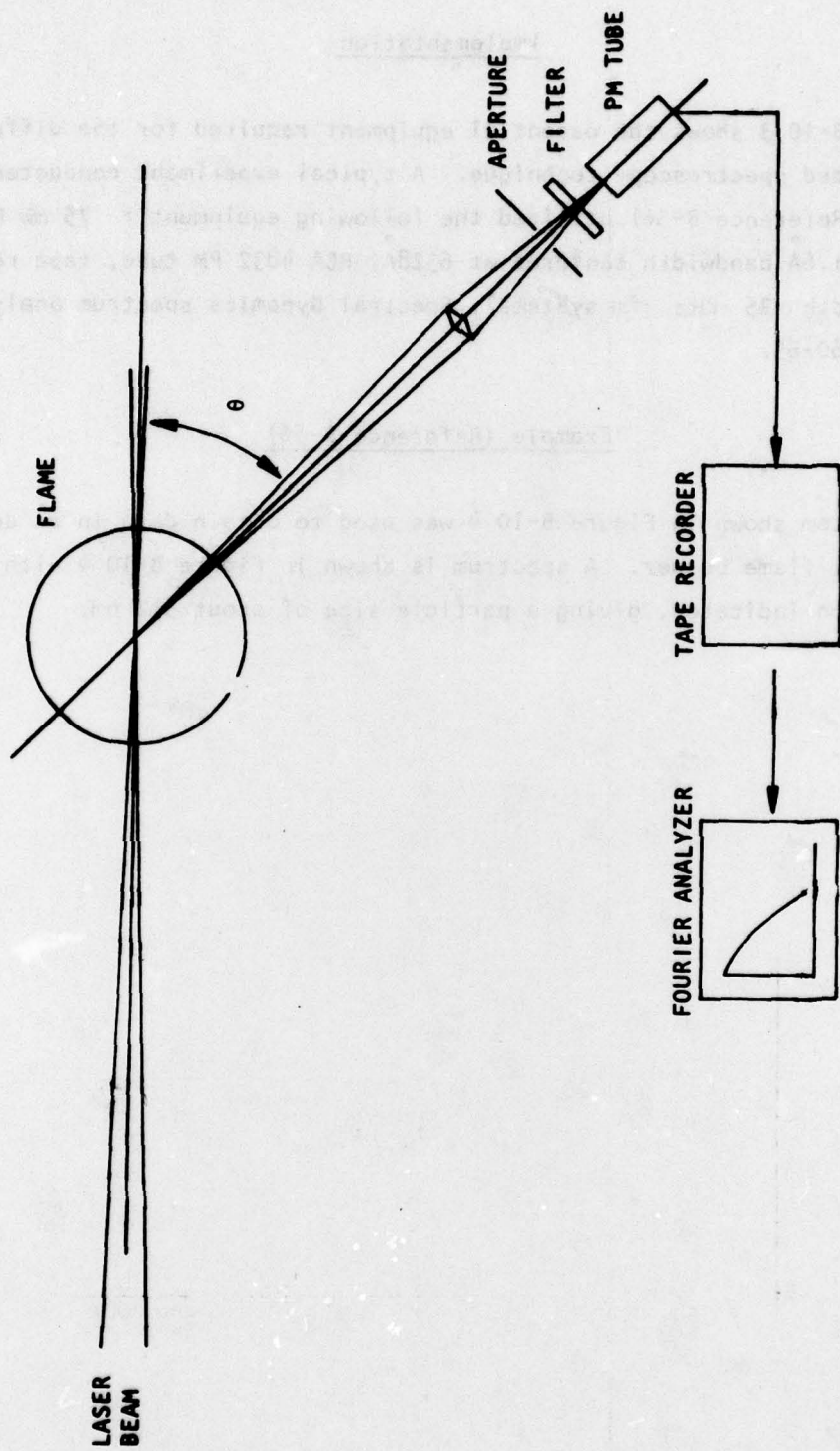


Figure B-10 3. Apparatus for Laser Doppler Line Shape Measurement.

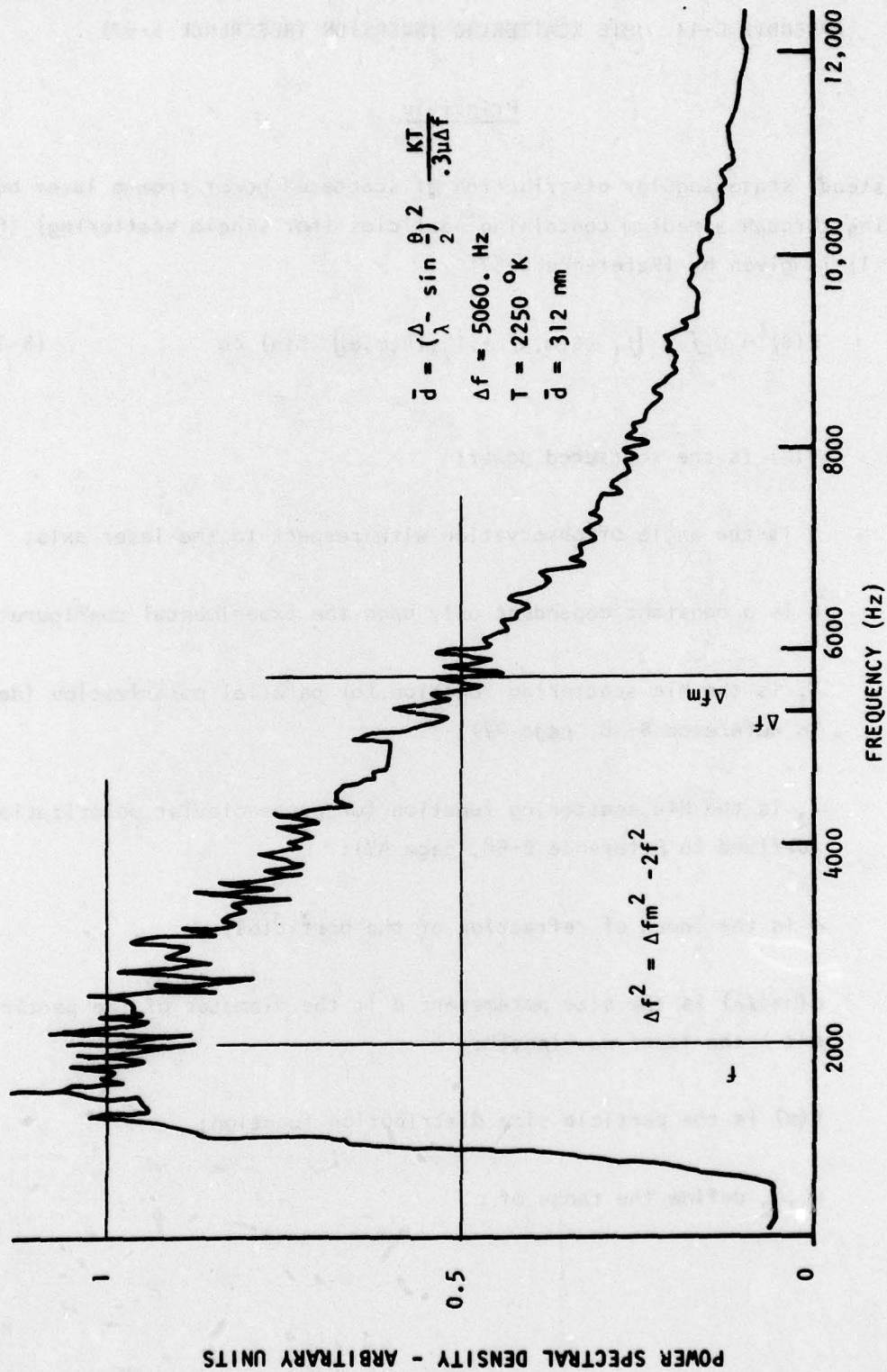


Figure B-10 4. Laser Scattered Power Spectrum from $C_2H_2-O_2$ Flame
(Scattering Angle - 60° , Height Above Burner Face - 3 cm, Equivalence Ratio - 2.5)

APPENDIX B-11. MIE SCATTERING INVERSION (REFERENCE B-57)

Principle

The steady state angular distribution of scattered power from a laser beam passing through a medium containing particles (for single scattering) (Figure B-11 1) is given by (Reference B-57)

$$P(\theta) = C \int_{\alpha_1}^{\alpha_2} [i_1(\theta, m, \alpha) + i_2(\theta, m, \alpha)] f(\alpha) d\alpha \quad (\text{B-11 1})$$

where $P(\theta)$ is the scattered power;

θ is the angle of observation with respect to the laser axis;

C is a constant dependent only upon the experimental configuration;

i_1 is the Mie scattering function for parallel polarization (defined in Reference B-58, page 47);

i_2 is the Mie scattering function for perpendicular polarization, (defined in Reference B-58, page 47);

m is the index of refraction of the particles;

$\alpha (= \pi d / \lambda)$ is the size parameter; d is the diameter of the particles and λ the laser wavelength;

$f(\alpha)$ is the particle size distribution function;

α_1, α_2 define the range of α .

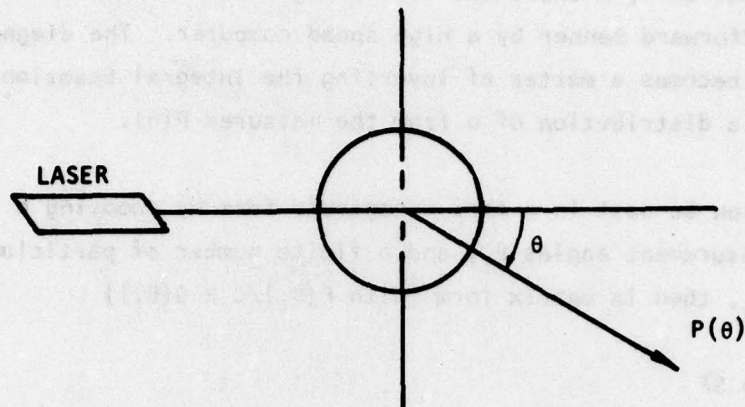


Figure B-11 1. Angular Scattering Orientation

The Mie scattering functions are given by Kerker as follows (Reference B-58),

$$i_1(\theta, m, \alpha) = \left| \sum_{n=1}^{\infty} \frac{2n+1}{n(n+1)} [A_n \pi_n(\cos \theta) + b_n \tau_n(\cos \theta)] \right|^2 \quad (\text{B-11 } 2)$$

$$i_2(\theta, m, \alpha) = \left| \sum_{n=1}^{\infty} \frac{2n+1}{n(n+1)} [A_n \tau_n(\cos \theta) + b_n \pi_n(\cos \theta)] \right|^2 \quad (\text{B-11 } 3)$$

where $\pi_n(\cos \theta) = \frac{P_n^{(1)}(\cos \theta)}{\sin \theta} \quad (\text{B-11 } 4)$

$$\tau_n(\cos \theta) = \frac{d}{d\theta} P_n^{(1)}(\cos \theta) \quad (\text{B-11 } 5)$$

$P_n^{(1)}(\cos \theta)$ are associated Legendre Polynomials of the first kind;
 $A_n(m, \alpha)$ and $b_n(m, \alpha)$ are linear combinations of Ricatti-Bessel
 functions.

For a given set of θ , m and α the scattering functions can be calculated in a straightforward manner by a high speed computer. The diagnostics problem then becomes a matter of inverting the integral Equation (B-11 1) to determine a distribution of α from the measured $P(\theta)$.

The problem can be cast in a more manageable form by choosing a finite number of measurement angles θ_i , and a finite number of particle size intervals $\Delta\alpha_k$, then in matrix form [with $P(\theta_i)/C \equiv G(\theta_i)$]

$$G = SF$$

(B-11 6)

where G is a column vector of the measurements at the θ_i , F is a column vector of the number of particles within each size element $\Delta\alpha_k$, and S is the square transformation matrix with elements $s_{ik}(\theta_i, m, \alpha_k)$ calculable from the scattering functions if the index of refraction is assumed. The inverse of the matrix Equation (B-11 6) constitutes the determination of the distribution function $f(\alpha_k)$. This inversion is far from a trivial numerical problem, as discussed in References B-57, B-59, and B-60.

The amount of information from a set of measurements may be doubled by selectively measuring the scattered parallel and perpendicularly polarized component of the intensity. Also, an additional piece of information is given by the extinction measurement at $\theta=0$. Various investigators (References B-60, B-61, and B-62, for example) have used combinations of angular, polarization, and extinction measurements to infer approximate particle size distributions.

Status

This technique is in the research stage with no successful general application reported to date. Lewis, et al, at AEDC (Reference B-60) have an operating computer program which they have used to generate particle size histograms when only two angular measurements could be made.

Restrictions and Weaknesses

1. The complex nature of the deconvolution (or inversion) process makes this technique difficult to access until some definitive application is made. Even more difficult may be the assignment of uncertainty limits to the data. The uncertainty problem is discussed in Reference B-57 in the context of its contributions to instability of the inversion calculation. Problems of uniqueness of the inversion have also been posed but are as yet unresolved.
2. The complex index of refraction must be known or must be determined as a third order iteration on the inversion. Currently, very little data on the index of refraction of materials of interest in rocket exhausts exist. This lack of data on the index of refraction may be the weakest link in the use of the technique.
3. Limits on the size range of applicability of the technique occur when the change in scattering function with size becomes asymptotically small. On the lower end the scattering function becomes relatively insensitive to size changes at a diameter of about 0.25λ (Rayleigh limit). On the upper end the limit on measurable particle size is probably about 10λ , although this limit is really a function of how well the back-scattered radiation can be measured.

Implementation

The apparatus necessary for this measurement consists of a laser having sufficient power to penetrate the particle laden flow and the appropriate detector systems. No suitable apparatus for rocket exhausts has been tested to date, although a system is under development at the AFRPL.

REFERENCES

- B-1. Goody, R. M., Atmospheric Radiation, Clarendon Press, Oxford, 1964.
- B-2. Young, S. J., "Nonisothermal Band Model Theory," Jou. Quantitative Spectroscopy and Radiative Transfer, Vol. 18, pp. 1-28, 1977.
- B-3. Ludwig, C. B., Malkmus, W., Reardon, J. E., and Thomson, J. A. L., "Handbook of Infrared Radiation from Combustion Gases," NASA SP-3080, 1973.
- B-4. Young, S. J., "Evaluation of Nonisothermal Band Models for H₂O," Jou. Quantitative Spectroscopy and Radiative Transfer, Vol. 18, pp. 29-45, 1977.
- B-5. Brewer, L. E. and Limbaugh, C. C., "Infrared Band Model Technique for Combustion Diagnostics," Applied Optics, Vol. 11 pp. 1200-1204, 1972.
- B-6. Brewer, L. E., "Development and Application of an Optical Technique for Determining Temperature and Specie Concentrations in Radiating Combustion Gases," PH.D. Dissertation, The von Karman Institute for Fluid Dynamics, Brussels, Belgium, May 1975.
- B-7. Krekow, B., Bahrov, H. J., McClay, G. J., and Arnold, C. B., "Use of the Curtis-Godson Approximation in Calculations of Radiant Heating by Inhomogeneous Hot Gases," Applied Optics, Vol. 5, p. 1791, 1966.
- B-8. Young, S. J., "Band Model Parameters for the 2.7 μ m Bands of H₂O and CO₂ in the 100-3000°K Temperature Range," SAMS0-TR-76-209, Los Angeles Air Force Station, CA, Jul. 1975.
- B-9. Young, S. J., "Band Model Parameters for the 4.3 μ m Fundamental Band of CO₂ in the 100-3000°K Temperature Range," SAMS0-TR-76-35, Los Angeles Air Force Station, CA, Feb. 1976.
- B-10. Young, S. J., Unpublished Progress Reports, RPL-sponsored NERD Emission/Absorption Program, AFRPL/PACP, Edwards AF Base, CA, 1977-78.
- B-11. Limbaugh, C. C., "An Uncertainty Propogations Analysis for an Infrared Band Model Technique for Combustion Gas Diagnostics," AEDC-TR-76-155, Arnold Air Force Station, TN, Apr. 1977.
- B-12. Davis, M. G., McGregor, W. K., Few, J. D., and Glassman, H. N., "The Transmission of Doppler Broadened Resonance Radiation Through Absorbing Media with Combined Doppler and Pressure Broadening (NO γ -Bands as an Example)," AEDC-TR-76-12, Feb. 1976.

REFERENCES

- B-13. Few, J. D., McGregor, W. K., and Glassman, H. N., "Comparison of UV Absorption Measurements with Probe Sampling Measurements of Nitric Oxide Concentration in a Jet Engine Combustor Exhaust," AEDC-TR-76-134, Sep. 1976.
- B-14. Few, J. D., McGregor, W. K., and Glassman, H. N., "Resonance Absorption Measurements of NO Concentration in Combustor Exhaust," Experimental Diagnostics in Gas Phase Combustion Systems, Ed. B. T. Zinn, AIAA Press, pp. 187-204, 1977.
- B-15. McGregor, W. K., Seiber, B. L., and Few, J. D., "Concentration of OH and NO in YJ93-GE-3 Engine Exhaust Measured In Situ by Narrow-Line UV Absorption," Proceedings of 2nd Conf. on the Climatic Impact Assessment Program, Cambridge, MA, Nov. 1972.
- B-16. Few, J. D., Bryson, R. J., and McGregor, W. K., "Evaluation of Probe Sampling Measurements of Nitric Oxide Concentrations in a Jet Engine Combustor Exhaust," AEDC-TR-76-180, Jan. 1977.
- B-17. Cattolica, R., Robben, F. and Talbot, L., "The Interpretation of the Spectral Structure of Rayleigh Scattered Light from Combustion Gases," in Experimental Diagnostics in Gas Phase Combustion System, Ed. B. T. Zinn, Progress in Astronautics and Aeronautics, Vol. 53, AIAA Press, 1977.
- B-18. Williams, W. D. and Lewis, J. W. L., "Rayleigh Scattering Studies of CO₂ Expansion Flow Fields," AEDC-TR-75-146, Arnold Engineering Development Center, TN, Dec. 1975.
- B-19. Lewis, J. W. L. and Williams, W. D., "Results of Visible Radiance, Temperature and Number Density for Vacuum Plume Expansion of a Liquid Bipropellant Engine," 10th JANNAF Plume Technology Meeting, San Diego, CA, 13-15 Sep. 1977.
- B-20. Pitz, R. W., Cattolica, R., Robben, F., and Talbot, L., "Temperature and Density in a Hydrogen-Air Flame from Rayleigh Scattering," Combustion and Flame, Vol. 27, pp. 313-320, 1976.
- B-21. Williams, W. D. and Lewis, J. W. L., "Rotational Temperature and Number Density Measurements of N₂, O₂, CO, and CO₂ in a Hypersonic Flow Field Using Laser-Raman Spectroscopy," AEDC-TR-75-37, Arnold Engineering Development Center, TN, July 1975.
- B-22. Leonard, D. A., "Field Tests of a Laser Raman Measurement System for Aircraft Engine Exhaust Emissions," AFAPL-TR-74-100, Air Force Aero Propulsion Laboratory, Wright-Patterson Air Force Base, OH, Oct. 1974.

REFERENCES

- B-23. Williams, W. D., Powell, H. M., et al, "Emitted Radiation from Special Engines (ERASE), Part III, Determination of Temperature and Species Number Density in the Exhaust Plume Utilizing Laser-Raman/Rayleigh Scattering," AEDC-TR-76-121, Arnold Engineering Development Center, TN, July 1977.
- B-24. Williams, W. D., Powell, H. M., et al, "Laser-Raman Diagnostics of Temperature and Number Density in the Mixing Region of a Rocket Engine Exhaust Plume and a Coflowing Air Stream," 10th JANNAF Plume Technology Meeting, San Diego, CA, 13-15 Sep. 1977.
- B-25. Griem, H. R., Plasma Spectroscopy, McGraw-Hill Book Co., Inc., New York, (1964).
- B-26. Mitchel, A. C. G. and Zemansky, M. W., "Resonance Radiation and Excited Atoms," Cambridge Press, London (Reprinted 1971).
- B-27. Limbaugh, C. C., "Determination of the Excited State Density Distribution within a Nonequilibrium Freely Expanding Argon Arcjet Plume," AEDC-TR-77-23, Arnold Engineering Development Center, TN, Mar. 1977.
- B-28. Neer, M. E., Drury, J. E., "Supersonic Combustion Flowfield Studies Using Absorption Spectroscopy," in Experimental Diagnostics in Gas Phase Combustion Systems (Ed B. T. Zinn), Progress in Astronautics and Aeronautics, Vol. 53, AIAA Press, New York (1977).
- B-29. Hanson, R. K., Kuntz, P. A., and Kruger, C. H., "High-Resolution Spectroscopy of Combustion Gases Using a Tunable IR Diode Laser," Applied Optics, Vol. 16, pp. 2045-2048, 1977.
- B-30. Daily, J. W. and Kruger, C. H., "Effects of Cold Boundary Layers on Spectroscopic Temperature Measurements in Combustion Gas Flows," J. Quant. Spectrosc. Radiat. Transfer, Vol. 17, pp. 327-328, 1977.
- B-31. Krakow, B., Kiech, E. A., McAdoo, H. A., "Isolated CO Lines for Use in Combustion Diagnostics," AEDC-TR-77-11, Arnold Engineering Development Center, TN, Sep. 1977.
- B-32. Muntz, E. P., "The Electron-Beam Fluorescence Technique," AGARD-ograph 132, Dec. 1968.
- B-33. Whitfield, D. L., Lewis, J. W. L., and Williams, W. D., "Specie Number Density, Pitot Pressure, and Flow Visualization in the Near Field of Two Supersonic Nozzle Banks Used for Chemical Laser Systems," AEDC-TR-73-11, Arnold Engineering Development Center, TN, May 1973.

REFERENCES

- B-34. Lewis, J. W. L., Williams, W. D., Price, L. L., and Powell, H. M., "Nitrogen Condensation in a Sonic Orifice Expansion Flow," AEDC-TR-74-36, Arnold Engineering Development Center, TN, July 1974.
- B-35. Price, L. L., Powell, H. M., and Moskalik, R. S., "Species Number Density Measurements in Plume Interactions with Free Stream Using an Electron Beam Technique," AEDC-TR-71-226, Arnold Engineering Development Center, TN, Nov. 1971.
- B-36. Daily, J. W., "Saturation Effects in Laser Induced Fluorescence Spectroscopy," Applied Optics, Vol. 16, pp. 568-571, 1977.
- B-37. Baronavski, A. P. and McDonald, J. R., "Measurement of C_2 Concentration in an Oxygen-Acetylene Flame: An Application of Saturation Spectroscopy," Jou. Chem. Phys., Vol. 66, pp. 3300-3301, 1977.
- B-38. Trolinger, J. D., "Laser Instrumentation for Flow Field Diagnostics," AGARDograph No. 186, March 1974.
- B-39. Weurker, R., Briones, R., and George, D., "Holography of Solid Propellant Combustion," AIAA Paper No. 77-977, AIAA/SAE 13th Propulsion Conference, Orlando, FL, July 11-13, 1977.
- B-40. Morse, H. L., Tullis, B., Siefert, H. S., and Babcock, W., "Development of a Laser Doppler Particle Sensor for the Measurement of Velocities in Rocket Exhausts," Jou. of Spacecraft and Rockets, Vol. 6, pp. 264-272, 1969.
- B-41. Yeh, Y. and Cummins, H. Z., "Localized Fluid Flow Measurements with a He-Ne Laser Spectrometer," Applied Physics Letters, Vol. 4, pp. 176-178, 1964.
- B-42. Brayton, D. B. and Goethert, W. H., "A New Dual-Scatter Laser Doppler Shift Velocity Measuring Technique," ISA Transactions, Vol. 10, p. 40, 1971.
- B-43. Rudd, M. J., "A New Theoretical Model for the Laser Doppler Meter," Jou. of Physics E, Vol. 2, pp. 55-58, 1969.
- B-44. Farmer, W. M., "Measurements of Particle Size, Number Density, and Velocity Using a Laser Interferometer," Applied Optics, Vol. 11, p. 2603, 1972.
- B-45. Chigier, N. A., "Combustion Diagnostics by Laser Velocimetry," Progress in Astronautics and Aeronautics, Vol. 53, Ed. B. T. Zinn, AIAA Press, p. 337, 1977.

REFERENCES

- B-46. Stevenson, W. H., "Principles of Laser Velocimetry," Progress in Astronautics and Aeronautics, Vol. 53, Ed. B. T. Zinn, AIAA Press, p. 307, 1977.
- B-47. Barnett, D. O. and Giel, T. V., "Application of a Two-Component Bragg-Diffracted Laser Velocimeter to Turbulence Measurements in a Subsonic Jet," AEDC-TR-76-36, Arnold Engineering Development Center, TN, May 1976.
- B-48. Bentley, H. T. and Bomar, B. W., "Development of a Laser Velocimeter System for Flame Studies," AEDC-TR-76-150, Arnold Engineering Development Center, TN, June 1977.
- B-49. Barnett, D. O. and Brayton, D. B., "Laser Velocimeter Utilization in Jet Engine Altitude Test Cells," AEDC-TR-77-21, Arnold Engineering Development Center, TN, June 1977.
- B-50. Hinds, W. and Reist, P. C., "Aerosol Measurement by Laser Doppler Spectroscopy - I Theory and Experimental Results for Aerosols Homogeneous," Aerosol Science. Vol. 3, pp. 501-514.
- B-51. Penner, S. S., Bernard, J. M., and Jerskey, T., "Power Spectra Observed in Laser Scattering from Moving, Polydisperse Particle Systems in Flames - I. Theory," Acta Astronautica, Vol. 3, pp. 69-91, 1976.
- B-52. Walker, C. T., "Light Scattering" in Physics of Quantum Electronics, Vol. 2 - Laser Applications to Optics and Spectroscopy, pp. 281-350, Addison-Wesley Publishing Co., Reading, MA, 1975.
- B-53. Benedek, G. B., "Optical Mixing Spectroscopy, with Applications to Problems in Physics, Chemistry, Biology and Engineering," in Polarization, Matter and Radiation, Presses Universitaires de France, Paris, pp. 49-84, 1969.
- B-54. Bernard, J. M. and Penner, S. S. "Determination of Particle Sizes in Flames from Scattered Laser Power Spectra" in AIAA Progress in Astronautics and Aeronautics Vol. 53, Experimental Diagnostics in Gas Phase Combustion Systems, AIAA Press, pp. 411-420, 1977.
- B-55. Penner, S. S., Bernard, J. M., and Chany, P., "Determination of Particle Sizes (or Temperatures) Using the Power Spectra of Scattered Radiation from Pulsed Lasers," (Unpublished Paper).

REFERENCES

- B-56. Driscoll, J. F., Mann, D. M., and McGregor, W. K., "Submicron Particle Measurements in an Acetylene-Oxygen Flame." Combustion Science & Technology (to be published).
- B-57. Chow, L. C. and Tien, C. L. "Inversion Techniques for Determining the Droplet Size Distribution in Clouds: Numerical Examination," Applied Optics, Vol. 15, pp. 378-383, 1976.
- B-58. Kerker, M., The Scattering of Light and Other Electro-Magnetic Radiation, Academic Press, New York, 1969.
- B-59. Twomey, S., "On the Numerical Solution of Fredholm Integral Equation of the First Kind by the Inversion of the Linear System Produced by Quadrature," Jou. Assoc. of Computing Machinery, Vol. 10, p. 97, 1963.
- B-60. Lewis, J. W. L., Curry, B. P., and Weaver D. P., "Determination of the Size Distribution Function for Particles in a Hypersonic Flowfield," AEDC-TR-77- , Arnold Engineering Development Center, TN (to be published).
- B-61. Pinnick, R. G., Carroll, D. E., and Hofmann, D. J., "Polarized Light Scattered from Monodisperse Randomly Oriented Nonspherical Aerosol Particles: Measurements," Applied Optics, Vol. 15, p. 334, 1976.
- B-62. Bonczyk, P. A., "Measurement of Particulate Size by In Situ Laser-Optical Methods," United Technology Research Center, Hartford, Conn., 1977 (internal report).